ISBN 978-82-326-0442-5 (printed version)
ISBN 978-82-326-0443-2 (electronic version)
ISSN 1503-8181

Shahla Gondal

Doctoral Thesis

Doctoral theses at NTNU, 2014:265

Shahla Gondal

Carbon dioxide absorption into hydroxide and carbonate systems

NTNU
Norwegian University of Science and Technology
Faculty of Natural Sciences and Technology
Department of Chemical Engineering

NTNU – Trondheim
Norwegian University of
Science and Technology

Doctoral theses at NTNU, 2014:265

NTNU

NTNU – Trondheim
Norwegian University of
Science and Technology

Shahla Gondal

Carbon dioxide absorption into hydroxide and carbonate systems

Thesis for the degree of Philosophiae Doctor

Trondheim, October 2014

Norwegian University of Science and Technology
Faculty of Natural Sciences and Technology
Department of Chemical Engineering

NTNU – Trondheim
Norwegian University of
Science and Technology

NTNU
Norwegian University of Science and Technology

Thesis for the degree of Philosophiae Doctor

Faculty of Natural Sciences and Technology
Department of Chemical Engineering

ISBN 978-82-326-0442-5 (printed version)
ISBN 978-82-326-0443-2 (electronic version)
ISSN 1503-8181

Doctoral theses at NTNU, 2014:265

Printed by Skipnes Kommunikasjon as

Dedicated to

Nature and its Creator…

Who created it in the most ordered form!

ABSTRACT

In the global warming scenario, a literature review on carbon dioxide capture technologies shows that CO_2 capture by chemical absorption seems to be the immediately viable route for sustainable energy supply in near future. The technology for chemical absorption is available and has been practiced in the industry. Development and identification of optimal absorbents for absorption is required to employ it on the scale required for CO_2 capture and to minimize the energy penalty of capture.

Hydroxide and carbonate systems have been used for absorption of CO_2 from the beginning of the 20^{th} century in different industrial processes. Though the use of hydroxides and carbonates remained persistent in special applications but the use of these systems in industrial gas cleaning units decreased after the introduction of alkanolamines as absorbents. During the last two decades, hydroxide and carbonate systems have regained interest in post combustion CO_2 capture by absorption. Potentially low energy requirements for the capture process based on hydroxide and carbonate systems and being environment friendly are advantages over the energy intensive amine based CO_2 capture solvents and environmental issues arising from degradation of amines.

This thesis contributes to the kinetics and equilibrium of CO_2 absorption into hydroxide and carbonate systems. The measured experimental data on CO_2 absorption and physical solubility of CO_2 (from N_2O solubility using N_2O analogy) into these systems, in addition to vapor liquid equilibrium (VLE) data were used to evaluate the activity based kinetics of the reaction of CO_2 with hydroxyl ion (OH^-) containing Li^+, Na^+ and K^+ counter ions. To study the kinetics of the CO_2 reaction with hydroxyl ion is important not only for hydroxide and carbonate systems but it is significant as this reaction occurs in all alkaline systems including alkanolamines.

The density and N_2O solubility data into aqueous hydroxides and blends of hydroxides with carbonates containing Li^+, Na^+ and K^+ counter ions were experimentally determined. The measured density data were compared with an empirical density model available in the literature. The measured N_2O solubility data were used for the refitting of parameters in an extensively used solubility

model available in the literature for up gradation to wider ranges of temperature and concentration.

The measured N_2O solubility data and VLE data collected from the literature were simultaneously regressed using an in-house equilibrium model to determine the interaction parameters in the Electrolyte-NRTL model. The determined Electrolyte-NRTL parameters were subsequently used for the estimation of liquid phase activities of CO_2 and OH^- in the systems containing Li^+, Na^+ and K^+ counter ions.

The kinetics of aqueous hydroxides and blends of hydroxides with carbonates containing Li^+, Na^+ and K^+ counter ions were experimentally measured using a string of discs contactor (SDC). The measured data were used for the parameter optimization in a widely used kinetics model available in the literature to a broader range of temperature.

Finally, the activity based kinetics of the CO_2 reaction with OH^- were determined using the measured kinetics data and the calculated liquid phase activities of CO_2 and OH^- in the aqueous solutions containing Li^+, Na^+ and K^+ counter ions.

Acknowledgements

All praise belongs to **Allah Almighty**, Who is Lord of all the worlds and I have grateful heart for all of His **Messengers** who contributed towards my intellect to appreciate the Creator and His creature.

I would like to express my gratitude to all those who provided me the possibility to complete this work. I am thankful to Faculty of Natural Sciences and Department of Chemical Engineering at NTNU to facilitate and finance this work by providing every possible facility and support.

My heart is indebted to my co-supervisor, Professor **Hallvard F. Svendsen** whose inspiration, motivation and stimulating suggestions enabled me to start this work. I deem it as my privilege to express my sincerest gratitude and heartfelt thankfulness to him for his guidance, expert opinions and encouraging remarks throughout the course of this work.

I owe my deepest gratitude to my supervisor Associate Professor **Hanna Knuutila** for her friendly, motivating and kind behavior during the completion of this work. Hanna, this would never be possible for me to complete this work without your constructive criticism, practical suggestions, swift follow-ups and compassionate guidance.

I would like to thank my friends for their continuous encouragement, summer students for performing experiments for me and all of my colleagues for their cooperation, especially Dr. Juliana G.M.S. Monteiro for her ever present support and help regarding computational work and execution of equilibrium model.

I want to pay tribute to my father, parents-in-law, brother, brothers-in-law, sisters-in-law and their families for sending best wishes and encouraging me during the course of this work.

I did not know that it would be my last meeting with my mother when I left for Norway on 13th September, 2008 to start my Masters in the Chemical Engineering Department of NTNU. My mother was the happiest person on earth when I started my doctoral work in August 2010 but she passed away in November 2010. Today while writing my acknowledgements for this thesis, I have a grieved heart for my

mother. She was a continuous source of prayers and will always remain source of inspiration behind every single success in my life.

Last but not least, I am indebted to love, care and cooperation of my family, my husband Naveed Asif, 12 years old daughter, Fatima, 3 years old son, Abdullah, and our daughter who is expected to breath in this world in January 2015. Just like death of my mother, I was unaware that I would be blessed with two more family members during the course of this work. I want to thank my husband for practically helping me in the completion of this work by performing most of my experimental work at NTNU during my parental leave and taking care of home and children when I am working in the University. Naveed, Fatima, Abdullah and my little angel, you are the real contributors to this work. Your love, care, encouragement, faith, and hope provided me the strength required to complete this work.

Contents

LIST OF SYMBOLS

Symbol	Definition	Units
	Uppercase Latin Letters	
A_{act}	Actual mass transfer area	m^2
$AARD$	Average Absolute Relative Deviation	-
C	Solubility	$kmol.m^{-3}$
C	Concentration	$kmol.m^{-3}$
D	Diffusivity	$m^2.s^{-1}$
E	Enhancement factor	-
E_A	Activation energy	J.mol^{-1}
I	Ionic strength	$mol.L^{-1}$
G	Gibbs free energy	J
H^{app}	Apparent Henry's law constant	$Pa.m^3.mol^{-1}$
H	Henry's law constant	Pa
Ha	Hatta Number	-
K	Equilibrium constant	-
K	Schenov constant	-
K_{ov_G}	Gas phase overall mass transfer coefficient	$mol.m^{-2}.Pa^{-1}.s^{-1}$
K_{ov_L}	Liquid phase overall mass transfer coefficient	$m.s^{-1}$
LMPD	Logarithmic mean of the partial pressure difference	Pa
M	Molarity	$mol.L^{-1}$
N	Flux	$mol.m^{-2}.s^{-1}$
NC	Number of components	-
NP	Number of phases	-
P	Pressure	Pa
P_i	Partial pressure	Pa
Q	Molar flow rate	$mol.s^{-1}$
R	Universal gas constant	$8.314\ J.mol^{-1}.K^{-1}$
T	Absolute temperature	K
V	Volume	m^3
Z	Compressibility factor	-
	Lowercase Latin Letters	
a	Activity	-
d	Distance	m
f	Fugacity coefficient	-
$\dot{g}^E$	Molar excess Gibbs free energy	$J.mol^{-1}$
h_{G_o}	Gas specific parameter	$m^3.kmol^{-1}$

h_i	Ion specific parameters	$m^3.kmol^{-1}$
h_T	Gas specific parameter for temperature effect	$m^3.kmol^{-1}.K^{-1}$
k_1	First order reaction rate constant	s^{-1}
k_2	Second order reaction rate constant	$m^3.mol^{-1}.s^{-1}$
k_g	Gas phase mass transfer coefficient	$mol.m^{-2}.Pa^{-1}.s^{-1}$
k_G	Gas phase mass transfer coefficient	$m.s^{-1}$
k_L	Liquid phase mass transfer coefficient with chemical reaction	$m.s^{-1}$
k_L^o	Liquid phase mass transfer coefficient without chemical reaction	$m.s^{-1}$
m	Mass	kg
n	Moles	mol
r	Rate of reaction	$mol.m^{-3}.s^{-1}$
s	Fractional rate of surface renewal	s^{-1}
t	Time	s
v	Gas velocity	$m.s^{-1}$
v_i	Partial molar volume	$m^3.mol^{-1}$
w	Thickness	m
x	Liquid phase mole fraction	-
y	Vapor phase mole fraction	-
z	Charge number of an ion	-
	Greek Letters	
Γ	Liquid wetting rate	$kg.m^{-1}.s^{-1}$
γ	Activity coefficient	-
δ	Film thickness	m
ϴ	Poynting factor	-
θ	Time of exposure of of liquid to gas	s
μ_i	Chemical potential of a component	$J.mol^{-1}$
μ	Viscosity	$Pa.s$
ρ	Density	$kg.m^{-3}$
τ	Interaction paremeter	-
φ	Fugacity coefficient	-
Φ	Ratio of diffusion time to reaction time	-
σ	Standard deviation	Same units as those of the property
Ψ	Surface element contact times distribution function	s^{-1}
	Subscripts	
b	Bulk	
G, g	Gas phase	
eq	Equivalent	

i	Species i , Interface, Internal
$inst$	Instantaneous
j	Reaction j
L	Liquid phase
R	Reactor
V	Vessel
sat	Saturation
tot	Total
V	Vapor
∞	Infinite enhancement
	Superscripts
app	Apparent
exp	Exponent, Experimental value
E	Excess
G, g	Gas phase
id	Ideal solution
L	Liquid phase
LR	Long range
o	Initial conditions
SR	Short range
$*$	Pure component, Equilibrium, Henry's law constant based on mole fraction
∞	Infinite dilution of solutes
	Abbreviations
APC	Air pollution control
AwR	Alkali absorption with regeneration
BECCS	Biomass energy with carbon capture and storage
C	Carbon
$CaCO_3$	Calcium carbonate
$Ca(OH)_2$	Calcium hydroxide
CO	Carbon mono oxide
CO_2	Carbon dioxide
CO_3^{2-}	Carbonate ion
e-NRTL	Electrolyte-Non Random Two Liquid
erf	Error function
GHGs	Greenhouse gases
H	Atomic Hydrogen
H_2O	Water

HCl	Hydrochloric acid
HCO_3^-	Bicarbonate ion
IEA	International Energy Agency
IPCC	Intergovernmental Panel on Climate Change
K^+	Potassium cation
K_2CO_3	Potassium carbonate
K_2SO_4	Potassium sulphate
KBr	Potassium bromide
KCl	Potassium chloride
$KHCO_3$	Potassium bicarbonate
KNO_3	Potassium nitrate
KOH	Potassium hydroxide
Li^+	Lithium cation
Li_2CO_3	Lithium carbonate
$LiHCO_3$	Lithium bicarbonate
$LiOH$	Lithium hydroxide
LWR	Long wave radiation
MSW	Municipal solid waste
N_2	Nitrogen gas
N_2O	Nitrous oxide gas
Na^+	Sodium cation
Na_2CO_3	Sodium carbonate
Na_2SO_4	Sodium sulphate
$NaCl$	Sodium chloride
$NaHCO_3$	Sodium bicarbonate
$NaNO_3$	Sodium nitrate
$NaOH$	Sodium hydroxide
O	Atomic Oxygen
OH^-	Hydroxyl ion
PM	Particulate matter
ppm	Part per million
R&D	Research and development
SDC	String of discs contactor
SWR	Shortwave radiation
UNIQUAC	UNIversal QUAsiChemical
UNFCCC	United Nations Framework Convention on Climate Change
VLE	Vapor Liquid Equilibria

1. Introduction and Motivation

Human activities have changed and continue to change the Earth's surface and atmospheric composition. Apprehension about global warming due to prolonged emissions of human-made greenhouse gases (GHGs) entered into force at the United Nations Framework Convention on Climate Change (UNFCCC) on 21st March 1994. As of March 2014, UNFCCC has 196 parties with the objective of stabilizing GHGs in the atmosphere at a level preventing "dangerous anthropogenic interference with the climate system." The Intergovernmental Panel on Climate Change (IPCC, 2013) shows that collective and significant global action is needed to reduce greenhouse gas emissions in order to keep global warming below 2°C. The IPCC report says that the longer we wait, the more expensive and technologically challenging meeting this goal will be (ECCA, 2014). The limit of 1°C global warming, aiming to avoid practically irreversible ice sheet and species loss tolerating maximum CO_2 ~ 450 ppm with reasonable control of other GHGs, has also been argued (Hansen et al., 2008).

The end product of current fossil fuel based electricity production technologies is CO_2, which is released to the biosphere. This anthropogenic CO_2 accumulates mainly in the atmosphere in a process which is practically irreversible in present scenario because natural carbon sequestration processes are very slow and the CO_2 binding potential of terrestrial plants has been considerably reduced as compared to previous centuries due to excessive industrialization and deforestation. Consequently, anthropogenic CO_2 emissions affect the equilibria of natural carbon cycles and the CO_2 concentration in the atmosphere (Budzianowski, 2011). The 400 ppm CO_2 level was recorded in 2013:

"In 2013, carbon dioxide concentrations for the first time in recorded history exceeded 400 parts per million (ppm) at Mauna Loa —considered a "global benchmark" monitoring site—in early May. This year (2014), CO_2 exceeded 400 ppm at Mauna Loa in mid-March, two months earlier than last year (2013). Concentrations at Mauna Loa have continued to top 400 ppm throughout much of April and are expected to stay at historic high levels through May and early June (2014." (NOAA/ESRL, 2014).

1.1. Green House Effect and Climate Change

The climate system of the Earth is driven by solar radiation as shown by Figure 1.1. Since the temperature of the Earth has been relatively constant over many centuries, the incoming solar energy must be in balance with outgoing radiation. Nearly half of the incoming solar shortwave radiation (SWR) is absorbed by the Earth's surface and about 30% of absorbed SWR is reflected back to space by gases, aerosols, clouds and by the Earth's surface (albedo) while about 20% is absorbed in the atmosphere (IPCC, 2013).

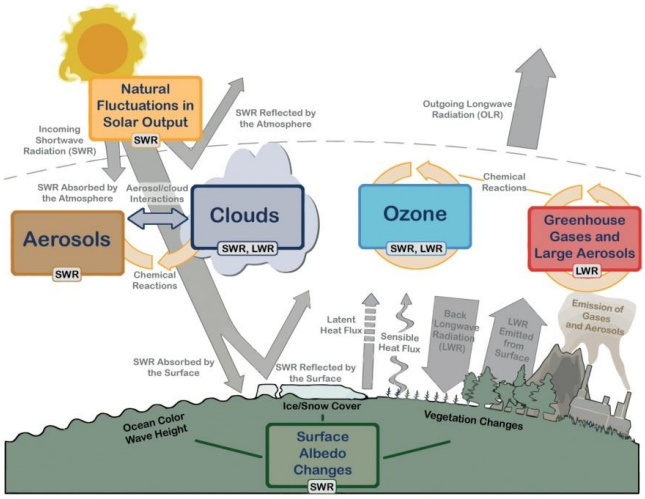

Figure 1.1: Main drivers of climate change. The radiative balance between incoming solar shortwave radiation (SWR) and outgoing longwave radiation (OLR) is influenced by global climate 'drivers'. Natural fluctuations in solar output (solar cycles) can cause changes in the energy balance (through fluctuations in the amount of incoming SWR). Human activity changes the emissions of gases and aerosols, which are involved in atmospheric chemical reactions, resulting in modified O_3 and aerosol amounts. [(Forster et al., 2007); (IPCC, 2013)].

Due to low temperature of the Earth's surface, most of the outgoing energy flux from the Earth is longwave radiation (LWR). The LWR emitted from the Earth's surface is largely absorbed by certain atmospheric constituents; clouds, water vapors, CO_2, CH_4, N_2O and other greenhouse gases (GHGs), which themselves emit LWR in all directions. The downward directed component of this LWR adds heat to the lower layers of the atmosphere and to the Earth's surface (greenhouse effect). The dominant energy loss of the infrared radiation from the Earth is from higher layers of the troposphere. The solar energy primarily falls in the tropics and the subtropics of Earth and this energy is then partially redistributed to middle and high latitudes by

atmospheric and oceanic transport processes. The radiative energy budget of the Earth is almost in balance as shown by Figure 1.1, but ocean heat content and satellite measurements indicate a small positive imbalance [(Murphy et al., 2009); (Trenberth et al., 2009); (Hansen et al., 2011)] that is consistent with the rapid changes in the atmospheric composition (IPCC, 2013).

To avoid imbalance of radiative energy and to achieve CO_2 stabilization targets below 450 ppm, demands that global net CO_2 emissions will eventually have to be reduced to near zero or may even need to become negative [(Azar et al., 2006); (Forster et al., 2007); (Knopf et al., 2009)]. Negative emissions can be attained by several techniques, including reforestation, direct air capture, and the combination of Bio Energy with Carbon Capture and Storage in power plants.

1.2. Cost Effective and Sustainable Energy Supply

Sustainable energy supply and reduction of CO_2 emissions are priorities on the global political agendas. Although the constraint for reduction in CO_2 emission is increasing, the cost of CO_2 capture remains a limiting factor for large scale application (Abu-Zahra et al., 2007). Reducing the cost of the capture step by improving the process and the solvent used must have top priority in order to apply this technology in the future. Much of the research in the area of CO_2 recovery and storage focuses on minimizing the energy required for CO_2 capture, as this step corresponds to the major cost contribution of the overall value chain (capture, transportation, injection) [(Rao and Rubin, 2002); (Rao et al., 2006); (Pires et al., 2011)].

Out of the traditional methods of CO_2 capture (absorption, adsorption, cryogenics and membrane processes), absorption is considered to be the best available technology for post-combustion applications (Abu-Zahra et al., 2013). The cost of capturing CO_2 depends on the type of power plant used, its overall efficiency and the energy requirements of the capture process.

In post-combustion absorption system, CO_2 is separated from the flue gas by passing the flue gas through a continuous scrubbing system. The system consists of an absorber and a stripper. Absorption processes utilize the reversible chemical reaction of CO_2 with an aqueous alkaline absorbent at 1-1.2 bar pressure and 40-60°C temperature. In the stripper, the absorbed CO_2 is desorbed from the absorbent and a

pure stream of CO_2 is sent for compression while the regenerated absorbent is sent back to the absorber. Heat is required in the reboiler to heat up the absorbent to the required temperature (100-120°C); to provide the heat of desorption and to produce steam (about at 2 bar) in order to provide the required driving force for CO_2 stripping from the absorbent. This leads to the main energy penalty on the power plant. In addition, energy is required to compress the CO_2 to the conditions needed for storage and to operate the pumps and blowers in the process.

1.2.1. Biomass as renewable energy resource

Apart from the electricity sector, renewable energy sources like bioenergy for the generation of heat and the use of environmental friendly bio-fuels for the transport sector will become more and more important in the future (Jäger-Waldau et al., 2011). Biomass fuels and residues can be converted to energy via thermal, biological and mechanical or physical processes. Wood, annual energy crops and residues from agricultural and forestry are some of the main bioenergy resources available. The biodegradable components of municipal solid waste (MSW) and wastes from commercial and industrial divisions are also significant bioenergy resources, although particularly in the case of MSW, they may require extensive processing before conversion (Bridgwater, 2006).

To mitigate the global warming, substitution of biomass for fossil fuels in energy consumption is irrevocable, and political action plans exist worldwide for an increased use of biomass. The use of biomass for energy can imply different economic and environmental advantages and disadvantages for the society and the energy sector. For the achievement of an increased and sustainable use of biomass for energy, synthesis and creation of new knowledge within the field is inevitable.

1.2.2. The BECCS approach

Energy portfolios from a broad range of energy technologies are required to attain desired concentrations of greenhouse gases. Scenario studies carried out by (Azar et al., 2010), to investigate the technological and economic attainability of reduced CO_2 concentrations, revealed that negative emission technologies e.g., biomass energy with carbon capture and storage (BECCS) can significantly enhance the possibility to achieve low concentration targets (at around 350 ppm CO_2). According to the

International Energy Agency (IEA), electricity generation from bioenergy should more than triple over the period (2013-2035), with China, United States and the European Union accounting for over half of the growth in New Policies Scenario, 2013-2035. Its share of total power generation doubles from 2% to 4% (IEA, 2013). The BECCS approach enhances natural biological processes that take CO_2 out of the atmosphere and sequester it in plants, soils, and marine sediments.

Biomass with capture provides an energy product i.e. electricity, hydrogen, or ethanol while simultaneously achieving capture of CO_2 from the air. This may result in nearly twice the effective CO_2 mitigation compared to conventional biomass energy systems (Keith et al., 2006). In a recent publication (Yılmaz and Selim, 2013), a detailed overview of methods for biomass to energy conversion systems design has been presented which describes the huge potential of biomass to energy conversion. According to (Möllersten et al., 2003), the biomass based energy conversion with CO_2 capture can be divided into four main process groups.

1. Gasification of biomass and pre combustion CO_2 capture
2. Oxy-combustion of biomass with water condensation and CO_2 capture
3. Biomass conversion to secondary fuels with CO_2 capture
4. Biomass combustion with CO_2 capture from the flue gases

However, a particular biomass source may be burnt in air, gasified, pyrolysed, fermented, digested, or undergo mechanical energy extraction. Theoretically the total energy obtainable or extractable from the resource is the same. Practically the actual amount of energy obtained and the form of that energy will vary from one conversion process technology to another (McKendry, 2002).

Biomass combustion with CO_2 capture from the flue gases is a technically mature process. Absorption is the most commonly used technology for capturing CO_2 from gas streams, whereby chemical or physical solvents are used to scrub the gases and collect the CO_2. Chemical absorption is a proven end of pipe method for capturing CO_2 from flue gases [(Möllersten et al., 2003); (White et al., 2003)].

1.2.3. Composition of biomass and flue gas emissions

The components of biomass comprise cellulose, hemicelluloses, lignin, lipids, proteins, sugars, starches, water, hydrocarbon, ash, and other compounds. The concentration of each class of compound differs depending on species, type of plant

tissue, phase of evolution, and growing conditions (Khan et al., 2009). The bulk composition of biomass in terms of carbon, hydrogen, and oxygen (CHO) does not differ much among different biomass sources. Common (dry basis) weight percentages for C, H, and O are 30 to 60%, 5 to 6%, and 30 to 45% respectively. C, H, O portions can be different for different fuels [(Faaij et al., 1997); (Faaij, 2004)]. Relative to coal, biomass generally has less carbon, more oxygen, more silica, chlorine and potassium, less aluminum, iron, titanium and sulfur, and sometimes more calcium.

According to the Biomass Energy Centre UK (BEC, 2014), there can be about 0.3% nitrogen, 0.1% sulphur, 0.1% chlorine, and trace quantities of various minerals such as calcium, potassium, silicon, phosphorus and sodium. Ash is the inorganic incombustible part of fuel which is left after complete combustion which contains the bulk of the mineral fraction of the original biomass.

The principal concerns about biomass emissions are due to small particulates (PM_{10} and $PM_{2.5}$; particles smaller than 10 microns and 2.5 microns respectively). Recently published review on flue gas cleaning from combustion of biomass (Singh and Shukla, 2014) throws light on different technologies addressing the problem.

Sulphur and chlorine together with nitrogen are responsible for gaseous emissions including SO_x, NO_x, and HCl and to a certain extent dioxins and furans (Khan et al., 2009). Water and CO_2 are inevitable consequences of burning any CHO containing material. Under conditions of insufficient oxygen supply or incomplete combustion, carbon monoxide (CO) and soot can also be formed.

Biofuels require comparatively longer residence times in the high temperature zone than coal (Khan et al., 2009). In a well-designed combustion system, which allows sufficient oxygen, time and turbulence within the combustion chamber for complete combustion, levels of CO within the flue gases can be kept to a minimum. NO_x formation can be avoided by using advanced burners and controlling flame temperature.

Although emissions from fossil fuel burning and from biomass combustion are widely varying both on constituent and concentration basis, all emissions except CO_2 can be either avoided/reduced or pre-treated before CO_2 capture.

1.3. CO_2 Absorption into Hydroxide and Carbonate Systems

CO_2 absorption into hydroxides and carbonates of alkali metals, especially lithium, sodium and potassium, has been studied and used for several applications since early 20^{th} century [(Hitchcock, 1937); (Welge, 1940); (Kohl and Nielsen, 1997)]. During the last two decades, due to increased environmental concerns and stringent conditions for CO_2 emissions from power plants, energy intensive regeneration of amine based CO_2 capture solvents, environmental issues arising from thermal degradation of amines (Rochelle, 2012b) and other socioeconomic factors, these systems have regained attention [(Cullinane and Rochelle, 2004);(Corti, 2004); (Knuutila et al., 2009); (Mumford et al., 2011); (Anderson et al., 2013); (Smith et al., 2013)].

Systems based on lithium hydroxide (LiOH) have been used for life support since the early days of space exploration and are employed in submarines to control CO_2 levels in case of an emergency[(Norfleet and Horn, 2003); (Matty, 2008)]. The technologies for CO_2 capture directly from ambient air [(Zeman, 2007); (Mahmoudkhani and Keith, 2009); (Goeppert et al., 2012)] involve chemical absorption by strong bases like NaOH, KOH, Na_2CO_3, K_2CO_3, $Ca(OH)_2$.

In a feasibility report commissioned by Australian National Low Emissions Coal R&D Program (Liu et al., 2012) alkali scrubbing of CO_2 and SO_2 with $NaOH/Na_2CO_3/NaHCO_3$ at atmospheric pressure was studied in semi- batch well stirred reactor. The report concluded that aqueous NaOH is an active solution to absorb both CO_2 and SO_2; the absorption of CO_2 is mainly liquid phase controlled and the absorption of SO_2 is mainly gas phase controlled. They recommended operational conditions for operation of practical scrubbers at a pH value window between 4 and 5.5 to minimize the consumption of the NaOH reagent yet still allow high rates of absorption during scrubbing. It was found that operation at pH value higher than 5.5 may lead to loss of caustic solution.

Recently, an innovative biogas upgrading method named Alkali absorption with Regeneration (AwR) that facilitates capture and storage of the separated CO_2 is investigated in pilot scale [(Baciocchi et al., 2013); (Lombardi and Carnevale, 2013)]. The process consists of CO_2 separation from biogas by chemical absorption

with an alkali aqueous solution (NaOH or KOH) followed by regeneration of the spent absorption solution from the upgrading process and the captured CO_2 is stored in a solid and thermodynamically stable form i.e. $CaCO_3$. The regeneration process is carried out by contacting the spent absorption solution, rich in carbonate and bicarbonate ions, with a waste material, Air Pollution Control (APC) residue from Waste-to-Energy plants characterized by a high content of calcium hydroxide, and leads to the precipitation of calcium carbonate.

The Shell, under-development, precipitating carbonate process (Moene et al., 2013) employs the carbonate to bicarbonate reaction for the absorption of CO_2 followed by precipitation and concentration of part of the bicarbonate before entering the regenerator. The process is claimed to be an attractive alternative to the present carbon capture technologies employed for post combustion, due to its potential for energy efficiency. Screening bench scale pilot plant experiments of the precipitating carbonate process have demonstrated sufficiently high cyclic loadings and established the operation for 90% removal of CO_2 from synthetic flue gas containing 4% CO_2 (Moene et al., 2013).

1.4. Scope of This Work

The goal of the present work is to study CO_2 absorption solvents which could be employed for energy producing technologies based on biomass. Due to the variability in composition and concentration of flue gas from biomass combustion, traditional amine based solvents may not be the best choice. Regained interest of hydroxide and carbonate systems in capture scenarios of zero or negative emissions; either in a BECCS approach or as an environment friendly absorption system, shaped the action plan of present work.

In this work the reaction between OH^- and CO_2 is studied. This reaction is important for all hydroxide and carbonate systems. The reaction is modeled based on both concentration and activity. The behavior of Henry's law constant, needed for kinetic modeling is studied experimentally for systems containing Li^+, Na^+ and K^+ as counter ions. The activities of CO_2 and OH^-, needed in the liquid phased, are calculated with a developed vapor-liquid equilibrium model able to predict both the partial pressure and physical solubility of CO_2.

1.4.1. Key contributions of thesis

This thesis is a contribution to research work carried out to study the absorption of CO_2 into hydroxide and carbonate systems in the following ways:

- Kinetics of CO_2 absorption into aqueous hydroxides (0.01–2.0 M) and blends of hydroxides and carbonates with mixed counter ions (1–3 M) containing Li^+, Na^+ and K^+ as counter ions were studied in a String of Discs Contactor (SDC). The temperature range was 25–63°C. The dependence of the reaction rate constant on temperature and concentration/ionic strength and the effect of counter ions were studied for the reaction of CO_2 with hydroxyl ions (OH^-) in these aqueous electrolyte solutions. The infinite dilution second order rate constant $k_{OH^-}^{\infty}$, valid up to 63°C, was derived as an Arrhenius temperature function and the parameters of Pohorecki and Moniuk model (Pohorecki and Moniuk, 1988) were refitted to model the ionic strength dependency of the second order rate constant, k_{OH^-}. The contribution of ions to the ionic strength and the model itself, were extended to the 3M concentration and 63°C temperature.
- The solubility of N_2O into aqueous solutions of hydroxides containing Li^+, Na^+ and K^+ counter ions and the hydroxide blends with carbonates were measured for a range of temperatures (25-80°C) and concentrations (0.08-3M). To evaluate the solubility experiments in terms of apparent Henry's law constant, the liquid densities of these systems were measured and compared to literature. By using the experimental data for N_2O solubility, the parameters in the model of Weisenberger and Schumpe (Weisenberger and Schumpe, 1996) were refitted for aforementioned systems to extend the validity range of the model up to 3M and 80°C.
- The equilibrium model (Monteiro, 2014) was employed for simultaneous regression of VLE (Vapor-Liquid Equilibria) and apparent Henry's law constant data for better prediction of activity coefficients. The presented Electrolyte-NRTL interaction parameters were obtained by simultaneous regression of P_{CO_2}, P_{total} and apparent Henry's law constant data.
- The total pressure data over aqueous LiOH solutions for a range of concentrations (0.25 – 8.5 wt.%) and temperatures (40 – 90°C) were

measured by ebulliometer and the measured data were used in fitting of the equilibrium model.

- The experimental kinetics data were re-evaluated by use of activity based kinetic expression. It was observed that the use of activities instead of concentrations eliminates the effect of both concentration and counter ion on the derived rate constant. The activity based rate constant and infinite dilution rate constants together with activities of CO_2 and hydroxyl ion were used to predict the rate of absorption of CO_2. The advantage of using activities in kinetic expressions is that fundamental description of kinetics and thermodynamics become consistent with each other.

1.4.2. Layout of thesis

This thesis consists of 9 chapters. First chapter is dedicated to the motivation behind the performance of this research work and gives a short introduction of experimental and modeling work that has been carried out. Chapter 2 gives a literature survey providing an overview of experimental work to measure required data and some models used to represent those data. Basic concepts of solution thermodynamics, equilibrium modeling and kinetics theories, used in the evaluation of experimental work, are presented in chapter 3. Chapter 4 summarizes the methods and equipment used to conduct the experimental work.

Paper I presenting measured N_2O solubility and density data with parameter optimization in the model of Weisenberger and Schumpe (Weisenberger and Schumpe, 1996) is presented in Chapter 5. Chapter 6 comprises of ***Paper II*** which present equilibrium modeling used in this work to calculate interaction parameters for calculation of activities of the species present in the hydroxide and carbonate systems containing Li^+, Na^+ and K^+ as counter ions. The kinetic data measured on string of discs contactor and rate constants based on concentration and parameter optimization in the model of Pohorecki and Moniuk (Pohorecki and Moniuk, 1988) are presented in Chapter 7. Chapter 8, containing Paper ***IV***, presents activity based kinetics of measured experimental data. Conclusions and suggestions for future work are summarized in Chapter 9.

1.4.3. Publications and conference proceedings

This thesis comprises of 4 publications which present all the experimental and modeling work carried out in this work. The publications, referred as ***Paper I***, ***Paper II***, ***Paper III*** and ***Paper IV*** in the text, are part of the thesis and comprise Chapter 6-8 respectively.

In *paper I*, the author performed part of experimental work, all calculations and parameter optimization in solubility model using MODFIT and was responsible for writing.

In *Paper II*, the author was responsible for collection of literature data, all calculations, parameter optimization using equilibrium model and writing.

In *Paper III*, the author was responsible for evaluation of experimental data, parameter optimization in kinetics model using MODFIT and writing.

In *Paper IV*, the author was responsible for activity based evaluation of kinetics data and writing.

Paper I: Gondal, S., Asif, N., Svendsen, H. F., and Knuutila, H. Density and N_2O solubility of aqueous Hydroxide and Carbonate Solutions in the temperature range from 25 to 80°C. *Accepted for publication in Chemical Engineering Science.*

Paper II: Gondal, S., Usman, M., Monteiro, J. G. M. S., Svendsen, H. F., and Knuutila, H. VLE and Apparent Henry's Law Constant Modeling of Aqueous Solutions of Unloaded and Loaded Hydroxides of Lithium, Sodium and Potassium. *To be submitted for publication.*

Paper III: Gondal, S., Asif, N., Svendsen, H. F., and Knuutila, H. Kinetics of the absorption of carbon dioxide into aqueous hydroxides of lithium, sodium and potassium and blends of hydroxides and carbonates. S*ubmitted for publication in Chemical Engineering Science.*

Paper IV: Gondal, S., Svendsen, H. F., and Knuutila, H. Activity based kinetics of CO_2-OH^- systems with Li^+, Na^+ and K^+ counter ions. *To be submitted for publication*.

Conference Proceedings:

1. Gondal, S., Asif, N., Svendsen, H. F., and Knuutila, H. Kinetics of carbonates and hydroxide systems for CO_2 capture. *2nd International Chairs Seminar on Carbon, Capture and Storage, 25-27 March, 2013 | Paris & Le Havre, France.*

2. Gondal, S., Asif, N., Svendsen, H. F., and Knuutila, H. Kinetics of the reaction of carbon dioxide with aqueous hydroxide solutions. *The 7th Trondheim CCS Conference (TCCS-7), June 4-6, 2013, Trondheim, Norway.*

3. Gondal, S., Asif, N., Monteiro, J. G. M. S., Svendsen, H. F., and Knuutila, H., Equilibrium Modeling of Carbonate and Hydroxide Systems, *2nd Post Combustion Capture Conference (PCCC2), September 17 - 20, 2013, Bergen, Norway.*

4. Gondal, S., Asif, N., Svendsen, H. F., and Knuutila, H. N_2O solubility of aqueous Hydroxide and Carbonate Solutions in the temperature range from 25 to 80°C", *UTCCS-2, January 28-30, 2014, University of Texas, Austin, USA.*

2. Literature Review

The study of carbon dioxide absorption into hydroxides and carbonates demands complete evaluation of vapor-liquid-equilibria (VLE) and kinetics of the absorption reaction. To study the VLE and kinetics of CO_2 absorption into these systems, physiochemical properties of absorbents such as density, viscosity and N_2O solubility are needed. Moreover, the determination of these properties is inevitable for the modeling and design of gas-liquid contactors of absorption equipment.

This chapter provides a brief literature overview of experimental work carried out for measurement of density, viscosity, VLE and kinetics of hydroxide and carbonate systems along with models used for prediction of experimental data. The purpose of this chapter is two-fold. Firstly, it provides literature sources for finding these properties and secondly, it gives a framework for designing experimental work to fill the gap where data required for calculations are either non-existing or show high discrepancies. As mentioned in the previous chapter, the absorption of CO_2 into hydroxides and carbonates has been studied by several researchers since the early decades of last century and the experimental measurements likewise for density, viscosity, and vapor-liquid-equilibrium are abundantly available in literature. This chapter includes most, but not all, available literature data sources for experimental measurements and some models to predict the experimental data.

2.1. Density

Density is an important property for evaluation of mass transfer, kinetics and physical solubility of CO_2 in the absorbent. Since hydroxides and carbonates of alkali metals are very common and industrially important electrolytes, density data for LiOH, NaOH, KOH, Na_2CO_3 and K_2CO_3 is available in literature from studies carried out over more than a century. Table 2.1 presents some literature data sources for densities of these hydroxides and carbonates. The table gives overall range of temperature and concentration for the experimental data found in these literature sources. It can be seen that the concentration range of experimental data found in literature is limited by the solubility of these chemicals in water. The temperature ranges mostly from 0-100°C except for NaOH where it goes up to 120°C and for LiOH where it is limited from 20°C to 75°C.

Table 2.1: Literature sources of density data for hydroxides and carbonates of Li^+, Na^+ and K^+

Hydroxides/ Carbonates	Overall Temp. Range [°C]	Overall Conc. Range [wt.%]	Reference
LiOH	20–75	2.4 – 11.33	(Hitchcock, 1937); (Roux et al., 1984b);(Herrington et al., 1986); (Sipos et al., 2000); (Taboada et al., 2005)
NaOH	0–120	0.0033– 52	(Hitchcock and McIlhenny, 1935); (Akerlof and Kegeles, 1939); (Huckel and Schaaf, 1959); (Roux et al., 1984b); (Hershey et al., 1984); (Herrington et al., 1986); (Magalhães et al., 2002); (Sipos et al., 2000); (Patterson et al., 2001); (Salavera et al., 2006); (Green, 2008)
KOH	0–100	0.084–59.46	(Hitchcock and McIlhenny, 1935); (Akerlof and Bender, 1941); (Mashovets et al., 1965); (Tham et al., 1967); (Roux et al., 1984b); (Herrington et al., 1986); (Sipos et al., 2000); (Patterson et al., 2001); (Salavera et al., 2006); (Green, 2008)
Na_2CO_3	0–100	0.042–30.8	(Hitchcock and McIlhenny, 1935); (Roberts and Mangold Jr, 1939); (Perron et al., 1975); (Correia et al., 1980); (Hershey et al., 1983); (Magalhães et al., 2002); (Graber et al., 2004); (Green, 2008); (Lide, 2008); (Knuutila et al., 2010b)
K_2CO_3	0–100	0–50	(Hitchcock and McIlhenny, 1935); (Roberts and Mangold Jr, 1939); (Correia et al., 1980); (Green, 2008); (Lide, 2008); (Knuutila et al., 2010b)

In some of the above mentioned sources, density is modeled with empirical correlations; either based on molality or weight fraction to calculate partial molar volumes. The density model based on literature density data presented in (Laliberte and Cooper, 2004) was found to be very useful, because it covers all the chemicals studied in this work and provides a common base for comparison. The model calculates partial molar volumes of solutes (hydroxides and carbonates in this work) and solvent (water) at a particular temperature based on their respective weight fractions and can be used as well for solutions containing more than one solutes. The densities of solutions at a particular temperature, with a known weight fraction can

be calculated from the calculated partial molar volumes and the density of water at that temperature.

2.2. Viscosity

Viscosity and diffusivity are required for the evaluation of kinetics parameters from mass transfer experiments; diffusivity is typically estimated form viscosity values using the Stokes-Einstein equation. Literature data sources for viscosities of aqueous solutions of hydroxides and carbonates of Li^+, Na^+ and K^+ are given in Table 2.2. The table shows overall range of temperature and concentration for the available literature data. It can be seen that the concentration range for the data available is almost the same as that for density data but temperature range is very limited. There is a need for experimental data at higher temperatures especially for LiOH and KOH where the available data is limited up to 40°C.

Table 2.2: Literature sources of viscosity data for hydroxides and carbonates of Li^+, Na^+ and K^+

Hydroxides/ Carbonates	Overall Temp. Range [°C]	Overall Conc. Range [wt.%]	Reference
LiOH	20–40	1.184–11.33	(Hitchcock, 1937); (Sipos et al., 2000); (Taboada et al., 2005)
NaOH	12.5–70	2–56	(Hitchcock and McIlhenny, 1935); (Krings, 1948); (Huckel and Schaaf, 1959); (Vázquez et al., 1996); (Sipos et al., 2000)
KOH	-14.1–40	2.8–51.86	(Hitchcock and McIlhenny, 1935); (Kelly et al., 1965); (Sipos et al., 2000)
Na_2CO_3	20–90	0.042–30.8	(Hitchcock and McIlhenny, 1935); (Correia et al., 1980)
K_2CO_3	19–89	1–58.24	(Hitchcock and McIlhenny, 1935); (Correia et al., 1980)

As mentioned for density, the empirical model based on literature viscosity data is also presented by (Laliberté, 2007). The model is very convenient as it provides a common base to calculate viscosity at a particular temperature of all solutions including blends of hydroxides and carbonates, used in this work, on the basis of their mass fractions in the solutions.

2.3. N_2O Solubility

Physical solubility of CO_2 into an absorbent, typically expressed as an apparent Henry's law constant of the absorbent is necessary in the development of kinetics and in thermodynamic models for the calculation of actual activity coefficient of CO_2.

Since CO_2 reacts in most of the absorbents, including hydroxide and carbonate systems as well, it is not possible to measure the physical solubility independently using CO_2. Hence it is suggested that the N_2O analogy can be employed to estimate the physical solubility [(Versteeg and Van Swaaij, 1988); (Xu et al., 2013)]. N_2O is used to estimate the properties of CO_2 as it has similarities in configuration, molecular volume and electronic structure and is a nonreactive gas under the normally prevailing reaction conditions.

The N_2O analogy was originally proposed by (Clarke, 1964), verified by (Laddha et al., 1981) and is being widely used by many researchers [(Haimour and Sandall, 1984); (Versteeg and Van Swaaij, 1988); (Al-Ghawas et al., 1989); (Hartono et al., 2008); (Knuutila et al., 2010b)]. Applying this analogy, the physical solubility of CO_2 in terms of an apparent Henry's law constant, H_{CO_2} can be calculated based on the solubility of CO_2 and N_2O into water and the solubility of N_2O in the system of interest by the equation:

$$H_{CO_2} = H_{N_2O}\left(\frac{H^{\circ}{}_{CO_2}}{H^{\circ}{}_{N_2O}}\right) \tag{2.1}$$

Here $H_{N_2O}[kPa.m^3.kmol^{-1}]$ represents the solubility of N_2O in the system of interest in terms of an apparent Henry's law constant, $H^{\circ}{}_{N_2O}[kPa]$ and $H^{\circ}{}_{CO_2}[kPa]$ are the Henry's law constants for N_2O and CO_2 in water respectively. The term apparent Henry's law constant is defined by:

$$H_{N_2O} = \frac{P_{N_2O}}{C^{L}_{N_2O}} \tag{2.2}$$

Table 2.3: Literature sources for N_2O solubility data

Hydroxides/ Carbonates	Temp. [°C]	Conc. /Ionic strength	Reference
K_2CO_3-KHCO3	25	0–1.5 gmol ion.L^{-1}	(Joosten and Danckwerts, 1972)
Na_2CO_3-$NaHCO_3$	25	0–15 wt.%	(Hikita et al., 1974)
Na_2CO_3	25–80	1–20 wt.%	(Knuutila et al., 2010b)
K_2CO_3	25–80	5–30 wt.%	(Knuutila et al., 2010b)

Table 2.3 gives literature data sources for N_2O solubility in carbonate-bicarbonate systems. No literature data were found for N_2O solubility in hydroxides. The N_2O solubility measured in potassium carbonate-potassium bicarbonate system at 25°C by (Joosten and Danckwerts, 1972) was used to estimate CO_2 solubility using a simple function depending only on ionic strength of the solution. The data for N_2O solubility in sodium carbonate-sodium bicarbonate system at 25°C by (Hikita et al., 1974) was used to show that N_2O solubility is not only the function of ionic strength but it also depends on the carbonate-bicarbonate ratio. Their data showed that the N_2O solubility decreases as the content of bicarbonate increases in the system. The N_2O solubility data for Na_2CO_3 and K_2CO_3 solutions for temperature range 25-80°C measured by (Knuutila et al., 2010b) was used by them to refit the parameters in the model of Weisenberger and Schumpe (Weisenberger and Schumpe, 1996).

The model of Weisenberger and Schumpe (Weisenberger and Schumpe, 1996) is widely used to predict the solubility of gases into electrolyte solutions [(Rischbieter et al., 2000); (Vas Bhat et al., 2000) (Kumar et al., 2001); (Dindore et al., 2005); (Rachinskiy et al., 2014)]. The model is very general and based on a large set of data. It describes the salting-out effect of 24 cations and 26 anions on the solubility of 22 gases but the model is reported to be valid only up to 40°C and up to electrolyte concentrations of about 2 kmol.m^{-3}. The model is based on an empirical model by Sechenov (Sechenov, 1889) who modelled the solubility of sparingly soluble gases into aqueous salt solutions with the equation

$$log\frac{C_{g_o}}{C_g}[-] = KC_s \qquad (2.3)$$

Here $C_{g_o}[kmol.m^{-3}]$ and C_g $[kmol.m^{-3}]$ are the gas solubilities in water and in salt solution, respectively, C_s $[kmol.m^{-3}]$ is the salt concentration and $K[m^3.kmol^{-1}]$ is the Sechenov constant. Schumpe (Schumpe, 1993) modified this model and in the model of Weisenberger and Schumpe (Weisenberger and Schumpe, 1996) the solubility was calculated from the equations given as follows:

$$log\frac{C_{g_o}}{C_g}[-] = \sum_{i}^{n}(h_i + h_g)C_i \tag{2.4}$$

$$h_g[m^3.kmol^{-1}] = h_{G_o} + h_T(T - 298.15K) \tag{2.5}$$

In these equations $h_i[m^3.kmol^{-1}]$ is an ion-specific parameter, $h_{G_o}[m^3.kmol^{-1}]$ is a gas specific parameter, $C_i[kmol.m^{-3}]$ is the concentration of ion and $h_T[m^3.kmol^{-1}.K^{-1}]$ is the gas specific parameter for the temperature effect.

As mentioned earlier, Knuutila (Knuutila et al., 2010b) updated h_T for N_2O and h_i for potassium and sodium in the model of Weisenberger and Schumpe (Weisenberger and Schumpe, 1996) using experimental data for carbonates of sodium and potassium from 25 to 80°C.

2.4. Vapor Liquid Equilibria

For the rational design of gas treating processes, vapor-liquid equilibrium data of CO_2 over aqueous solutions of absorbents are essential besides the mass transfer and rate of chemical kinetics. A wide collection of experimental vapor liquid equilibrium (VLE) data for aqueous hydroxides and carbonates of Li^+, Na^+ and K^+ containing CO_2 are available in literature from early 20th century till date.

The concentration and loadings found in the literature data sets were recalculated and are presented as wt.% of hydroxide and loadings are recalculated as moles of CO_2 per mole of the cation present in the solution.

Table 2.4: Literature sources for equilibrium data of hydroxides and carbonates of lithium (Li^+)

Reference	P_{H_2O} [kPa] P_{CO_2} [kPa]	*Conc. as LiOH [wt.%]	*Loading [mol CO_2/ mol Li^+]	Temp. [°C]
Vapor pressure of water over LiOH solutions P_{H_2O} [kPa]				
(Aseyev, 1999)	0.58 – 462.4	2 – 10	0	0 – 150
Partial pressure of CO_2 over CO_2-Li_2CO_3-$LiHCO_3$ equilibrium solutions, P_{CO_2} [kPa]				
(Walker et al., 1927)	0.03 – 0.04	0.013–0.96	0.51 – 0.92	25 – 37

*** The concentrations of Li_2CO_3 solutions are recalculated as LiOH solutions with 0.5 loading [mol CO_2/mol Li^+]. **The physical solubility for CO_2 was calculated from N_2O solubility data by using N_2O analogy.**

The literature sources for VLE data of hydroxides and carbonates of lithium (Li^+) are given in Table 2.4. The equilibrium data include vapor pressure of water, P_{H_2O} [kPa] over LiOH solutions and partial pressure of CO_2, P_{CO_2} [kPa] over CO_2 -Li_2CO_3-$LiHCO_3$ equilibrium solutions. The only CO_2-Li_2CO_3-$LiHCO_3$ equilibrium data found in literature are from (Walker et al., 1927).

The VLE data found in literature, as shown by Table 2.4, for LiOH are very limited and there is a need for more equilibrium data at temperatures higher than 37°C. The N_2O solubility for estimation of physical solubility of CO_2, for the hydroxide/carbonate systems containing Li^+ counter ion is also needed.

The literature sources for VLE data of hydroxides and carbonates of sodium (Na^+) are given in Table 2.5. The data include vapor pressure of water P_{H_2O} [kPa] over aqueous solutions of hydroxides and carbonates of Na^+, partial pressure of CO_2, P_{CO_2} [kPa] over CO_2-Na_2CO_3-$NaHCO_3$ equilibrium solutions, total pressure, P_{total} [kPa] for CO_2 solubility in NaOH solutions at high pressures, partial pressure of CO_2, P_{CO_2} [kPa] for CO_2 solubility in $NaHCO_3$ solutions at high pressures and N_2O solubility in terms of apparent Henry's law constant, H_{N_2O} [kPa.m^3/mol].

As shown by the table, the literature VLE data available for sodium covers a wide variety and range of concentrations, temperatures and loadings but the low CO_2 pressure data, at higher temperatures, above 37°C, is still needed. More data for N_2O solubility, especially in hydroxides, is also required.

Table 2.5: Literature sources for equilibrium data of hydroxides and carbonates of sodium (Na^+)

Reference	P_{H_2O} [kPa] P_{total} [kPa] P_{CO_2} [kPa] $H_{N_2O}^{NaOH}$ [kPa.m^3.mol^{-1}]	*Conc. as NaOH [wt.%]	*Loading [molCO$_2$/mol Na$^+$]	Temp. [°C]
Vapor pressure of water over NaOH solutions, P_{H_2O} [kPa]				
(Don and Robert, 2008)	0.013 – 16479	0 – 98.8	0	0 – 350
Total pressure over *Na_2CO_3 solutions, P_{total} [kPa]				
(Knuutila et al., 2010a)	3.48 – 101.28	7.87 – 25.86	0.5	27 – 105
(Don and Robert, 2008)	2.17 – 97.46	3.77 – 25.86	0.5	0 – 100
(Taylor, 1955)	22.64 – 84.57	0.8 – 17.44	0.5	65 – 95
Partial pressure of CO_2 over CO_2-Na_2CO_3-$NaHCO_3$ equilibrium solutions, P_{CO_2} [kPa]				
(Walker et al., 1927)	0.031 – 0.039	0.02 – 0.62	0.64 – 0.93	25 – 37
(Hertz et al., 1970)	0.17– 5.05	0.4 – 4.3	0.67 – 0.88	30
(Mai and Babb, 1955)	0.95 – 18.03	0.4 – 3.9	0.78 – 0.98	20 – 65
(Ellis, 1959)	4.3 – 108.9	0.7 – 3.7	0.8 – 0.93	119 – 197
(Knuutila et al., 2010a)	0.16 – 19.17	6.3 – 9.8	0.55 – 0.85	40 – 80
Total pressure for CO_2 solubility in NaOH solutions at high pressures, P_{total} [kPa]				
(Rumpf et al., 1998)	12.7– 10163	3.69 – 3.7	0 – 2.03	40 – 160
(Lucile et al., 2012)	320 – 5020	3.84	0.99 – 2.11	20 – 60
Partial pressure of CO_2 for CO_2 solubility in *$NaHCO_3$ solutions at high pressures, P_{CO_2} [kPa]				
(Gao et al., 1997)	5000 – 57600	0.96 – 3.46	1.14 – 8.18	50 – 130
(Wong et al., 2005)	100	0.4 – 2.1	1.05 – 1.61	5 – 25
(Han et al., 2011)	310 – 2035	0.2 – 4.2	1.04 – 10.21	40 – 60
****N_2O solubility in terms of apparent Henry's law constant, $H_{N_2O}^{*Na_2CO_3}$,[kPa.m^3.mol^{-1}]**				
(Knuutila et al., 2010b)	4.56– 75.56	0.8 – 16.5	0.5	25 – 80

***The concentrations of Na_2CO_3 solutions are recalculated as NaOH solutions with 0.5 loading [mol CO_2/mol Na^+] and those of $NaHCO_3$ solutions are recalculated as NaOH solutions with 1 loading [mol CO_2/mol Na^+]. **The physical solubility for CO_2 can be calculated from N_2O solubility data by using N_2O analogy.**

The literature sources for VLE data of hydroxides and carbonates containing potassium (K^+) are presentd in Table 2.6. The data include total pressure, P_{total} [kPa], above aqueous solutions of K_2CO_3 and CO_2, total pressure, P_{total} [kPa], over CO_2-K_2CO_3-$KHCO_3$ equilibrium solutions, Partial pressure of CO_2, P_{CO_2} [kPa], over CO_2-K_2CO_3-$KHCO_3$ equilibrium solutions, and N_2O solubility in terms of apparent Henry's law constant, H_{N_2O} [kPa.m^3.mol^{-1}].

Although the literature database for potassium is not as wide as that for sodium; the data from (Tosh et al., 1959) covers a wide range of temperature at moderate pressures. The need for low CO_2 pressure data at higher temperatures, above 37°C is still there. The N_2O solubility data for KOH is also lacking in literature.

Table 2.6: Literature sources for equilibrium data of hydroxides and carbonates of potassium (K^+)

Reference	P_{H_2O} [kPa] P_{total} [kPa] P_{CO_2} [kPa] $H_{N_2O}^{KOH}$ [kPa.m^3.mol^{-1}]	*Conc. as KOH [wt.%]	*Loading [mol CO_2 / mol K^+]	Temp. [°C]
Total pressure over CO_2-K_2CO_3-$KHCO_3$ equilibrium solutions, P_{total} [kPa]				
(Tosh et al., 1959)	23.86–979.1	17.34– 37.2	0.5 – 0.89	70– 140
(Pérez-Salado Kamps et al., 2007)	267.2–9237	4.61–16.55	0.84– 2.29	40– 120
Partial pressure of CO_2 over CO_2-K_2CO_3-$KHCO_3$ equilibrium solutions, P_{CO_2} [kPa]				
(Walker et al., 1927)	0.03–0.038	0.03– 1.74	0.62 – 0.93	25 – 37
(Tosh et al., 1959)	0.21–923.9	17.34– 37.2	0.5 – 0.89	70– 140
(Park et al., 1997)	5.42–2230	4.13– 8.39	0.79– 1.39	25 – 50
(Jo et al., 2012)	0.4–1465.4	26.93	0.54– 1.01	100– 120
****N_2O solubility in terms of apparent Henry's law constant, $H_{N_2O}^{*K_2CO_3}$,[kPa.m^3.mol^{-1}]**				
(Knuutila et al., 2010b)	5.42–39.65	4.12– 26.93	0.5	25 – 80

*** The concentrations of K_2CO_3 solutions are recalculated as KOH solutions with 0.5 loading [mol CO_2/mol K^+]. **The physical solubility for CO_2 can be calculated from N_2O solubility data by using N_2O analogy.**

2.5. Mass Transfer and Kinetics

The reactions occurring during absorption of CO_2 into aqueous solutions of hydroxides and carbonates, with significant concentrations of OH^- (pH>10) (Liu et al., 2012) where formation of carbonic acid route is disregarded, can be expressed by the following equations:

$$CO_{2_{(g)}} \leftrightarrow CO_{2_{(l)}} \tag{2.6}$$

$$CO_{2_{(l)}} + OH^- \leftrightarrow HCO_3^- \tag{2.7}$$

$$HCO_3^- + OH^- \leftrightarrow CO_3^{-2} + H_2O \tag{2.8}$$

The rate of physical dissolution of gaseous CO_2 into the liquid solution, Equation (2.6) is high and the equilibrium at the interface can be described by Henry's law (Pohorecki and Moniuk, 1988). Since the reaction given by Equation (2.8) is a proton transfer reaction, it has a very much higher rate constant than the reaction given by Equation (2.7) [(Liu et al., 2012) (Hikita et al., 1976)]. Hence, reaction given by Equation (2.7) governs the overall rate of the process. Hydration of CO_2, Equation (2.7), is second order, i.e. first order with respect to both CO_2 and OH^- ions and the rate of reaction on concentration basis can be expressed by the equation:

$$r[kmol.m^{-3}.s^{-1}] = k_{OH^-}[OH^-][CO_2] \quad (2.9)$$

Here k_{OH^-} $[m^3.kmol^{-1}.s^{-1}]$ is the second order rate constant, $[OH^-]$ and $[CO_2]$ are molar concentrations $[kmol.m^{-3}]$ of hydroxide and carbon dioxide respectively.

The available literature for experiment work carried out to study the CO_2 absorption into hydroxide and carbonate systems is presented in Table 2.7. As mentioned earlier, these systems have been studied by several researchers due to their theoretical importance and several industrial applications. Most of the studies mentioned in the table were carried out at low temperatures. In the studies conducted before 1960s, the kinetic rates were typically reported as gas side overall mass transfer coefficients and simple empirical models were employed to predict the effect of chemical reaction on absorption.

The reaction rate constant for the chemical reaction, Equation (2.7), has previously been published by several authors [(Knuutila et al., 2010c), (Kucka et al., 2002), (Pohorecki and Moniuk, 1988), (Pohorecki, 1976), (Barrett, 1966), (Nijsing et al., 1959), (Himmelblau and Babb, 1958), (Pinsent et al., 1956), (Pinsent and Roughton, 1951)].

The rate constants measured by above mentioned authors were either based on only one counter ion (Na^+ or K^+) or were limited to low temperatures. Moreover, the values of predicted rate constants show diversity and scatter as indicated by infinite dilution values, $lnk^{\infty}_{OH^-}$, presented by Table 3 and Figure 7 in *Paper III*. The scatter in the value of second order rate constant, k_{OH^-}, is more profound. Most of the authors have tried to model the kinetic constants using different methods.

Classically, the kinetic constant for electrolyte solutions is expressed as function of ionic strength (Astarita et al., 1983)

$$logk_{OH^-} = logk^{\infty}_{OH^-} + bI \quad (2.10)$$

In Equation (2.5), $k^{\infty}_{OH^-}$is the infinite dilution reaction rate constant, I is the ionic strength of solution and b is a solution dependent constant.

Table 2.7: Literature sources for the CO_2 absorption into hydroxide and carbonate systems

Hydroxides/ Carbonates	Temp. [°C]	Apparatus	Reference
NaOH	25	Batch reactor	(Ledig and Weaver, 1924)
KOH, K_2CO_3	25-90	Baffle tower, Pebble packed tower, Absorption box	(Williamson and Mathews, 1924)
NaOH, KOH	25	Glass absorption vessel	(Weber and Nilsson, 1926)
Na_2CO_3	27-84	Bubble cap column	(Whitman and Davis, 1926)
NaOH, Na_2CO_3, $NaHCO_3$		Absorption tower packed with glass rings	(Payne and Dodge, 1932)
Na_2CO_3	25-63	Wetted wall column	(Harte Jr et al., 1933)
NaOH, KOH	30	Batch reactor	(Hitchcock, 1934)
Na_2CO_3, K_2CO_3	30	Batch reactor	(Hitchcock and Cadot, 1935)
Na_2CO_3, K_2CO_3	24-61	String of discs	(Roper, 1955)
NaOH	0–40	Rapid thermal method	(Pinsent et al., 1956)
$NaHCO_3$	0–20	Radioactive tracing	(Himmelblau and Babb, 1958)
NaOH	0–25	Stopped flow	(Sirs, 1958)
NaOH, NaOH+ Na_2CO_3, Na_2CO_3+ $NaHCO_3$	25	Rotating drum	(Danckwerts and Kennedy, 1958)
Na_2CO_3, K_2CO_3	20	Wetted wall column	(Nijsing et al., 1959)
NaOH, Na_2CO_3+ $NaHCO_3$	25	Packed column	(Danckwerts et al., 1963)
NaOH+ Na_2CO_3	25	Stirred cell, Packed column	(Danckwerts and Alper, 1975)
NaOH, NaOH+ Na_2CO_3	25–30	Wetted wall column	(Hikita et al., 1976)
K_2CO_3+ $KHCO_3$+KCl+NaOCl, NaOH+ Na_2CO_3	20	Laminar jet, sieve tray absorption column, Perspex column	(Pohorecki, 1976)
LiOH+KCl, NaOH blends with Na_2CO_3 , NaCl, $NaNO_3$, Na_2SO_4, KBr and K_2CO_3, KOH blends with KCl, KNO_3, K_2SO_4, KBr, K_2CO_3 and K_2CO_3	18–41 60–100	Laminar jet Wetted wall column	(Pohorecki and Moniuk, 1988) (Pohorecki and Kucharski, 1991)
NaOH, KOH	20–50	Stirred cell	(Kucka et al., 2002)
Na_2CO_3, K_2CO_3	25–69	String of discs contactor	(Knuutila et al., 2010c)

Ideally, the infinite dilution kinetic constant for the hydration of CO_2 should be independent of cation and be an Arrhenius type temperature function expressed as:

$$k_{OH^-}^{\infty}[m^3.kmol^{-1}.s^{-1}] = Aexp\left(\frac{E_A}{RT}\right) \quad (2.11)$$

where A [$m^3.kmol^{-1}.s^{-1}$] is the pre-exponential factor, E_A [$kJ.kmol^{-1}$] is the reaction activation energy, R [8.3144 $kJ.kmol^{-1}.K^{-1}$] is the ideal gas law constant and T[K] is absolute temperature.

In the model proposed by (Pohorecki and Moniuk, 1988), they theoretically justified that it seems more logical to use a correlation containing contributions characterizing the different ions, rather than different compounds present in the solution. They proposed the model given by Equation (2.12).

$$log\frac{k_{OH^-}}{k_{OH^-}^{\infty,e}} = \sum b_{ion}I_{ion} \quad (2.12)$$

where I_{ion} [$kmol.m^{-3}$] is the ionic strength of an ion, b_{ion} [$m^3.kmol^{-1}$] is an ion specific parameter and $k_{OH^-}^{\infty,e}$ is the apparent rate constant for the reaction, Equation (2.7), in the infinitely dilute solution. Its value at any temperature (18-41°C) can be calculated by Equation (2.13) (Pohorecki and Moniuk, 1988).

$$logk_{OH^-}^{\infty,e} = 11.916 - \frac{2382}{T[K]} \;\; ; where \;\; k_{OH^-}^{\infty,e}[m^3.kmol^{-1}.s^{-1}] \quad (2.13)$$

Recently, use of activities instead of concentration or ionic strength in the kinetic expressions and thermodynamics modeling with chemical reactions has gained interest due to consistency in fundamentals of thermodynamics and kinetics. The activity based kinetics finds its applications mainly in the modeling of integrated processes like reactive absorption (as studied in this work), reactive distillation and reactive extraction where both thermodynamics and kinetics, are of essential importance and activity coefficients deviate substantially from ideal behavior (Haubrock et al., 2007).

The activity based kinetics for the CO_2 hydration reaction with Li^+, Na^+ and K^+ counter ions have been published by (Haubrock et al., 2007). Knuutila et al., (Knuutila et al., 2010c) have also evaluated their kinetic data of CO_2 absorption into aqueous solutions of Na_2CO_3 and K_2CO_3; both on concentration and activity basis.

2.6. Framing the Experimental and Modeling Work

As previously mentioned the literature review not only provided with the relevant data and modeling sources but it also played an important role in shaping the experimental and modeling work carried out in this work.

The literature review showed that though a large data bank for density and viscosity of hydroxides and carbonates is found in the literature, differences in concentration and temperature for particular measurements do not allow using these data unless a model to interpolate between temperatures and concentrations is present. Density and viscosity models based on literature data [(Laliberte and Cooper, 2004); (Laliberté, 2007)] were used respectively for comparison with density data measured in this work, as presented in ***Paper I***, and calculation of viscosities used in the kinetics evaluations, as presented in ***Paper III***.

The kinetic evaluations found in literature have discrepancies in the values of determined kinetic constants and most of the data for hydroxides were either available only at room temperature or maximum up to 41°C. The kinetic experiments performed in this work, up to 60°C, are a small contribution to available data sources for these systems. The work is presented in ***Paper III***.

As previously mentioned, N_2O solubility is inevitable for evaluation of kinetics data, hence experiments were conducted for solubility of N_2O into these systems; containing Li^+, Na^+ and K^+ counter ions for a wider range of concentration (0.01-3M) and temperature (25-80°C). The N_2O solubility data collected in this work is also presented in ***Paper I***.

The upper limits of temperature, 40°C and 41°C for respectively the solubility and kinetics models of (Weisenberger and Schumpe, 1996) and (Pohorecki and Moniuk, 1988) respectively provided a motivation for execution of experiments at higher temperatures and concentrations for subsequent refitting of parameters as presented in ***Paper I*** and ***Paper III***.

The VLE data gathered form literature provided a base for equilibrium modeling in ***Paper II***. The VLE data available for the LiOH-H_2O-Li_2CO_3-$LiHCO_3$ system are very few and non-consistent. The ebulliometric data for aqueous solutions of LiOH

was measured in this work. There were sufficient data found in the literature for CO_2 partial pressure and total pressure for hydroxides of sodium and potassium so no VLE data were measured for these systems. The measured ebulliometric data and N_2O solubility data for hydroxides, measured in this work, were used in addition to literature VLE data for equilibrium modeling presented in ***Paper II***. The motivation behind the equilibrium modeling, ***paper II***, was to obtain interaction parameters for the calculation of activities by simultaneous regression of the apparent Henry's law constant and VLE data which was not done previously by any equilibrium model available in literature. The Electrolyte NRTL parameters obtained from equilibrium modeling as presented in ***Paper II*** were used to calculate activity coefficients for both CO_2 and OH^-. The calculated activity coefficients are applied for evaluation of activity based kinetics of the CO_2-OH^- system as presented in ***Paper IV.***

3. Theoretical Background

This chapter presents a brief overview on solution thermodynamics, thermodynamic equilibrium modeling and mass transfer in chemical absorption processes and the mechanisms used to interpret the reactions between CO_2 and systems studied in this work. The remaining parts of the chapter are dedicated to the fundamental study of kinetics, both based on concentration and activities, of the reaction between reactant A (CO_2 in this work) and reactant B (hydroxyl ion in this work, which is the actual rate determining reactant in both hydroxide and carbonate systems). The mechanisms were used to interpret experimental data from a string of discs contactor apparatus. This chapter provides the basic theory for the ***Papers II-IV*** presented in Chapters 6-8.

3.1. Basic Concepts of Solution Thermodynamics

Before the discussion of phase behavior of absorption systems employed in this work, which are solutions of water, hydroxides and/or carbonates, introduction to some important thermodynamic properties is necessary.

3.1.1. Partial molar and excess properties

The pure components are characterized by molar quantities but solutions or mixtures are characterized by their partial molar correspondents, e.g. partial molar volume, $v_i[m^3.mol^{-1}]$, or partial molar Gibbs free energy, $g_i[\,\mathrm{J}.mol^{-1}]$.

Excess functions are thermodynamic properties of a solution that are in excess of an ideal (or non-ideal- dilute) solution at the same conditions of temperature, pressure and composition. For an ideal solution all excess properties are zero (Prausnitz et al., 1999). A general excess function is defined as:

$$e^E = e^{real} - e^{ideal} \tag{3.1}$$

The partial molar volume, $v_i\ [m^3.mol^{-1}]$ of a component i in a system corresponds to the partial derivative of the total volume, $V[m^3]$ with respect to the molar amount of that component, $n_i[mol]$, given as:

$$v_i[m^3.mol^{-1}] \equiv \left(\frac{\partial V}{\partial n_i}\right)_{P,T,n_{j\neq i}} \tag{3.2}$$

The density measurements of real aqueous solutions and density of pure water are used for the calculation of partial molar volumes and excess partial molar volumes.

The partial molar Gibbs free energy, which is also called the chemical potential, provides the criterion for phase equilibrium of multi-component systems:

$$\mu_i[J.mol^{-1}] \equiv \left(\frac{\partial G}{\partial n_i}\right)_{P,T,n_{j\neq i}} \tag{3.3}$$

The chemical potential is the key quantity in the discussion of both phase equilibrium and chemical equilibrium of multi-component systems. The equilibrium condition for solutions or mixtures is equality of chemical potential of component i in all the phases given as:

$$\mu_i^1 = \mu_i^2 = \cdots = \mu_i^\pi \tag{3.4}$$

3.1.2. Fugacity and fugacity coefficients

The fugacity of component i, f_i, in a mixture at constant T for any system; solid, liquid, gas, pure, mixed, ideal or non-ideal is expressed as:

$$\mu_i - \mu_i^o = RTln\frac{f_i}{f_i^o} \tag{3.5}$$

Both $\mu_i^o[J.mol^{-1}]$ and $f_i^o[Pa]$ are arbitrary but may not be chosen independently; if one is chosen, the other will be fixed. Writing analogous expressions for the liquid and vapor phase give:

$$\mu_i^V - \mu_i^{oV} = RTln\frac{f_i^V}{f_i^{oV}} \quad and \quad \mu_i^L - \mu_i^{oL} = RTln\frac{f_i^L}{f_i^{oL}} \tag{3.5a}$$

At equilibrium, the chemical potential in all phases are equal as given by Equation (3.4) thus:

$$\mu_i^{oV} + RTln\frac{f_i^V}{f_i^{oV}} = \mu_i^{oL} + RTln\frac{f_i^L}{f_i^{oL}} \tag{3.5b}$$

If the standard state for liquid and gas are the same, i.e. $\mu_i^{oV} = \mu_i^{oL}$ and $f_i^{oV} = f_i^{oL}$, this leads to additional criteria for equilibrium called *isofugacity*:

$$f^V = f^L = \cdots = f^\pi \tag{3.6}$$

This infers that the equilibrium condition in terms of chemical potential can be replaced, without loss of generality, by an equation in terms of fugacity.

For a pure ideal gas, the fugacity is equal to the pressure, and for a component i in a mixture of ideal gases, it is equal to its partial pressure, $y_i P[Pa]$. For all systems at

very low pressures, the gas behaves like an ideal gas and the fugacity is therefore equal to the partial pressure as defined by the limit:

$$\lim_{P\to 0} \frac{f_i}{y_i P} \equiv 1 \tag{3.7}$$

The fugacity coefficient, $\varphi_i[-]$, is the ratio of fugacity to real gas pressure defined as:

$$\frac{f_i}{y_i P} \equiv \varphi_i[-] \tag{3.8}$$

Fugacity coefficient is a measure of non-ideality and is used to characterize the Gibbs excess function at fixed temperature and pressure. In a mixture of ideal gases, $\varphi_i = 1$.

3.1.3. Activity and activity coefficients

The concept of activity is an alternative approach to express the chemical potential in a real solution. The activity of component i at given temperature, T[K], pressure, P[Pa], and composition, $x_i[-]$, is defined as the ratio of the fugacity of the component, f_i at these conditions, to the fugacity, f_i^o, at standard state (T^o[K], P^o[Pa] and $x_i^o[-]$). Activity of a substance gives an indication of how active a substance is relative to its standard state, it is defined as:

$$a_i[-] \equiv \frac{f_i}{f_i^o} \tag{3.9}$$

Substitution of Equation (3.9) into Equation (3.5) gives a relationship between chemical potential and activity.

$$\mu_i - \mu_i^o = RTlna_i \tag{3.10}$$

A general expression for the chemical potential in an ideal solution in terms of ideal mixing could be written as:

$$\mu_i^{ideal} - \mu_i^o = RTlnx_i \tag{3.11}$$

The activity coefficient, $\gamma_i[-]$, gives a measure of non-ideality of a solution, defined as a ratio of the activity of component i to its concentration, usually the mole fraction.

$$\gamma_i[-] \equiv \frac{a_i}{x_i} \tag{3.12}$$

In an ideal solution the activity is equal to the mole fraction and the activity coefficient is equal to unity. Substitution of Equation (3.12) into Equation (3.10) gives:

$$\mu_i - \mu_i^o = RTlnx_i + \ RTln\gamma_i \tag{3.13}$$

Subtraction of Equation (3.11) from Equation (3.13) gives

$$\mu_i - \mu_i^{ideal} = RTln\gamma_i \tag{3.14}$$

Equation (3.14) shows that the activity coefficient relates chemical potential in an ideal solution to the chemical potential in a real solution, thus representing a measure of non-ideality. There are two conventions for reference states for activity coefficient; ***Symmetric Convention***: In this convention the activity coefficient of each component

i is unity as its mole fraction approaches unity, i.e. solutes and solvents are liquids in their pure reference state. This convention leads to an ideal solution in the Raoult's law sense;

$$\gamma_i \to 1 \quad as \ \ x_i \to 1 \tag{3.15}$$

Asymmetric Convention: This convention applies when the pure component is solid or gas at the system temperature and pressure. The reference state is defined as the infinite dilute state and the activity coefficient is chosen to be unity as the mole fraction approaches zero. This convention leads to an ideal dilute solution in the sense of Henry's law. The asymmetric activity coefficient, $\gamma_i^*[-]$, is the ratio of the actual activity coefficient and the activity coefficient at infinite dilution, $\gamma_i^\infty[-]$, defined as:

$$\gamma_i^*[-] = \frac{\gamma_i}{\gamma_i^\infty} \tag{3.16}$$

$$For\ solvents\ (water\ in\ this\ work),\ \gamma_i \to 1 \quad as \ \ x_i \to 1 \tag{3.16a}$$

$$For\ ionic\ or\ molecular\ solutes, \quad \gamma_i^\infty \to 1 \quad as \ \ x_i \to 0 \tag{3.16b}$$

This convention is said to be asymmetric because solvent and solute are not normalized in the same manner.

3.1.4. Raoult's Law and Henry's law

Raoult's law is one of the important applications of chemical potential (Prausnitz et al., 1999). The chemical potential of component i in the gas phase and in the liquid phase, for an ideal solution, can be calculated from Equation (3.5) and Equation

(3.11) respectively. At equilibrium, as mentioned, the chemical potential of component i must be equal in the gas and liquid phases, i.e. $\mu_i^L = \mu_i^V$, which lead to the following equation:

$$\mu_i^{oL} + RTlnx_i = \mu_i^{oV} + RTln\frac{f_i}{f_i^o} \quad (3.17)$$

For a pure component i, $x_i = 1$ and Equation (3.17) reduces to:

$$\mu_i^{oL}[J.mol^{-1}] = \mu_i^{oV} + RTln\frac{f_i^*}{f^o} \quad (3.18)$$

Here $f_i^*[Pa]$ is the fugacity of pure component i. Subtraction of Equation (3.18) from Equation (3.17) gives:

$$f_i[Pa] = x_i\, f_i^* \quad (3.19)$$

At low pressures, the gas phase behaves ideally and fugacities are equal to the pressures, which leads to:

$$P_i[Pa] = x_i\, P_i^* \quad (3.20)$$

Thus in an ideal solution, the partial pressure of component i, $P_i[Pa]$, depends on the vapor pressure of the pure component, $P_i^*[Pa]$, and its liquid phase mole fraction, $x_i[-]$. This is the definition of Raoult's law.

For a system at equilibrium, assuming the same reference state in both phases, the fugacity of a solute in gas phase is equal to the fugacity in the liquid phase. For a dilute solution, the concentration of the solute is approximately proportional to its mole fraction and for low pressures; the fugacity in gas phase is approximately equal to the pressure of the solute absorbed into liquid. Then the Henry's law can be written as:

$$\lim_{x_1 \to 0}\left(\frac{P_i}{x_i}\right) = H_i\ [Pa] \quad (3.21)$$

3.2. Thermodynamic Equilibrium Modeling

The absorption or desorption of CO_2 into or from an absorbent involves coexistence of gaseous and liquid phases under normal operating conditions. Although equilibrium is achieved neither in the absorber nor in the stripper column, these unit operations are typically modeled by discretization of the columns into a set of equilibrium stages, and considering an approach to equilibrium or an efficiency model (Taylor et al., 2003). A phase equilibrium model, therefore, is needed for the

calculation of compositions, enthalpies, entropies and other required properties of system.

Non-equilibrium or rate-based modeling is the most recent approach to model absorption processes; however the assumption that equilibrium at the interface is achieved is still used in these models (Taylor et al., 2003). Hence an equilibrium model is inevitable even if a non-equilibrium approach is adopted. Moreover, in rate-based models, the driving forces for mass transfer are more rigorously represented by use of the component fugacities, instead of concentrations or mole fractions.

The use of species activities instead of concentrations in kinetic expressions is gaining great attention in recent years [(Sandoval et al., 2001); (Haubrock et al., 2007); (Knuutila et al., 2010c)]. Nevertheless, the available models for calculation of species activities, e.g., Wilson, NRTL, UNIQUAC, are parameterized and the required parameters are regressed against experimental equilibrium data. This procedure also demands a good equilibrium model.

Classical thermodynamics provides a framework for calculating the equilibrium distribution of species between a vapor and liquid phase in a closed system through the equality of their chemical potential among the contacting phases. The vapor liquid equilibrium model is based on phase equilibrium conditions for neutral species and chemical equilibria for all elementary chemical reactions in the system.

The CO_2 containing components in the liquid phase and aqueous hydroxide/carbonate systems, used in this work, are, apart from molecular CO_2, all electrolytes. They dissociate in the aqueous phase to form a mixture of nonvolatile (ionic) or volatile (H_2O, CO_2) species. As previously mentioned the equilibrium distribution of these species between a vapor and liquid phase are governed by the equality of their chemical potential among the contacting phases. Chemical potential or partial molar Gibbs free energy is related to the activity coefficient of the species through partial molar excess Gibbs free energy, given as:

$$\dot{g}^E[J.mol^{-1}] = RT\sum_i x_i ln\gamma_i \qquad (3.22)$$

Equation (3.22) forms the basis for calculation of activity coefficients from excess Gibbs free energy models. An activity coefficient model (or excess Gibbs energy model) is an essential component of VLE models. The most important is to develop a valid excess Gibbs energy function, taking into consideration interactions between all species (molecular or ionic) in the system. In this regard, both apparent and

rigorous thermodynamic models have been proposed by various researchers to correlate and predict the vapor-liquid equilibrium.

3.2.1. The Electrolyte-NRTL model

The Electrolyte-NRTL (Non Random Two Liquid) model, based on excess Gibbs free energy of an electrolytic solution, was first proposed by Chen and coworkers [(Chen et al., 1979); (Chen et al., 1982)] and then extended by Chen, Evans and Mock [(Chen and Evans, 1986); (Mock et al., 1986)]. Augsten (Austgen et al., 1989) has summarized previous attempts to model the VLE of electrolyte systems. The Electrolyte-NRTL model assumes that the excess Gibbs free energy in the electrolyte system is the sum of two contributions [(Chen et al., 1982); (Chen and Evans, 1986); (Austgen et al., 1989)]:

1. Short-range forces between all the species that include the local ion-molecule, ion-ion, and molecule-molecule interactions.
2. Long-range electrostatic ion-ion interactions

The Electrolyte NRTL model is based on two fundamental assumptions (Chen et al., 1982):

1. Like-ion repulsion assumption: Due to the large repulsive forces between ions of the same charge, it is assumed that the local composition of cations around cations and anions around anions is zero.

2. Local electro neutrality assumption: It is assumed that the distribution of cations and anions around a central solvent molecule is such that the net local ionic charge is zero.

Thus, the expression for the excess Gibbs free energy as calculated by the Electrolyte

NRTL model can be expressed as:

$$\dot{g}^{E}[J.mol^{-1}] = \dot{g}^{E,LR} + \dot{g}^{E,local} \quad (3.23)$$

Where $\dot{g}^{E}[J.mol^{-1}]$ is the molar excess Gibbs free energy, $\dot{g}^{E,LR}[J.mol^{-1}]$ is the molar excess Gibbs free energy contribution from long range forces, $\dot{g}^{E,local}[J.mol^{-1}]$ is the molar excess Gibbs free energy contribution from local forces.

The long range contributions are represented as a combination of the Pitzer-Debye-Hückel contribution (Pitzer, 1980) and the Born expression (Robinson and Stokes,

1970). The local interaction contributions or short range contributions are derived as per the NRTL model.

The model used in this work, as presented in [(Monteiro et al., 2013); (Monteiro, 2014)] adopts the model presented by (Austgen et al., 1989). The local or short range interactions are described as functions of non-randomness and energy parameters, which may vary with temperature. The expressions for calculating the activity coefficients as a function of these parameters can be found in (Chen and Evans, 1986). The non-randomness parameters were fixed as described by (Hessen et al., 2010). The parameters for H_2O-CO_2 system were fixed as Aspen plus Electrolyte NRTL default values. The temperature dependent energy parameters were modelled according to Equation (3.24) (Hessen et al., 2010).

$$\tau_{ij} = a_{ij} + \frac{b_{ij}}{T} \tag{3.24}$$

3.2.2.Equilibrium modeling with reactive absorption

This work deals with reactive absorption where phase equilibria go together with chemical reactions between chemically reactive species. There are two strategies typically adopted for solving the chemical phase equilibria problems; the direct minimization of the Gibbs free energy, and the solution of a system of algebraic equations representing the phase and chemical equilibria. In the later approach, phase equilibrium is formulated as the equality of fugacities (Monteiro, 2014). In addition to phase equilibrium, the chemical equilibrium needs to be solved. In this work, this is accomplished by solving the nonstoichiometric equation given as (Monteiro, 2014):

$$min\ G(\underline{n})[J] = \sum_{k=1}^{NP}\sum_{i=1}^{NC} n_i^k \left[\Delta G_{i,k}^f + RTln\left(\frac{f_i^k}{f_i^{ok}}\right)\right] \tag{3.25}$$

Here NP represents the number of phases (either liquid or vapor in this work), NC is the number of chemical species, f_i^k represents the fugacity of component i in phase k, $n_i^k[mol]$ represents the number of moles of component i present in phase k and $f_i^k[-]$ represents the fugacity coefficient of component i in phase k.

The vapor liquid equilibrium of a system at constant temperature and pressure can be described by using the condition of isofugacity as shown by Equation (3.6). Applying definitions of fugacity coefficient, $\varphi_i[-]$ from Equation (3.8),

activity, $a_i[-]$ from Equation (3.9), and activity coefficient, $\gamma_i[-]$ from Equation (3.12), relates the fugacity coefficients to activity coefficients as:

$$\varphi_i y_i P = \gamma_i x_i f_i^{oL} \tag{3.26}$$

For the hydroxides and carbonate systems the ionic components can be considered to be non-volatile and phase equilibrium will be formulated only for water and CO_2. The reference fugacity of water is typically pure water at the system temperature and pressures and activity of water approaches unity as the mole fraction of water approaches unity (Deshmukh and Mather, 1981). The reference fugacity is specified to be the saturation pressure of water at the system temperature and can be expressed as a function of temperature only as given by:

$$f_{H_2O}^{oL}\ (T) = P_{H_2O}^{sat}\ (T)\varphi_{H_2O}^{sat}\ (T) \tag{3.27}$$

Introducing Equation (3.27) in Equation (3.26) defines the vapor liquid equilibrium as a function of system temperature, T[K], pressure, P[Pa], liquid and vapor phase mole fractions (x, y, x_{H_2O}, y_{H_2O}) given as:

$$\varphi_{H_2O}(T,P,y) y_{H_2O} P = \gamma_{H_2O}(T,P,x) x_{H_2O} P_{H_2O}^{sat}\ (T)\varphi_{H_2O}^{sat}\ (T) \tag{3.28}$$

For the gaseous solute CO_2 the reference state fugacity is infinite dilution and the vapor liquid equilibrium can be expressed as:

$$\varphi_{CO_2}(T,P,y) y_{CO_2} P\ =\ \gamma_{CO_2}^{\infty}(T,P,x) x_{CO_2} H_{CO_2}^{\infty}\ (T) \tag{3.29}$$

Here $H_{CO_2}^{\infty}\ [Pa]$ is the Henry's law constant of the solute at infinite dilution in water and $\gamma_{CO_2}^{\infty}[-]$ is the activity coefficient with infinite dilution as the reference state. In the Equations (3.28) and Equation (3.29), $\gamma_{H_2O}[-]$ follows the *symmetric* convention as given by Equation (3.16a), while $\gamma_{CO_2}^{\infty}[-]$ follows the *asymmetric* convention as given by Equation (3.16b).

A correction term called the Poynting factor is used to relate fugacities at different pressures and is given as:

$$\Theta[-] = \frac{f_2(T,P_2)}{f_1(T,P_1)} = exp\left(\int_{P_1}^{P_2} \frac{v_i dP}{RT}\right) \tag{3.30}$$

After introduction of Poynting factor, the phase equilibrium expressions become;

For water:

$$\varphi_{H_2O}(T,P,y) y_{H_2O} P = \gamma_{H_2O}(T,P,x) x_{H_2O} P_{H_2O}^{sat}\ (T)\varphi_{H_2O}^{sat}\ (T) exp\left[\frac{v_{H_2O}\left(P - P_{H_2O}^{sat}\right)}{RT}\right] \tag{3.31}$$

For CO_2:

$$\varphi_{CO_2}(T,P,y)y_{CO_2}P = \gamma_{CO_2}(T,P,x)x_{CO_2}H^{\infty *}_{CO_2}(T)exp\left[\frac{v^{\infty}_{CO_2}\left(P - P^{sat}_{H_2O}\right)}{RT}\right] \quad (3.32)$$

In Equation (3.31) and Equation (3.32) $v_{H_2O}[m^3.mol^{-1}]$ and $v^{\infty}_{CO_2}[m^3.mol^{-1}]$ are the partial molar volumes respectively of water and CO_2 at infinite dilution in water and $H^{\infty *}_{CO_2}[Pa]$ is infinite dilution Henry's law constant based on mole fraction.

3.3. Basics of Mass Transfer and Kinetics

In the chemical absorption process, reaction kinetics of the absorbent is critical in determining the absorber performance and to enable optimal design. Absorption of gases into liquids takes place by diffusion and convective mechanisms. Diffusion is caused by the random molecular transport of dissolved gas in the presence of a concentration gradient. Diffusion can be the only transport mechanism in a stagnant liquid. This mechanism alone is not realistic for an industrial absorption process. Convective transport combined with diffusion is typical for an absorption process since the liquid is always, to some extent, agitated and the mass transfer itself may result in a net convective flow. Convective mass transfer involves bulk fluid motion where mass transport occurs between a boundary surface and a moving fluid, or between immiscible fluids as a result of driving forces created by concentration difference between a boundary and the bulk phase (Kays et al., 2005). Gas absorption into an agitated liquid is influenced by two sets of factors: physicochemical factors such as solubility and diffusivity of gas in liquid, reagent concentration, reaction velocity constant, reaction-equilibrium constant and hydrodynamic factors such as geometry and scale of the equipment; viscosity, density, liquid flow rate (Danckwerts and Kennedy, 1954).

Mass transfer of a gas solute, A, into liquid can occur with or without a chemical reaction. When mass transfer into the liquid phase occurs without chemical reaction (physical absorption) the mass transfer rate in terms of flux, $N^o_A[mol.m^{-2}.s^{-1}]$ in the liquid phase is given by:

$$N^o_A[mol.m^{-2}.s^{-1}] = k^o_L(C_{A,i} - C_{A,b}) \quad (3.33)$$

Here $k^o_L[m.s^{-1}]$ is the liquid mass transfer coefficient without chemical reaction, $C_{A,i}[mol.m^3]$ and $C_{A,b}[mol.m^3]$ are the concentrations at the interface and bulk

liquid respectively. If the absorption is accompanied by chemical reaction; the actual mass transfer rate in terms of flux, $N_A[mol.m^{-2}.s^{-1}]$, may be larger than values for physical absorption and can be expressed as:

$$N_A[mol.m^{-2}.s^{-1}] = k_L(C_{A,i} - C_{A,b}) \quad (3.34)$$

Where $k_L[m.s^{-1}]$ is the liquid side mass transfer coefficient with chemical reaction. The ratio between the actual liquid phase mass transfer coefficient, observed under the same driving force, with and without chemical reaction is known as the enhancement factor, $E_A[-]$ (Astarita et al., 1983).

$$E_A[-] = \frac{k_L}{k_L^o} \quad (3.35)$$

In a reactive absorption system information on the enhancement factor is required if an enhancement factor based mass transfer model is utilized. A large number of enhancement factor expressions based on different mass transfer models are found in literature; ranging from the simpler two film model (Lewis and Whitman, 1924) to the more complex penetration model (Higbie, 1935a) and surface renewal model (Danckwerts, 1970a). The enhancement factor expression used depends on whether a reversible or irreversible reaction is assumed. Summaries of enhancement factor expressions for various reactions can be found in (Van Swaaij and Versteeg, 1992). The E_A expression can be simplified when a pseudo first order irreversible reaction approach can be assumed, (see Paper III).

3.3.1.Chemical absorption models

The two-film theory model (Lewis and Whitman, 1924) is the simplest model to describe the mass transfer that occurs when a gas phase is in contact with a liquid phase. It assumes the existence of a stagnant film of thickness, $\delta[m]$, near the gas-liquid interface through which mass transfer can only take place by molecular diffusion while the rest of the liquid phase is perfectly well mixed. Thus the concentration at a depth, $\delta[m]$, from the interface is equal to the bulk-liquid concentration for all species. Mass transport was assumed to take place by steady state molecular diffusion through the film while mass transfer by convection within this layer was assumed to be insignificant. Beyond the thin layers mixing is sufficient to eliminate concentration gradients (as shown in Figure 3.1).

The mass transfer from gas phase to liquid phase with a first order reaction is determined at steady state from the mass balance of the solute gas, given as:

$$D_A \frac{\partial^2 C_A}{\partial x^2} = 0 \text{ for } 0 \leq x \leq \delta \tag{3.36}$$

with boundary conditions:

$$x = 0,\ C_A = C_{A,i} \quad and \quad x = \delta,\ C_A = C_{A,b} \tag{3.37}$$

The solution will give the flux of solute through the gas-liquid interface as given by Equation 3.34, where the mass transfer coefficient is given as:

$$k_L[m.s^{-1}] = \frac{D_A}{\delta}[m.s^{-1}] \tag{3.38}$$

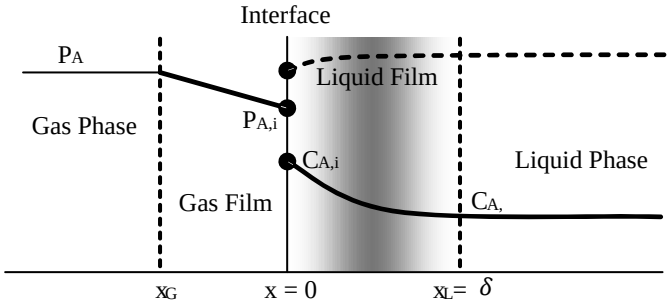

Figure 3.1. The two-film theory for mass transfer between a gas and a liquid

For a pseudo first order irreversible reaction, Hatta (Hatta, 1932) presented the analytical solution for the mass transfer for the film model. Starting from the mass balance for the solute:

$$D_A \frac{\partial^2 C_A}{\partial x^2} = k_1 C_A \text{ for } 0 \leq x \leq \delta \tag{3.39}$$

With boundary conditions as given below:

$$x = 0, \quad C_A = C_{A,i} \quad and \quad x = \delta,\ D_A \left[\frac{\partial C_A}{\partial x}\right]_\delta = 0 \tag{3.40}$$

The solution resulted in an enhancement factor given as:

$$E_{A,film}[-] = \frac{Ha}{\tanh(Ha)} \tag{3.41}$$

$$where\ Ha[-] = \frac{\sqrt{k_1 D_A}}{k_L^o} \tag{3.42}$$

Here $Ha[-]$ is the Hatta number and $k_1[s^{-1}]$ is the first order rate constant. The Hatta number compares the maximum rate of reaction in a liquid film to the rate of diffusion through the film.

The penetration model (Higbie, 1935a) for mass transfer assumes that the gas-liquid interface is made up of a variety of small liquid elements, which are continuously brought to the surface from the bulk of the liquid by the motion of the liquid phase itself. Each liquid element is considered to be stagnant, and the concentration of the dissolved gas in the element is considered to be equal to the bulk-liquid concentration when the element reaches the surface. The residence time at the phase interface is the same for all elements. Mass transfer takes place by unsteady molecular diffusion in the various elements of the liquid surface. The mass transfer from gas phase to liquid phase is determined as an unsteady state condition from the mass balance of the solute as:

$$D_A \frac{\partial^2 C_A}{\partial x^2} = \frac{\partial C_A}{\partial t} \tag{3.43}$$

With following initial and boundary conditions in space and time:

$$C_A(x,0) = C_{A,b};\ C_A(0,t) = C_{A,i};\ C_A(\infty,t) = C_{A,b} \tag{3.44}$$

The solution will lead to an average rate of mass transfer over the time interval 0 to $t^*[s]$ given by Equation 3.34, where the mass transfer coefficient is given as:

$$k_L[m.s^{-1}] = 2\sqrt{{}^{D_A}/_{\pi t^*}} \tag{3.45}$$

For a pseudo first-order irreversible reaction, the enhancement factor can be expressed as [(Danckwerts, 1970a); (Van Swaaij and Versteeg, 1992)]:

$$E_{A,pen}[-] = Ha\left[\left\{1 + \frac{\pi}{8Ha^2} erf\left(\sqrt{\frac{4Ha^2}{\pi}}\right) + \frac{1}{2Ha} exp\left(\frac{4Ha^2}{\pi}\right)\right\}\right] \tag{3.46}$$

The surface renewal, a more complex model was first introduced by (Danckwerts, 1951). The model is an extension of the penetration theory where it was assumed that the liquid elements stay the same time at the phase interface. In the surface renewal model the liquid elements do not stay the same time at the phase interface. The distribution of surface element contact times is described by a distribution function:

$$\Psi(t) = \frac{1}{t^*} \; for \; t < t^* \; and \; \Psi(t) = 0 \; for \; t > t^* \tag{3.47}$$

where $\Psi(t) = se^{-st}$ and $s[s^{-1}]$ is the is the fraction of the area of surface which is replaced with fresh liquid per unit time.

The rate of absorption at the surface is taken as the average of the rates of absorption in each element and can be expressed as:

$$N_A = \int_0^\infty N_{A,inst}\,(t)\Psi(t)dt = \sqrt{\frac{D_A}{\pi}}\left(C_{A,i} - C_{A,b}\right)\int_0^\infty \frac{se^{-st}}{\sqrt{t}}dt = k_L(C_{A,i} - C_{A,b}) \tag{3.48}$$

The mass transfer coefficient resulting from this model is then $k_L = \sqrt{D_A s}$

In both the penetration and surface renewal models, the unknown thickness of the film has disappeared and been replaced by an unknown contact time $t^*[s]$ or an unknown retention time distribution parameter $s[s^{-1}]$.

For a pseudo first-order irreversible reaction, the mass balance for the solute for the diffusion, reaction and accumulation can be written as:

$$D_A\frac{\partial^2 C_A}{\partial x^2} - k_1 C_A = \frac{\partial C_A}{\partial t} \tag{3.49}$$

With following boundary conditions:

$$C_A(x,0) = 0;\; C_A(0,t) = C_{A,i};\; C_A(\infty,t) = 0 \tag{3.50}$$

Here $k_1[s^{-1}]$ is the first order rate constant. Implementing the Laplace transform with the boundary conditions, and using inverse transformation, the solution of Equation (3.48) can be written as the distribution of concentration $C_A(x,t)$ as:

$$\frac{C_A}{C_{A,i}}[-] = \frac{1}{2}\,exp\left[-x\sqrt{\frac{k_1}{D_A}}\right]erf\left[\frac{x^2}{2D_A t} - \sqrt{k_1 t}\right] + \frac{1}{2}\,exp\left[x\sqrt{\frac{k_1}{D_A}}\right]erf\left[\frac{x^2}{2D_A t} + \sqrt{k_1 t}\right] \tag{3.51}$$

Equation (3.50) can be simplified for large value of $\sqrt{k_1 t}$ to:

$$\frac{C_A}{C_{A,i}}[-] = \; exp\left[-x\sqrt{\frac{k_1}{D_A}}\right] \tag{3.52}$$

The rate of absorption in an element having a surface 'age' $t[s]$ can be calculated as:

$$N_A(t)[mol.m^{-2}.s^{-1}] = \sqrt{k_1 D_A}\;\; C_{A,i}\left[erf\left(\sqrt{k_1 t} + \frac{e^{-k_1 t}}{\sqrt{\pi k_1 t}}\right)\right] \tag{3.53}$$

The average absorption rate at the surface can be determined using Danckwert's 'age' function as:

$$N_A(t) = \sqrt{D_A(k_1 + s)}\ C_{A,i} = \sqrt{D_A\left(k_1 + \frac{k_L^2}{D_A}\right)}\ C_{A,i} = k_L C_{A,i}\sqrt{1 + \frac{k_1 D_A}{k_L^2}} \qquad (3.54)$$

Hence the enhancement factor for this model can be expressed as:

$$E_{A,surf}[-] = \sqrt{1 + \frac{k_1 D_A}{k_L^{o\,2}}} = \sqrt{1 + Ha^2} \qquad (3.55)$$

For the **pseudo-first-order irreversible reaction**, the enhancement factors derived from the three different models for mass transfer are very similar. The largest deviation among the model is found to be 7.6 % for $Ha = 1$ (Van Swaaij and Versteeg, 1992). Hence it can be concluded that for a **pseudo-first-order irreversible reaction:**

$$If\ Ha \gg 1;\ \ then\ \ E_{A,film} \cong Ha, E_{A,pen} \cong Ha, E_{A,surf}\ \cong Ha \qquad (3.56)$$

The regime of the reaction can be determined from the absolute value of $Ha[-]$ and the ratio between $Ha[-]$ and $E_{A,\infty}[-]$ (the infinite enhancement factor) given as:

Slow reaction regime ($Ha < 0.3$), no enhancement caused by the chemical reaction. The absorption flux depends on the physical mass transfer coefficient and since the mass transfer coefficient is strongly liquid flow rate dependent, the absorption flux will also depend on the liquid flow rate.

Fast reaction/ pseudo-first order regime ($3 < Ha \ll E_{A,\infty}$), gives weak to strong enhancement of the mass transfer rate due to the reaction. In this regime the absorption flux is independent of the physical mass transfer coefficient and, hence independent of liquid flow rate.

Instantaneous reaction regime ($3 < E_{A,\infty} \ll Ha$), the reaction is said to be instantaneous with respect to the mass transfer and the absorption flux is limited by diffusion of the reactants.

A transition regime ($0.3 < Ha < 3$) also exists. This region falls between slow reaction regime and fast reaction regime.

Expressions for the infinite enhancement factor for the different mass transfer models can also be found in (Van Swaaij and Versteeg, 1992).

(Astarita et al., 1983) uses a term called the '*ratio of the diffusion time,* $t_D[s]$, *over the reaction time,* $t_R[s]$,' , denoted by, $\Phi[-] = \frac{t_D}{t_R}$, to classify the reaction regimes based on the film model. The diffusion time, $t_D[s]$, is the time needed for molecular diffusion to make the concentration uniform, and the reaction time, $t_R[s]$, is the time required for the chemical reaction to proceed to such an extent that the concentration of the limiting reactant is changed significantly. Three different regimes can be represented as

Slow reaction ($\Phi[-] \ll 1$, $E_A = 1$), the reaction is too slow to have any significant influence on the diffusion phenomena and no enhancement will take place, $t_R = 10^{-2}s$.

Fast reaction ($\Phi[-] \gg 1$, $E_A = \sqrt{\Phi}$), the reaction is fast enough to result in a significant change in limiting reactant concentration and rate enhancement results. Liquid at the interface is not in chemical equilibrium with the gas phase. Reaction proceeds at finite rate and equilibrium is not established instantaneously, $10^{-2}s > t_R > 10^{-6}s$.

Instantaneous reaction($\Phi[-] \to \infty, _A = E_{A,\infty}$), the reaction is infinitely fast and chemical equilibrium is established instantaneously, $t_R < 10^{-6}\, s$. All resistance to mass transfer has been eliminated due to chemical kinetics.

3.3.2.Gas-side resistance and overall mass transfer coefficient

In a gas mixture of soluble and insoluble gases, the soluble gas must diffuse through the insoluble gas to reach the interface. Thus the partial pressure of the soluble gas at the interface is generally less than that in the bulk gas. The *'gas film resistance'* is then the stagnant film of gas of finite thickness across which the soluble gas is transferred by molecular diffusion alone, while the bulk of the gas has a uniform composition (Danckwerts, 1970a). The two-film model as shown by Figure 3.1, could be used to describe the phenomena on both the liquid and gas sides of the interface. The soluble gas is being transported across both films by a steady-state process. This can be expressed as:

$$N_A[mol.m^{-2}.s^{-1}] = k_g\left(P_A - P_{A,i}\right) = E_A k_L^o (C_{A,i} - C_{A,b}) \qquad (3.57)$$

Introducing an apparent Henry's law constant, $H_A^{app}[Pa.m^3.mol^{-1}]$, at interface, $P_{A,i} = H_A^{app} C_{A,i}$, to eliminate interfacial concentrations and use of Equation (3.35) gives:

$$N_A[mol.m^{-2}.s^{-1}] = \frac{P_A - H_A^{app} C_{A,b}}{\frac{1}{k_g} + \frac{H_A^{app}}{k_L}} = \frac{\frac{P_A}{H_A^{app}} - C_{A,b}}{\frac{1}{k_L} + \frac{1}{H_A^{app} k_g}} \quad (3.58)$$

Or

$$N_A[mol.m^{-2}.s^{-1}] = K_{ov_G}\left(P_A - H_A^{app} C_{A,b}\right) = K_{ov_L}\left(\frac{P_A}{H_A^{app}} - C_{A,b}\right) \quad (3.59)$$

Where

$$\frac{1}{K_{ov_G}} = \frac{1}{k_g} + \frac{H_A^{app}}{k_L} \quad and \quad \frac{1}{K_{ov_L}} = \frac{1}{k_L} + \frac{1}{H_A^{app} k_g} \quad (3.60)$$

Thus Equation (3.60) gives the overall mass transfer coefficients, $K_{ov_G}[mol.m^{-2}.Pa^{-1}.s^{-1}]$ and $K_{ov_L}[m.s^{-1}]$, as reciprocals of the sum of resistances in the two films. In reality the values of $k_g[mol.m^{-2}.Pa^{-1}.s^{-1}]$ and $k_L[m.s^{-1}]$ are likely to vary from point to point, the average overall resistance will then be the average of the local values obtained by summing the local resistances and not the sum of the average overall resistances. Mannford-Doble (Mannford-Doble, 1966) concluded through careful experiments that average overall resistances and the sum of the two averaged resistances are not significantly different for practical purposes.

Equation (3.58) and Equation (3.59) show that there are two possible limiting behaviors in the system considered namely:

Gas-Phase Control

$$\text{If } \frac{k_L}{H_A^{app} k_G}[-] \gg 1 \quad then \; N_A = K_{ov_G}\left(P_A - H_A^{app} C_{A,b}\right) \quad (3.61)$$

This implies that the value of liquid film mass transfer coefficient, $k_L[m.s^{-1}]$, is much higher than that of gas film mass transfer coefficient, $k_g[mol.m^{-2}.Pa^{-1}.s^{-1}]$ and the mass transfer in the liquid phase is much easier than in gas phase, hence only a negligible fraction of the driving force, $\left(\frac{P_A}{H_A^{app}} - C_{A,b}\right)$, is utilized in the liquid phase. Thus $C_{A,i}[mol.m^{-3}]$ is almost equal to $C_{A,b}[mol.m^{-3}]$.

Liquid-Phase Control

$$\text{If } \frac{k_L}{H_A^{app} k_G}[-] \ll 1 \quad then \; N_A = K_{ov_L}\left(\frac{P_A}{H_A^{app}} - C_{A,b}\right) \tag{3.62}$$

In this case mass transfer is easier in the gas phase than in the liquid phase. Thus the overall driving force is almost entirely utilized in the liquid phase so that $P_{A,i}$ is almost equal to P_A . As seen from Equation (3.62), liquid phase control is more likely to occur for systems with high value of apparent Henry's constant (low solubility of gas in liquid).

3.3.3. Concentration and activity based kinetics

For an irreversible second order reaction in liquid phase as follows:

$$A(l) + B(l) \rightarrow P(l) \tag{3.63}$$

The reaction rate is given by:

$$r_A[mol.m^{-3}.s^{-1}] = k_2 C_A C_B \tag{3.64}$$

$$If \; C_B \gg C_A \qquad then \quad r_A = k_1 C_A \tag{3.65}$$

Here $C_A[mol.m^{-3}]$ and $C_B[mol.m^{-3}]$ are the molar concentrations of the components A and B respectively.

The expression given by Equation (3.65) is the same as that for a first order reaction. This simplification for fast second order reactions, as previously mentioned, is called the pseudo-first order approximation. By use of this approximation, a second-order chemical reaction can be treated as if it were a first-order reaction and the enhancement factor expressions, approaching the value of the Hatta number, as derived from different mass transfer models in section 3.3.1., can be used. The reaction condition requirements for the application of the pseudo-first order approximation as given in section 3.3.1. can be found in (Danckwerts, 1970a) and ***Paper III*** as presented in Chapter 7.

For reaction, as given by Equation (3.63), the pseudo first order reaction rate constant, $k_1[s^{-1}]$, can be calculated by use of Equation (3.35), Equation (3.42) and Equation (3.60) for $K_{ov_G}[mol.m^{-2}.Pa^{-1}.s^{-1}]$ to eliminate $k_L[m.s^{-1}]$.

$$k_1[s^{-1}] = \frac{H_A^{app\,2}}{\left(\frac{1}{K_{ov_G}} - \frac{1}{k_g}\right)^2 D_A} \tag{3.66}$$

The second order rate constant, $k_2[m^3.mol^{-1}.s^{-1}]$, can now be calculated by:

$$k_2[m^3.mol^{-1}.s^{-1}] = \frac{k_1}{C_B} \tag{3.67}$$

The concentration based kinetic constant will be a function of the composition of the system at a given temperature and is not a real constant because it will depend on the concentrations of ions in the solution as well as the type of ions, see [(Pinsent et al., 1956); (Pohorecki and Moniuk, 1988); (Kucka et al., 2002); (Knuutila et al., 2010c)] and ***Paper III*** as presented in Chapter 7.

A kinetic expression based on activities can be expressed as:

$$r[mol.m^{-3}.s^{-1}] = k_2^{\gamma} C_A C_B \gamma_A \gamma_B \tag{3.68}$$

The activity based kinetic constant, k_2^{γ}, as presented in Equation (3.68) should be independent of the concentration and type of ions present in the reaction solution and behave like an Arrhenius type function which is only temperature dependent. The activity based kinetic constants are expected to be real constants at a particular temperature, because activities of the reactants should take care of the changes in reaction rate with nature and composition of reactants, see [(Haubrock et al., 2007); (Knuutila et al., 2010c)] and ***Paper IV*** as presented in Chapter 8.

In activity based VLE models like the Pitzer (Pitzer, 1980), Electrolyte NRTL (Chen and Evans, 1986) the distribution of CO_2 between the vapor and liquid phase is normally modeled based on the Henry's law constant at infinite dilution in water with Equation (3.32). In the calculation of kinetic constants, the concentration of species A is typically calculated based on measurements through an apparent Henry's law constant. Introduction of apparent molar based Henry's law constant based on mole fraction, $H_A^{app*}[Pa] = P_{A,i}/x_{A,i}$ in Equation (3.32), with Poynting factor set equal to 1, gives:

$$H_A^{app*}[Pa] = \gamma_A H_A^{\infty *} \tag{3.69}$$

The mass transfer equation or flux based on activities can be rewritten as (Knuutila et al., 2010c):

$$\mathrm{N_A}[mol.m^{-2}.s^{-1}] = E^{\gamma} k_L^o \left(a_{A,i} - a_{A,b}\right) \tag{3.70}$$

Combining Equation (3.57) (for A=CO_2) and Equation (3.70) with the apparent Henry's law, the overall gas side mass transfer coefficient, K_{ov_G}, can be expressed as:

$$K_{ov_G}[mol.m^{-2}.Pa^{-1}.s^{-1}] = \frac{1}{\frac{1}{k_g} + \frac{\frac{H_A^{\infty *}}{\rho_{tot}}}{E^{\gamma} k_L^o}} = \frac{1}{\frac{1}{k_g} + \frac{H_A^{\infty}}{E^{\gamma} k_L^o}} \tag{3.71}$$

Here $H_A^{\infty *}[Pa]$ and $H_A^{\infty}[Pa.m^3.mol^{-1}]$ are the mole fraction ($x_A[-]$) based and molar concentration ($C_A[mol.m^{-3}]$) based values of the infinite dilution Henry's law constant respectively, $\rho_{tot}[mol.m^{-3}]$ is the total molar density of the solution (solvent plus all solutes). At infinite dilution of all solutes in an aqueous solution; CO_2, hydroxides and carbonates in this work, $\rho_{tot}[mol.m^{-3}] \cong \rho_{water}[mol.m^{-3}]$. Hence $H_A^{\infty *}[Pa]$ can be converted to $H_A^{\infty}[Pa.m^3.mol^{-1}]$ by division with molar density of the total solution, which is equal to the molar density of water in case of infinite dilution of aqueous solutions.

The enhancement factor for the pseudo-first order reaction should also be calculated from the activity based kinetic constant. The film theory for irreversible first order reaction gives the rate constant as:

$$r[mol.m^{-3}.s^{-1}] = k_1^{\gamma} \gamma_A C_A \tag{3.72}$$

If the activity of component A, CO_2 in this case, is considered to be constant in the film, for high values of Hatta number, it can be shown that (Knuutila et al., 2010c):

$$Ha^{\gamma}[-] = \frac{\sqrt{k_1^{\gamma} \gamma_A D_A}}{k_L^o} = E^{\gamma} \tag{3.73}$$

Combining Equation (3.71) and Equation (3.73) gives the activity based first order rate constant as:

$$k_1^{\gamma}[s^{-1}] = \frac{H_A^{\infty 2} \gamma_A}{\left(\frac{1}{K_{ov_G}} - \frac{1}{k_g}\right)^2 D_A} \tag{3.74}$$

The second order kinetic based rate constant can be calculated as:

$$k_2^{\gamma}[m^3.mol^{-1}.s^{-1}] = \frac{k_1^{\gamma}}{C_B \gamma_B} \quad (3.75)$$

When the concentration of all solutes approaches zero or at infinite dilution of both components A and B, where the activity coefficients; $\gamma_A[-]$ and $\gamma_B[-]$, are unity, Equation (3.68) reduces to(Knuutila et al., 2010c):

$$r[mol.m^{-3}.s^{-1} = k_2^{\gamma} C_A C_B \quad (3.76)$$

The concentration based rate equation at infinite dilution can be written as:

$$r[mol.m^{-3}.s^{-1}] = k_2^{\infty} C_A C_B \quad (3.77)$$

A comparison of Equation (3.76) and Equation (3.77) gives:

$$k_2^{\infty}[m^3.mol^{-1}.s^{-1}] = k_2^{\gamma}[m^3.mol^{-1}.s^{-1}] \quad (3.78)$$

Thus the infinite dilution values of the second order rate constants based on concentration and based on kinetics must be equal (Knuutila et al., 2010c). This means that with the infinite dilution kinetic constant and an equilibrium model to precisely predict the activities of hydroxyl ion and CO_2, the kinetics of any concentration can be predicted.

4. Experimental Work

This chapter provides a short review of the materials, experimental methodology and equipment used for execution of research work described in this thesis. The density, N_2O solubility, ebulliometric measurements of water vapor pressure over LiOH solutions and mass transfer experiments performed on string of discs contactor (SDC) are summarized in this chapter. All the aforementioned experimental measurements were required for equilibrium modeling and kinetics evaluation, both on concentration and activity basis, of hydroxide and carbonate systems presented in this work.

4.1. Materials and Solutions Preparation

The purity and suppliers of all chemicals used for the experimental work are given in Table 4.1. The purity of KOH as provided by the chemical batch analysis report from MERCK was relatively low. Thus it was determined analytically by titration against 0.1N HCl and was found to be 88 wt.%; the rest being water. All other chemicals were used as provided by the manufacturer without further purification or correction.

Table 4.1: Purity and suppliers of chemicals used for experimental work

Name of Chemical	Purity	Supplier
LiOH	Powder, reagent grade, > 98%	SIGMA-ALDRICH
NaOH	> 99 wt.%, Na_2CO_3 < 0.9% as impurity	VWR
KOH	*88 wt.%	MERCK
Na_2CO_3	> 99.9 wt.%	VWR
K_2CO_3	> 99 wt.%	SIGMA-ALDRICH
N_2O gas	≥ 99.999 mol%	YARA-PRAXAIR
CO_2 gas	≥ 99.999 mol%	YARA-PRAXAIR
N_2 gas	≥ 99.6 mol%	YARA-PRAXAIR

*** The purity is based on the titration results against 0.1M HCl. Since the purity was relatively low, all experimental data of KOH are presented after correction for purity.**

All the solutions of hydroxides and blends (hydroxides + carbonates) used for HCl titration (KOH for purity), density measurements, N_2O solubility, ebulliometric measurements and absorption experiments were prepared at room temperature on

molar basis by dissolving known weights of chemicals in deionized water and the total weight of deionized water required to make a particular solution was also noted. Thereby the weight fractions of all chemicals and water for all molar solutions were always known.

4.2. Experimental Procedures

4.2.1. HCl-titration for KOH purity

The simplest method to analyze the purity of supplied KOH was the titration of KOH solution of known molarity with a standard HCl solution. The 2M solution of KOH was prepared by dissolving KOH in deionized solution. A sample of about 1ml of prepared solution was weighed and dissolved into 60 mL of deionized water and the solution was titrated against a standard 0.1M HCl solution. The actual concentration of KOH was calculated as follows:

$$C_{KOH}[mol.L^{-1}] = \frac{v_{HCl}\, C_{HCl}\, \rho_{sample}}{m_{sample}} \quad (4.1)$$

Here $v_{HCl}[L]$, $C_{HCl}[0.1 mol.L^{-1}]$, $m_{sample}[g]$ and $\rho_{sample}[g.L^{-1}]$ are the volume of standard HCl solution used for titration, concentration of that HCl solution, mass of sample KOH solution added to deionized water and density of that KOH solution respectively. Two parallel titrations were carried out for the sample. The density of KOH solution was measured at 25°C by an Anton Paar Stabinger Density meter DMA 4500.

The purity of KOH solutions was calculated on the basis of following:

$$\textbf{Purity of KOH}[\textbf{weight}\,\%] = \frac{\textbf{Actual concentration of KOH obtained from titration}}{\textbf{Concentration on the basis of prepared KOH solution}} \times 100 \quad (4.2)$$

4.2.2. Density measurements

Accurate density measurements were required for determination of KOH purity by titration presented above, the calculations of the N_2O solubility into hydroxides and blends and evaluation of kinetic experiments performed on SDC. The densities of all the prepared molar solutions of hydroxides and blends were measured by an Anton Paar Stabinger Density meter DMA 4500 for the temperature range 25 to 80°C. The nominal repeatability of the density meter, as described by the manufacturer, was 1×10^{-5} g.cm^{-3} and 0.01°C with a measuring range from 0 to 3 g.cm^{-3}. A sample of

10±0.1 mL was placed in a test tube, and put into the heating magazine with a cap on. The temperature in the magazine was controlled by the Xsampler 452 H heating attachment. For each temperature and solution, the density was calculated as an average value of two parallel measurements. The density meter was compared with water in the temperature range from 25 to 80°C before start and after the end of every set of experiments. The repeatability of the density meter established by experimental data obtained for water was 6×10^{-4} g.cm^{-3}.

The density and N_2O measurements described in this section are basis for the ***Paper I*** as given in Chapter 5 and all experimental results obtained are presented there.

4.2.3. N_2O solubility measurements

The physical solubility of N_2O into deionized water and aqueous solutions of hydroxides and carbonates was measured using the apparatus shown in Figure 4.1.

The apparatus consists of a stirred, jacketed reactor (Büchi Glass reactor 1L, up to 200°C and 6 bara) and a stainless steel gas holding vessel (Swagelok SS-316L cylinder 1L). The exact volumes of reactor, V_R and gas holding vessel, V_v, calculated after calibration, were 1069 cm^3 and 1035 cm^3 respectively.

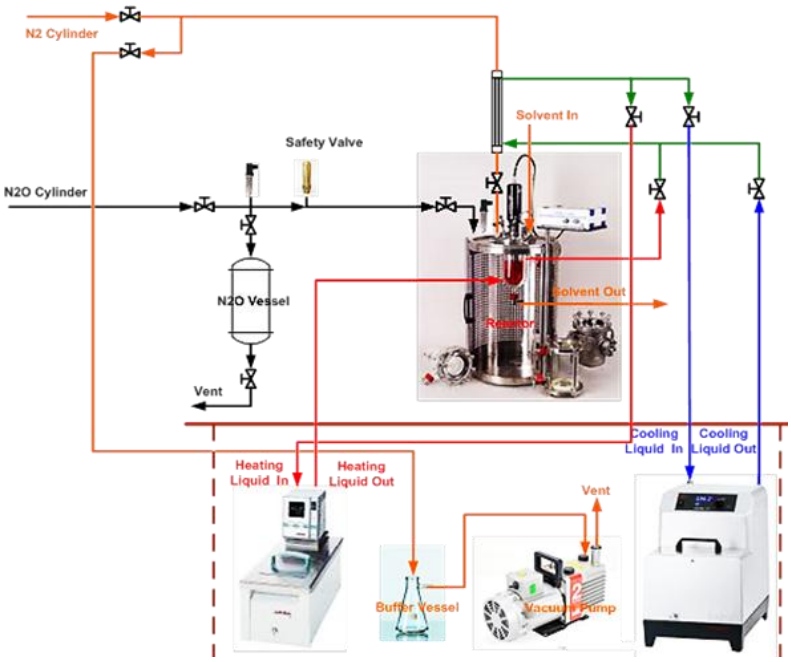

Figure 4.1. The experimental set-up for N_2O solubility experiments

A known mass of absorbent (water, aqueous solutions of hydroxides and/or carbonates in this work) was transferred into the reactor. The system was degassed at room temperature (25°C) once under vacuum by opening (about for one minute) a vacuum valve at the top of reactor until a vacuum around 4±0.5 kPa was obtained in the reactor. To minimize solvent loss during degassing, a condenser at the reactor outlet was installed. The temperature of the condenser was maintained at 4°C (corresponding to a water saturation pressure of 0.8 kPa) with the help of a Huber Ministat 230-CC water cooling system.

After degassing, the reactor was heated to desired temperatures, ranging from 25 to 80°C for all experiments, except for some water experiments which ranged from 25-120°C. The equilibrium pressure profiles before addition of N_2O were obtained for aforementioned temperature range starting from 25°C. The reactor temperature was controlled by a Julabo-F6 with heating silicon oil circulating through the jacketed glass reactor and a heating tape at the top of the reactor.

N_2O gas was added at the highest operating temperature (80°C or 120°C in this work), by shortly opening the valve between the N_2O steel gas holding vessel and the reactor. The initial and final temperatures and pressures in the N_2O gas holding vessel were recorded. After the addition of N_2O, starting with the highest temperature (80°C or 120°C), equilibrium was established sequentially once again at all the same temperatures for which equilibrium pressures without N_2O were obtained previously. The pressures in the gas holding vessel and reactor were recorded by pressure transducers PTX5072 with range 0-6 bar absolute and accuracy 0.04% of full range. Gas and liquid phase temperatures were recorded by PT-100 thermocouples with an uncertainty ±0.05°C. All data were acquired using FieldPoint and LabVIEW data acquisition systems.

It was possible to operate the setup in both manual and automated mode. The only difference in manual and automated mode was the selection of temperature set-points. In manual mode, the temperature set points were selected manually after achieving equilibrium at each temperature. The equilibrium in the reactor at a particular temperature was established after 3 to 4 hours when P_R, T_L and T_G; representing pressure in the reactor and temperatures of liquid and gas phases in reactor respectively, were stable and difference in T_L and T_G was not more than ±0.5 °C.

In the automated mode the temperature set-points (25-80°C) were selected after degassing and the system was allowed to achieve equilibrium at each set-point. The establishment of equilibrium was determined automatically by certain criteria of variance in temperatures and pressures. The equilibrium criteria are given as:

$$T_G - T_L = 0.1°C;\ T_{L_{variance}} = 0.015\ °C;\ T_{G_{variance}} = 0.025°C;\ \ P_{R_{variance}} = 0.5\ kPa$$

The above mentioned criteria state that equilibrium would be considered to be established when the temperature difference in the reactor between gas and liquid phase was less than 0.1°C, the variance in liquid phase temperature was less than 0.015°C, the variance of gas phase temperature was less than 0.025°C and the variance in reactor pressure was less than 0.5 kPa during an interval of half an hour. The criterion for the gas temperature variance was kept less strict than that for the liquid phase because it was more difficult to achieve temperature stability in the gas phase as compared to the liquid phase. For automated mode, equilibrium in the reactor at a particular temperature was usually attained in 2 to 3 hours, but for some experiments with LiOH, it took up to six hours to meet the above mentioned criteria of temperature and pressure variance.

The equilibrium partial pressure of N_2O, $P_{N_2O}[kPa]$, in the reactor at any temperature was taken as the difference between the total equilibrium pressure in the reactor before and after addition of N_2O at a particular temperature.

$$P_{N_2O}[Pa] = P_{R_{after\ addition\ of\ N_2O}} - P_{R_{before\ addition\ of\ N_2O}} \tag{4.3}$$

The use of Equation (4.3) assumes that the addition of N_2O does not change the vapor liquid equilibria of the absorbents (water or aqueous solutions of hydroxides and/or carbonates in this work). When the total volume of the reactor $V_R[m^3]$, the amount of liquid in the reactor $m_L[kg]$ and the density of liquid $\rho_L[kg.m^{-3}]$ are known, the amount of N_2O in the gas phase can be calculated by:

$$n^G_{N_2O}[mol] = \frac{P_{N_2O}(V_R - m_L\rho_L)}{zRT_R} \tag{4.4}$$

Here $R[kpa.m^3.kmol^{-1}]$ is the ideal gas constant, $T_R[K]$ is the reactor temperature ($T_R = T_L = T_G \pm 0.1K$) and $z[-]$ is the compressibility factor for N_2O at equilibrium temperature and pressure. The compressibility factor was calculated using the Peng–

Robinson equation of state using critical pressure of 7280 kPa, critical temperature of 309.57 K and acentric factor of 0.143 (Green, 2008).

The total amount of N_2O added to the reactor can be calculated by the pressure and temperature difference in the gas vessel before and after adding N_2O to the reactor.

$$n_{N_2O}^{added}[mol] = \frac{V_v}{R}\left(\frac{P_{v_1}}{T_{v_1}Z_1} - \frac{P_{v_2}}{T_{v_2}Z_2}\right) \quad (4.5)$$

Here $V_v[m^3]$, $P_v[kPa]$ and $T_v[K]$ are the volume, pressure and temperature of the gas holding vessel respectively, $Z[-]$ is the compressibility factor for N_2O and $R[Pa.m^3.mol^{-1}]$ is the universal gas constant. Subscripts "1" and "2" denote the parameters before and after the transfer of N_2O to the reactor. The amount of N_2O absorbed into the liquid phase of the reactor can be calculated as the difference between N_2O added to the reactor and N_2O present in the gas phase and the concentration of N_2O in the liquid phase, $C_{N_2O}^{L}[mol.m^{-3}]$, can then be calculated by

$$C_{N_2O}^{L}[mol.m^{-3}] = \frac{n_{N_2O}^{added} - n_{N_2O}^{G}}{V_{absorbent}} \quad (4.6)$$

The N_2O solubility into the solution can be expressed by an apparent Henry's law constant defined as:

$$H_{N_2O}[Pa.m^3.mol^{-1}] = \frac{P_{N_2O}}{C_{N_2O}^{L}} \quad (4.7)$$

Here H_{N_2O} is the apparent Henry's law constant for absorption of N_2O into the absorbent; $P_{N_2O}[Pa]$ is the partial pressure of N_2O present in the gas phase and $C_{N_2O}^{L}[mol.m^{-3}]$ is the amount [mol] of N_2O present per unit volume [m^3] of absorbent (water or aqueous solutions of hydroxides and/or carbonates).

4.2.4. Water vapor pressure over LiOH solutions measurements

The equilibrium modeling needed for the calculations of activities, to be used in activity based kinetics evaluation, requires equilibrium data. The N_2O solubility measurements performed in this work and literature equilibrium data available for hydroxides and carbonates, as presented in Chapter 2, was good enough to provide the basis for equilibrium modeling presented in ***paper II*** given as Chapter 6 for

systems containing Na^+ and K^+ counter ions. However the available equilibrium data for lithium were very limited in literature; a number of experiments were conducted to measure water vapor pressure over 0.25-8.5 wt.% solutions of LiOH for a range of temperature 40-90°C.

The measurements were performed in a modified Swietoslawski ebulliometer. The scheme of the experimental setup is shown in Figure 4.2. Detailed description of equipment can be found in (Ha´la et al., 1958) and (Rogalski and Malanowski, 1980)

The ebulliometer, which is made of glass, has a volume of 200 mL. It is designed for operation at temperatures up to 200°C and pressures of 1bar at the maximum. The temperatures were measured with calibrated Pt-100 resistance thermo sensors with an uncertainty of ±0.05°C. These were logged online via Chub-E4 thermometer readout (Hart Scientific, Fluke). The pressure was measured and controlled with a calibrated DPI520 rack mounted pressure controller (Druck, Germany). The uncertainty of the pressure controller was 0.3 kPa.

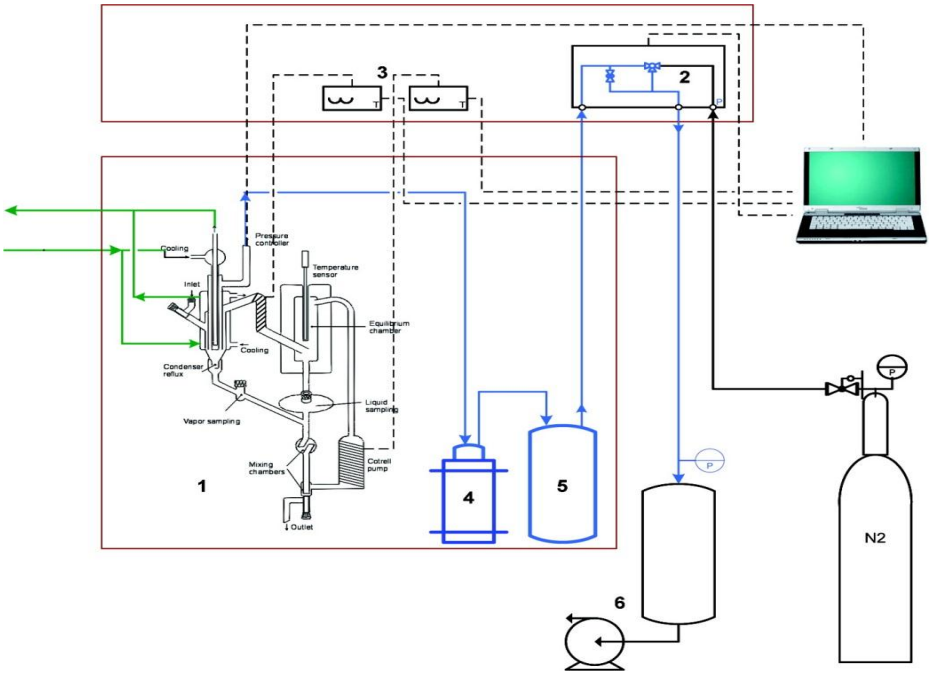

Figure 4.2: Experimental setup: 1, ebulliometer; 2, pressure controller; 3, temperature controllers; 4, cold trap; 5, buffer vessel; 6, vacuum pump with a buffer vessel (Kim et al., 2008).

An ebulliometer can be used either under isothermal or isobaric mode, to measure the boiling point of liquids by measuring the temperature of the vapor-liquid equilibrium. In isobaric mode pressure is kept constant and temperature is changed while in case of isothermal mode, temperature is kept constant and pressure is changed to get the equilibrium. Isothermal mode was used for the measurements used in this work. First of all, ebulliometer was washed and boiled with water and data was collected by running water only to validate the accuracy of equipment and experimental procedure. For better and more accurate results, the ebulliometer was washed and boiled three to four times with the desired solution prior to start of the experiment with that solution. Then, ebulliometer was charged with 95-100 mL of the LiOH solution of known weight concentration and purged with nitrogen.

Pressure was lowered by using vacuum pump and apparatus was checked for any leakages by observing the fluctuation in pressure operating line for very low pressure inside ebulliometer. Pressure was adjusted gradually by introducing N_2 gas to get the desired equilibrium temperature. The liquid would be heated and evaporated partially. The Cottrell pump carries the overhead liquid and vapor condensate to equilibrium chamber. This process continued until equilibrium was established with smooth boiling and temperature was almost a constant value (with fluctuations not more than 0.05°C) for more than 10-15 minutes. The value of equilibrium pressure was noted which is the vapor pressure of water over LiOH solution of desired concentration.

4.2.5. Kinetics measurements with string of discs contactor (SDC)

A string of a discs contactor (SDC) as shown in Figure 4.3 was used to perform the kinetic experiments with aqueous solutions of hydroxides and carbonates. The string of discs is made of unglazed ceramic material. It comprises an arrangement of $n_d = 43$ discs each with diameter, $d = 1.5 \times 10^{-2}\, m$ and thickness , $w = 4 \times 10^{-3}\, m$. The inner diameter of the glass column is $D_i = 2.6 \times 10^{-2}\, m$. The equivalent diameter is, $d_{eq} = 2.9 \times 10^{-2}\, m$. The characteristic active length of the column is about, $L = 6.45 \times 10^{-1}\, m$.

The actual mass transfer area is, $A_{act} = 2.19 \times 10^{-2}\, m^2$ and can be calculated by:

$$A_{act}[m^2] = \left[2\pi\left(\frac{d}{2}\right)^2 + \pi d w - 2w^2\right] n_d \qquad (4.8)$$

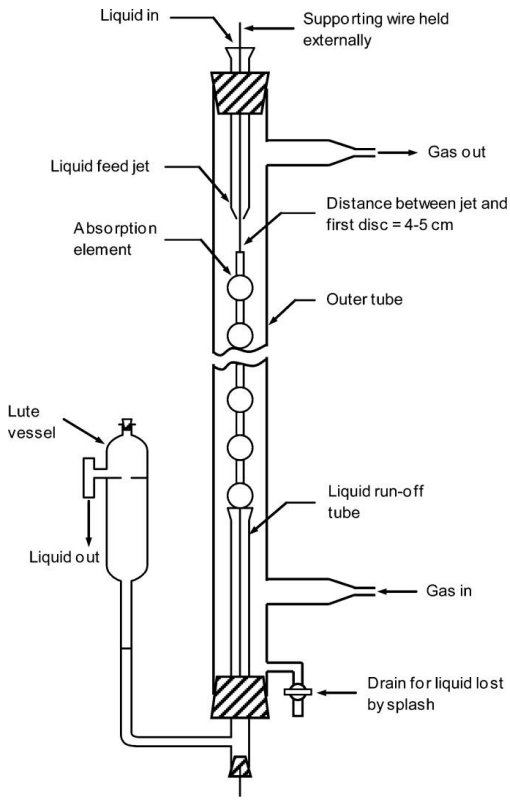

Figure 4.3: Arrangement of string of discs (SDC) absorption column (Ma'mun et al., 2007)

The discs are arranged on a string in a vertical row at alternating straight angles as shown in Figure 4.3.

The set-up used for measurements is shown in Figure 4.4. The string of discs column is operated counter-currently with liquid flowing from top to bottom and gas flowing upwards. The liquid flows through a tube that ends in a jet. The liquid is removed with a small tube from the funnel. The gas is fed from the bottom with long enough distance from the first disc to ensure a smooth gas flow. The liquid and gas flow rates are independently adjustable by use of a peristaltic liquid pump (EH Promass 83) and a gas blower. The flow of the blower is controlled by a Siemens Micro Master Frequency Transmitter and it has a maximum flow rate of 1.75 $Nm^3.hr^{-1}$.The concentration of feed mixture of gases, N_2 and CO_2, is controlled by two Bronkhorst Hi-Tec mass flow controllers and the concentration of CO_2 in bleed is measured by using an IR Fisher-Rosemount BINOS 100 NDIR CO_2 analyzer. Five K-type

thermocouples were used to register the 4 inlet and outlet gas and liquid temperatures and the temperature inside the chamber.

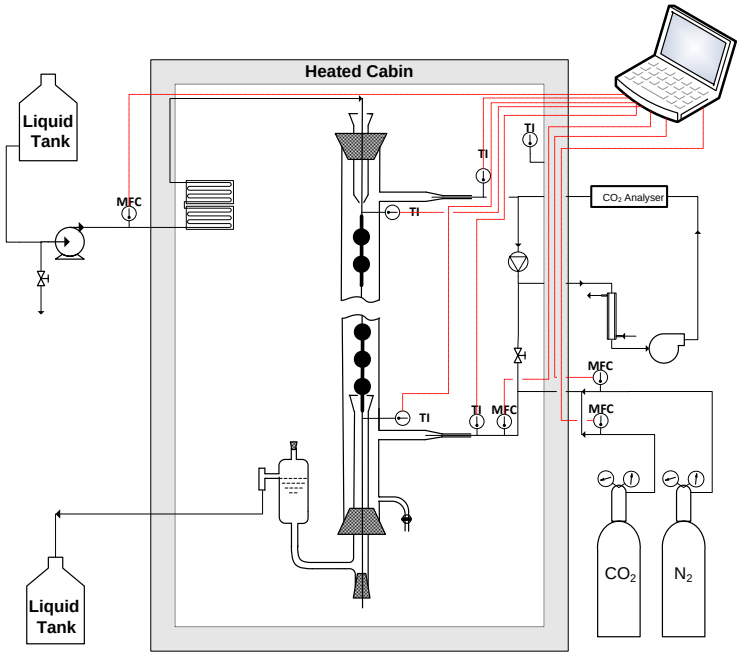

Figure 4.4: Experimental set-up of the string of discs (SDC) absorption column (Hartono et al., 2009)

The absorbents (aqueous solutions of hydroxides and blends of hydroxides and carbonates) were fed to the column at a flow rate which is in the range where the absorption rate is independent of liquid flow rate. This is to ensure that the absorption takes place in the fast reaction regime in which the kinetic parameters can be measured. To estimate this range, preliminary experiments with varying the liquid flow rate at a given temperature were required and then the constant absorption rate range was determined from a plot of CO_2 flux against the liquid flow rate (Ma'mun et al., 2007).

The cabinet was heated until desired temperature was reached; afterwards a known mixture of CO_2 and N_2 was fed into the column. A small amount of nitrogen has to enter the system, in addition to CO_2, because the pressure in the system is maintained constant by small amounts of gas bleeding out of a water lock. Typically the pressure in the apparatus will be about 50 Pa higher than the atmospheric pressure because of this water lock. The difference is considered negligible.

The experiments were run until steady state was achieved and were terminated when the temperature had reached a stable value at the desired level and a constant concentration level of CO_2 was obtained from the analyzer. The rate of absorption of CO_2 into the liquid was calculated from a solute mass balance over the entire system, i.e. CO_2 entering, $Q_{CO_2}^{in}[mol.s^{-1}]$, and going out, $Q_{CO_2}^{out}[mol.s^{-1}]$, from the system and can be expressed as:

$$r_{CO_2}^{absorbed}[mol.s^{-1}] = Q_{CO_2}^{in} - Q_{CO_2}^{out} \quad (4.9)$$

The amount of CO_2 entering, $Q_{CO_2}^{in}[mol.s^{-1}]$, in the system can be determined from the CO_2 mass flow controller while the amount of CO_2 going out, $Q_{CO_2}^{out}[mol.s^{-1}]$, from the system through the constant pressure bleed and can be calculated as:

$$Q_{CO_2}^{out}[mol.s^{-1}] = \frac{Q_{N_2}^{in} y_{CO_2}^{out}}{1-\left[\frac{P_{solution}}{P}\right]-y_{CO_2}^{out}} \quad (4.10)$$

The amount of N_2 entering into the system, $Q_{N_2}^{in}[mol.s^{-1}]$, is determined from the mass flow controller. Raoult's law was used to predict the vapor pressure of the solution, $P_{solution}[Pa]$. $y_{CO_2}^{out}[-]$ is the molar concentration of CO_2 in the gas phase in the circulating gas.

4.2.5.1. Characterization of the string of discs contactor

The unknown hydrodynamics of both gas and liquid flow in the string of discs contactors are the major drawback of the set-up and it is necessary to establish the gas and liquid side mass transfer resistance of the column by conducting experiments. In a string of discs type apparatus, the gas phase mass transfer resistance can be calculated by an expression based on Stephen and Morris (Stephens and Morris, 1951).

$$\frac{k_g P}{v\rho_A} = 0.328\Gamma^{0.13}\left(\frac{vd\rho}{\mu}\right)^{-0.33}\left(\frac{\mu}{\rho D_{A,G}}\right)^{-0.56}\left(\frac{P}{P_A}\right) \quad (4.11)$$

Here, $k_g[mol.m^{-2}.Pa^{-1}.s^{-1}]$ is the gas side mass transfer coefficient, $P[Pa]$ is the total pressure, $v[m.s^{-1}]$ is the gas velocity, $\rho_A[mol.m^{-3}]$ is the molar density of the solute gas, $d[m]$ is the equivalent diameter of the gas flow, $\mu[kg.m^{-1}.s^{-1}]$ and $\rho[kg.m^{-3}]$ are the average gas viscosity and density respectively, $D_{A,G}[m^2.s^{-1}]$

and $P_A[Pa]$ are the diffusivity and partial pressure of the solute gas respectively and $\Gamma[kg.m^{-1}.s^{-1}]$ is the liquid wetting rate in the apparatus defined as:

$$\Gamma[kg.m^{-1}.s^{-1}] = \frac{Liquid\ flow\ rate[kg.s^{-1}] \times Length\ of\ string[m]}{Surface\ area\ of\ string[m^2]} \quad (4.12)$$

The gas-side mass transfer coefficient, used in this work, was taken from earlier work in the same apparatus (Ma'mun et al., 2007). They used absorption of SO_2 into aqueous NaOH solution to measure the gas-side mass transfer resistance where the absorption of the solute was assumed to follow an instantaneous irreversible reaction with the reaction plane forming at the gas-liquid interface. The correlation developed by (Ma'mun et al., 2007) is given as:

$$\frac{k_G d}{D} = 0.12\left(\frac{vd\rho}{\mu}\right)^{0.79}\left(\frac{\mu}{\rho D}\right)^{0.44} \quad (4.13)$$

The gas film mass transfer coefficient $k_g[mol.m^{-2}Pa^{-1}.s^{-1}]$ having same units as those for overall mass transfer coefficient, $K_{ov_G}[mol.m^{-2}.Pa^{-1}.s^{-1}]$, can be calculated as:

$$k_g[mol.m^{-2}.Pa^{-1}.s^{-1}] = \frac{k_G[m.s^{-1}]}{RT[Pa.m^3.mol^{-1}]} \quad (4.14)$$

where $[Pa.m^3.mol^{-1}.K^-]$ is ideal gas law constant and $T[K]$ is the absolute temperature.

The liquid-side mass transfer coefficient, expressed as $\frac{k_L^o}{D}\left(\frac{\mu}{\rho D}\right)^{0.5}$ as a function of modified Reynolds number $\left(\frac{4\Gamma}{\mu}\right)$, shows strong dependence on liquid flow rate (Ma'mun et al., 2007). The results of (Ma'mun et al., 2007) agreed very well with earlier works and they proposed a correlation, based on the interpretation of original correlation by (Stephens and Morris, 1951) given as:

$$\frac{k_L^o}{D_A} = 17.92\left(\frac{4\Gamma}{\mu}\right)^{1.0}\left(\frac{\mu}{\rho D}\right)^{0.55} \quad (4.15)$$

The gas side and liquid side mass transfer coefficients, as mentioned earlier, used in this work were calculated by Equations 4.13-4.15 proposed by (Ma'mun et al., 2007) .

4.2.5.2. Calculation of the gas side overall mass transfer coefficient

The overall mass transfer coefficient based on gas side, $K_{ov_G}[mol.m^{-2}.Pa^{-1}.s^{-1}]$, as mentioned in Equations 3.59-3.61can be calculated for the whole string of discs by:

$$K_{ov_G}[mol.m^{-2}.Pa^{-1}.s^{-1}] = \frac{N_{CO_2}}{\Delta p_{CO_2,LM}} \tag{4.16}$$

The CO_2 flux, $N_{CO_2}[mol.m^{-2}.s^{-1}]$, can be calculated by use of Equations 4.8-4.9 as:

$$N_{CO_2}[mol.m^{-2}.s^{-1}] = \frac{r_{CO_2}^{absorbed}[mol.s^{-1}]}{A_{act}[m^2]} \tag{4.17}$$

The log mean pressure difference, $\Delta p_{CO_2,LM}[Pa]$, is used to replace the local driving force for absorption $(P_{CO_2} - P_{CO_{2,b}})$ by the average logarithmic driving force over the whole string of discs since the pressure is not uniform throughout the column. $\Delta p_{CO_2,LM}[Pa]$ can be calculated as:

$$\Delta p_{CO_{2,LM}}[kPa] = \frac{\left(P_{CO_2}^{in} - P_{CO_{2,b}}^{in}\right) - \left(P_{CO_2}^{out} - P_{CO_{2,b}}^{out}\right)}{ln\frac{\left(P_{CO_2}^{in} - P_{CO_{2,b}}^{in}\right)}{\left(P_{CO_2}^{out} - P_{CO_{2,b}}^{out}\right)}} \tag{4.18}$$

Here $P_{CO_{2,b}}^{in}[kPa]$ and $P_{CO_{2,b}}^{out}[kPa]$ are the equilibrium pressures of CO_2 over the liquid at the SDC contactor inlet and outlet. These can be considered to be zero because when the solution enters the column; it is either unloaded, in case of hydroxides, or with no CO_2 giving off in gas phase, in case of carbonates, and the degree of absorption of CO_2 in the column is very small. It should be noted that since the gas flow rate in the SDC is large compared to the flow of CO_2 through the system, the difference between $P_{CO_2}^{in}$ *and* $P_{CO_2}^{out}$ is very small and the driving force can be equally well calculated by the arithmetic mean $(P_{CO_2}^{in} + P_{CO_2}^{out})/2$. The overall mass transfer coefficient, $K_{ov_G}[mol.m^{-2}.Pa^{-1}.s^{-1}]$, can be used for the evaluation of both concentration based and activity based rate constants by use of Equations (3.66-3.67) and Equations (3.74-3.75) respectively.

5. Paper I

Density and N_2O solubility of aqueous Hydroxide and Carbonate Solutions in the temperature range from 25 to 80°C

*Shahla Gondal, Naveed Asif, Hallvard F. Svendsen, Hanna Knuutila**

Department of Chemical Engineering, Norwegian University of Science and Technology, N-7491 Trondheim, Norway

ABSTRACT

The solubility of N_2O in aqueous solutions of hydroxides containing Li^+, Na^+ and K^+ counter ions and the hydroxide blends with carbonates were measured for a range of temperatures (25-80°C) and concentrations (0.08-3M). To evaluate the solubility experiments in terms of apparent Henry's law constant [$kPa.m^3.kmol^{-1}$], the accurate liquid densities of these systems were measured by an Anton Paar Stabinger Density meter DMA 4500. The measured densities were compared with Laliberté and Cooper's density model (Laliberte and Cooper, 2004) with less than 0.3% AARD (Average Absolute Relative Deviation). By using the experimental data for N_2O solubility, the parameters in the model of Weisenberger and Schumpe (Weisenberger and Schumpe, 1996) were refitted for aforementioned systems. The ion specific and temperature dependent parameters for these systems in the original model, valid up to 40°C and 2M concentration, were refitted to extend the validity range of the model up to 3M and 80°C with 4.3% AARD.

*** Corresponding Author: Hanna.Knuutila@ntnu.no**

1. Introduction

CO_2 absorption into aqueous hydroxide and carbonate solutions of alkali metals, in particular lithium, sodium and potassium, has been widely studied and used for several applications since the early 20th century [(Hitchcock, 1937); (Welge, 1940); (Kohl and Nielsen, 1997)]. During the last two decades, due to increased environmental concerns and stringent conditions for CO_2 emissions from power plants, energy intensive regeneration of amine based CO_2 capture absorbents, environmental issues arising from thermal degradation of amines (Rochelle, 2012a) and other socio-economic factors, these systems have regained attention [(Cullinane and Rochelle, 2004); (Corti, 2004); (Knuutila et al., 2009); (Mumford et al., 2011); (Anderson et al., 2013); (Smith et al., 2013)].

One of the most important issues in evaluating an absorbent is to determine the kinetic parameters which are typically derived from the mass transfer experiments. To evaluate the kinetics from mass transfer experiments, data on physical diffusivity and solubility of CO_2 in the absorbents are required. Since CO_2 reacts in most of the absorbents, including hydroxide and carbonate systems, it is not possible to measure the physical solubility independently using CO_2. Hence it is suggested that the N_2O analogy can be employed to estimate the above mentioned physicochemical properties [(Versteeg and Van Swaaij, 1988); (Xu et al., 2013)]. N_2O can be used to estimate the properties of CO_2 as it has similarities in configuration, molecular volume and electronic structure and is a nonreactive gas under the normally prevailing reaction conditions.

The N_2O analogy was originally proposed by (Clarke, 1964), verified by (Laddha et al., 1981) and is being widely used by many researchers [(Haimour and Sandall, 1984); (Versteeg and Van Swaaij, 1988); (Al-Ghawas et al., 1989); (Hartono et al., 2008); (Knuutila et al., 2010b)]. Applying this analogy, the physical solubility of CO_2 in terms of an apparent Henry's law constant, $H_{CO_2}[kPa.m^3.kmol^{-1}]$, can be calculated based on the solubility of CO_2 and N_2O into water and the solubility of N_2O in the system of interest, by the equation:

$$H_{CO_2}[kPa.m^3.kmol^{-1}] = H_{N_2O}\left(\frac{H^{\circ}_{CO_2}}{H^{\circ}_{N_2O}}\right) \quad (1)$$

Here H_{N_2O} represents the solubility of N_2O in the system of interest in terms of an apparent Henry's law constant, $H^{\circ}_{N_2O}$ and $H^{\circ}_{CO_2}$ are the Henry's law constants for N_2O and CO_2 in water respectively. The term apparent Henry's law constant, as defined by Equation 11, refers to the physical solubility of a gas in the absorption systems (water, aqueous solutions of hydroxides and/or carbonates in this work).

It has been affirmed by several authors that the N_2O solubility in aqueous solutions exhibits an exponential dependency on the absorbent concentration in aqueous systems (carbonates and/or hydroxides in this work) [(Joosten and Danckwerts, 1972); (Hikita et al., 1974); (Knuutila et al., 2010b)]. The same behavior was assumed in the model of Weisenberger and Schumpe [(Schumpe, 1993); (Weisenberger and Schumpe, 1996)].

The model of Weisenberger and Schumpe (Weisenberger and Schumpe, 1996) is widely used to predict the solubility of gases into electrolyte solutions [(Rischbieter et al., 2000); (Vas Bhat et al., 2000) (Kumar et al., 2001); (Dindore et al., 2005); (Rachinskiy et al., 2014)]. The

model is very general and based on a large set of data. It describes the salting-out effect of 24 cations and 26 anions on the solubility of 22 gases. However, the model is reported to be valid only up to 40°C and up to electrolyte concentrations of about 2 kmol.m^{-3}. The model is based on an empirical model by Sechenov (Sechenov, 1889) who modelled the solubility of sparingly soluble gases into aqueous salt solutions with the equation

$$log\frac{C_{g_o}}{C_g}[-] = KC_s \quad (2)$$

Here $C_{g_o}[kmol.m^{-3}]$ and $C_g\ [kmol.m^{-3}]$ are the gas solubilities in water and in salt solution respectively, $C_s\ [kmol.m^{-3}]$ is the salt concentration and $K[m^3.kmol^{-1}]$ is the Sechenov constant. Schumpe (Schumpe, 1993) modified this model and in the model of Weisenberger and Schumpe (Weisenberger and Schumpe, 1996) the solubility was calculated from the equations

$$log\frac{C_{g_o}}{C_g}[-] = \sum_i^n (h_i + h_g)C_i \quad (3)$$

$$h_g[m^3.kmol^{-1}] = h_{G_o} + h_T(T - 298.15K) \quad (4)$$

In these equations $h_i[m^3.kmol^{-1}]$ is an ion-specific parameter, $h_{G_o}[m^3.kmol^{-1}]$ is a gas specific parameter, $C_i[kmol.m^{-3}]$ is the ion concentration and $h_T[m^3.kmol^{-1}.K^{-1}]$ is a gas specific parameter for the temperature effect.

Knuutila et al., 2010 (Knuutila et al., 2010b) updated h_T for N_2O and h_i for potassium and sodium in the model of Weisenberger and Schumpe (Weisenberger and Schumpe, 1996) using experimental data for carbonates of sodium and potassium from 25 to 80°C.

For the evaluation of hydroxides and carbonates as candidates for a CO_2 capture system, kinetic data are needed for a wide range of concentrations and for temperatures above 40°C. This is lacking in the literature. As previously mentioned, the N_2O solubility is essential for evaluation of mass transfer data into kinetic constants and hence, experiments were conducted to obtain solubility of N_2O into these systems; containing Li^+, Na^+ and K^+ counter ions for a wider range of concentrations and temperatures. Densities required for evaluation of experimental data were also measured.

2. Experimental section

2.1. Materials

Details on purity and supplier for all chemicals used are provided in Table 1. The purity of KOH as provided by the chemical batch analysis report from MERCK was relatively low. Thus it was determined analytically by titration against 0.1N HCl and was found to be 88 wt.%; the rest being water. All other chemicals were used as provided by manufacturer without further purification or correction.

Table 1. Details of chemicals used in experimental work

Name of Chemical	Purity	Supplier
LiOH	Powder, reagent grade, > 98%	SIGMA-ALDRICH
NaOH	> 99 wt.%, Na_2CO_3 < 0.9% as impurity	VWR
KOH	*88 wt.%	MERCK
Na_2CO_3	> 99.9 wt.%	VWR
K_2CO_3	> 99 wt.%	SIGMA-ALDRICH
CO_2 gas	≥ 99.999 mol%	YARA-PRAXAIR
N_2O gas	≥ 99.999 mol%	YARA-PRAXAIR
N_2 gas	≥ 99.6 mol%	YARA-PRAXAIR

*** The purity is based on the titration results against 0.1M HCl. Since the purity was relatively low, all experimental data of KOH is presented after correction for purity.**

2.2. Density

Accurate density measurements are required for the calculations of the N_2O solubility. The densities of the aqueous carbonate and hydroxide solutions were measured by an Anton Paar Stabinger Density meter DMA 4500 for the temperature range 25 to 80°C. The nominal repeatability of the density meter, as described by the manufacturer, was 1×10^{-5} g.cm^{-3} and 0.01°C with a measuring range from 0 to 3 g.cm^{-3}. The repeatability of the density meter established by experimental data obtained for water was 6×10^{-4} g.cm^{-3}. The reported experimental repeatability is based on average standard deviations of 60 density data points for water at six different temperatures as shown in Table A1.

The solutions were prepared at room temperature on molar basis by dissolving known weights of chemicals in deionized water and total weight of deionized water required to make a particular solution was also noted. Thereby the weight fractions of all chemicals and water for all molar solutions were always known. A sample of 10±0.1 mL was placed in a test tube, and put into the heating magazine with a cap on. The temperature in the magazine was controlled by the Xsampler 452 H heating attachment. For each temperature and solution the density was calculated as an average value of two parallel measurements. The density meter was compared with water in the temperature range from 25 to 80°C before start and after the end of every set of experiments. Density results from the apparatus were verified against the density of water data given in Table A1. The experimental results for water densities show 0.053% AARD (average absolute relative deviation) from the water density model given by (Wagner and Pruß, 2002). The standard deviation and %AARD were calculated by the equations:

$$\text{Standard Deviation } [g.cm^{-3}] = \sqrt[2]{\frac{\sum_{j=1}^{n}(\rho_i - \frac{1}{n}\sum_{j=1}^{n}\rho_i)^2}{n}} \quad (5)$$

$$AARD\ [\%] = \frac{1}{n}\sum_{i=1}^{n} 100\frac{\left|\rho_i^{Exp} - \rho_i^{Model}\right|}{\left|\rho_i^{Exp}\right|} \quad (6)$$

2.3. N_2O solubility

The physical solubility of N_2O into deionized water and aqueous solutions of hydroxides and carbonates was measured using the apparatus shown in Figure 1. The solubility apparatus

was a modified and automated version of the solubility apparatus previously described by [(Hartono et al., 2008); (Knuutila et al., 2010b) and (Aronu et al., 2012)]. The apparatus consists of a stirred, jacketed reactor (Büchi Glass reactor 1L, up to 200°C and 6 bara) and a stainless steel gas holding vessel (Swagelok SS-316L cylinder 1L). The exact volumes of reactor, V_R and gas holding vessel, V_v, calculated after calibration, were 1069 cm^3 and 1035 cm^3 respectively.

A known mass of absorbent (water, aqueous solutions of hydroxides and/or carbonates in this work) was transferred into the reactor. The system was degassed at room temperature (25°C) once under vacuum by opening (about for one minute) a vacuum valve at the top of reactor until a vacuum around 4±0.5 kPa was obtained in the reactor. To minimize solvent loss during degassing a condenser at the reactor outlet was installed. The temperature of the condenser was maintained at 4°C (corresponding to a water saturation pressure of 0.8 kPa) with the help of a Huber Ministat 230-CC water cooling system.

After degassing, the reactor was heated to desired temperatures, ranging from 25 to 80°C for all experiments except set 2 of water which ranged from 25-120°C. The equilibrium pressure profiles before addition of N_2O were obtained for aforementioned temperature range starting from 25°C. The reactor temperature was controlled by a Julabo-F6 with heating silicon oil circulating through the jacketed glass reactor and a heating tape at the top of the reactor. N_2O gas was added at the highest operating temperature (80°C or 120°C in this work), by shortly opening the valve between the N_2O steel gas holding vessel and the reactor. The initial and final temperatures and pressures in the N_2O gas holding vessel were recorded. After the addition of N_2O, starting with the highest temperature (80°C or 120°C), equilibrium was established sequentially once again at all the same temperatures for which equilibrium pressures without N_2O were obtained previously. The pressures in the gas holding vessel and reactor were recorded by pressure transducers PTX5072 with range 0-6 bar absolute and accuracy 0.04% of full range. Gas and liquid phase temperatures were recorded by PT-100 thermocouples with an uncertainty ±0.05°C. All data were acquired using FieldPoint and LabVIEW data acquisition systems. The precision of the modified experimental method was within 2% in the Henrys law constant as shown by the results in Table A4 for 3 experimental sets for water and for 2 sets of identical solutions of 2.5M LiOH. For the previous version of the solubility apparatus the precision was reported to be within 3% (Hartono et al., 2008).

It was possible to operate the setup in both manual and automated mode. The only difference in manual and automated mode was the selection of temperature set-points. In manual mode, the temperature set points were selected manually after achieving equilibrium at each temperature. The equilibrium in the reactor at a particular temperature was established after 3 to 4 hours when P_R, T_L and T_G; representing pressure in the reactor and temperatures of liquid and gas phases in reactor respectively, were stable and difference in T_L and T_G was not more than ±0.5°C.

In the automated mode the temperature set-points (25-80°C) were selected after degassing and the system was allowed to achieve equilibrium at each set-point. The establishment of equilibrium was determined automatically by certain criteria of variance in temperatures and pressures. The equilibrium criteria are given as:

$$T_G - T_L = 0.1°C; \quad T_{L_{variance}} = 0.015\ °C; \quad T_{G_{variance}} = 0.025°C; \quad P_{R_{variance}} = 0.5\ kPa$$

The above mentioned criteria state that equilibrium would be considered to be established when the temperature difference in the reactor between gas and liquid phase was less than 0.1°C, the variance in liquid phase temperature was less than 0.015°C, the variance of gas phase temperature was less than 0.025°C and the variance in reactor pressure was less than

0.5 kPa during an interval of half an hour. The criterion for the gas temperature variance was kept less strict than that for the liquid phase because it was more difficult to achieve temperature stability in the gas phase as compared to the liquid phase. For automated mode, equilibrium in the reactor at a particular temperature was usually attained in 2 to 3 hours, but for some experiments with LiOH, it took up to six hours to meet the above mentioned criteria of temperature and pressure variance.

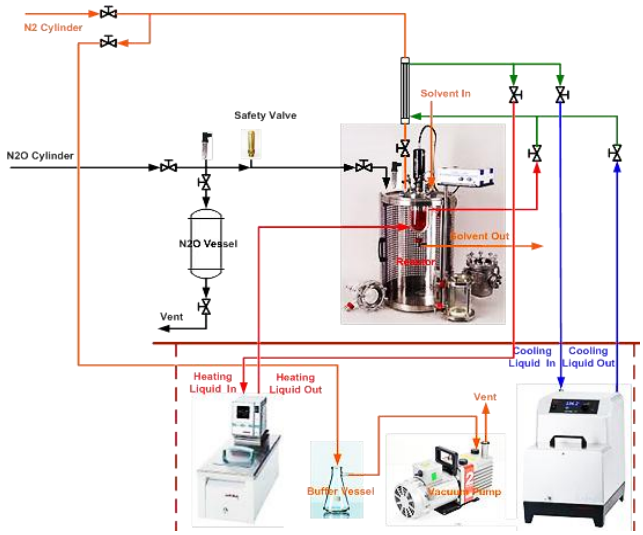

Figure 1. The experimental set-up for N_2O solubility experiments

The equilibrium partial pressure of N_2O, $P_{N_2O}[kPa]$, in the reactor at any temperature was taken as the difference between the total equilibrium pressure in the reactor before and after addition of N_2O at a particular temperature.

$$P_{N_2O}[kPa] = P_{R_{after\ addition\ of\ N_2O}} - P_{R_{before\ addition\ of\ N_2O}} \quad (7)$$

The use of Equation (7) assumes that the addition of N_2O does not change the vapor liquid equilibria of the absorbents (water or aqueous solutions of hydroxides and/or carbonates in this work). When the total volume of the reactor $V_R[m^3]$, the amount of liquid in the reactor $m_L[kg]$ and the density of liquid $\rho_L[kg.m^{-3}]$ are known, the amount of N_2O in the gas phase can be calculated by

$$n^G_{N_2O}[kmol] = \frac{P_{N_2O}\,(V_R - m_L\rho_L)}{zRT_R} \quad (8)$$

Here $R[kpa.m^3.kmol^{-1}]$ is the ideal gas constant, $T_R[K]$ is the reactor temperature ($T_R = T_L = T_G \pm 0.1K$) and $z[-]$ is the compressibility factor for N_2O at equilibrium temperature and pressure. The compressibility factor was calculated using the Peng–Robinson equation of state using critical pressure of 7280 kPa, critical temperature of 309.57 K and acentric factor of 0.143 (Green and Perry, 2007).

As the densities of the N_2O containing solutions were not measured, the liquid density used in Equation (8) is the density of the liquid without N_2O. The solubility of N_2O into the solutions is small (from 0.3 to 2.2 kg $N_2O.m^{-3}$ over the range of our experiments). The density

variation in the experiments was from 940 kg.m^{-3} to 1144 kg.m^{-3}. This means that wt.% of N_2O in the solutions ranged from 0.03% to 0.19%. Assuming that the added N_2O only influences the weight and not the volume a sensitivity analysis showed that the effect of this increase results in an increase in the calculated value of the apparent Henry's law constant by 0.02% to 1.2% respectively and is considered part of the experimental uncertainty.

The total amount of N_2O added to the reactor can be calculated by the pressure and temperature difference in the gas vessel before and after adding N_2O to the reactor.

$$n_{N_2O}^{added}[kmol] = \frac{V_v}{R}\left(\frac{P_{v_1}}{T_{v_1}z_1} - \frac{P_{v_2}}{T_{v_2}z_2}\right) \quad (9)$$

Here $V_v[m^3]$, $P_v[kPa]$ and $T_v[K]$ are the volume, pressure and temperature of the gas holding vessel respectively, $z[-]$ is the compressibility factor for N_2O and $R[kpa.m^3.kmol^{-1}]$ is the universal gas constant. Subscripts "1" and "2" denote the parameters before and after the transfer of N_2O to the reactor. The amount of N_2O absorbed into the liquid phase of the reactor can be calculated as the difference between N_2O added to the reactor and N_2O present in the gas phase and the concentration of N_2O in the liquid phase, $C_{N_2O}^{L}[kmol.m^{-3}]$, can then be calculated by

$$C_{N_2O}^{L}[kmol.m^{-3}] = \frac{n_{N_2O}^{added} - n_{N_2O}^{G}}{V_{absorbent}} \quad (10)$$

The N_2O solubility into the solution can be expressed by an apparent Henry's law constant defined as:

$$H_{N_2O}[kPa.m^3.kmol^{-1}] = \frac{P_{N_2O}}{C_{N_2O}^{L}} \quad (11)$$

Here H_{N_2O} is the apparent Henry's law constant for absorption of N_2O into the absorbent; $P_{N_2O}[kPa]$ is the partial pressure of N_2O present in the gas phase and $C_{N_2O}^{L}[kmol.m^{-3}]$ is the amount [kmol] of N_2O present per unit volume [m^3] of absorbent (water or aqueous solutions of hydroxides and/or carbonates).

3. Results

3.1. Density

Densities of hydroxides (LiOH, NaOH, KOH) and blends of hydroxides with carbonates (Na_2CO_3 and K_2CO_3) measured in this work are presented in Table A2 and Table A3 respectively.

The experimental results for hydroxide solutions densities were compared with literature data [(Randall and Scalione, 1927); (Lanman and Mair, 1934); (Hitchcock and McIlhenny, 1935); (Akerlof and Kegeles, 1939); (Tham et al., 1967); (Hershey et al., 1984); (Roux et al., 1984a); (Sipos et al., 2000)]. The agreement with literature data was very good (0.08 % average difference) for all hydroxides. No literature data could be found for blends of hydroxides and carbonates.

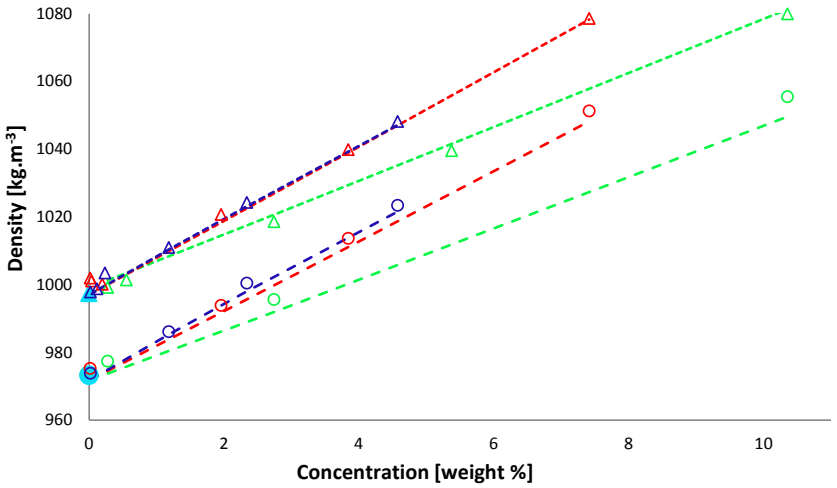

Figure 2. Density of LiOH, NaOH and KOH as a function of concentration at 25°C and 80°C; Points: Experimental data this work, Triangles (Δ): 25°C, Circles (○): 80°C, Lines: Laliberté and Cooper's Density Model. Turquoise: Water, Blue: LiOH, Red: NaOH, Green: KOH.

The experimental density data for water, hydroxides and blends obtained in this work along with density data for Na_2CO_3 and K_2CO_3 from Knuutila et al., 2010 (Knuutila et al., 2010b) were also compared with Laliberté and Cooper's density model (Laliberte and Cooper, 2004) which is based on literature density data. The Laliberté and Cooper density model, with validated parameters for 59 electrolytes, was established on the basis of an extensive and critical review of the published literature for solutions of single electrolytes in water with over 10 700 points included (Laliberte and Cooper, 2004). The Laliberté and Cooper density model predicts the density of a solution based on calculation of the specific apparent volume, $v_{app,i}[m^3.kg^{-1}]$, of dissolved solutes (LiOH, NaOH, KOH, Na_2CO_3 and K_2CO_3) and solvent (water) in solution. The apparent specific volumes were calculated by empirical coefficients suggested by the density model and the mass fraction of a solute in solution. The empirical coefficients for all solutes were obtained by fitting an apparent volume curve to experimental density data available in the literature from late 1800s and including all the above mentioned references. The statistical details of a comparison between this model and experimental density data for carbonates from (Knuutila et al., 2010b) in addition to all measured data in this study are provided in Table 2.

Figure 2 shows the density of the hydroxides studied in this work as function of concentration at 25°C and 80°C which brackets the entire concentration and temperature ranges of experimental data. It can be observed that Laliberté and Cooper's density model predicts the experimental data with less than 0.3% AARD. The largest deviations are observed for the lowest concentration of NaOH at 25°C and highest concentration of KOH at 80°C where the model under-predicts the experimental data by 0.47% and 0.55% respectively. It can also be seen that at zero concentration, the densities of all the three hydroxides reduce to the density of water as shown by the turquoise filled points on the y-axis.

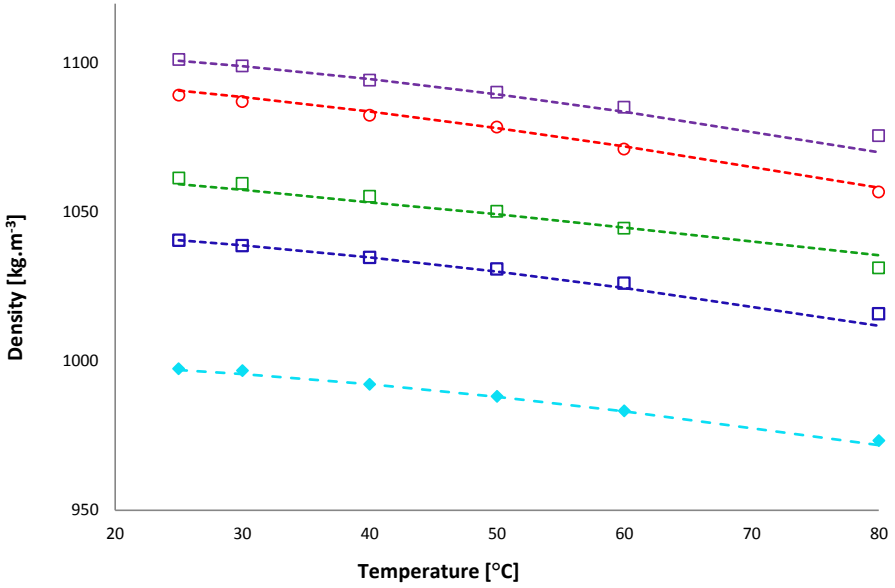

Figure 3. Density of water and blends of hydroxides and carbonates as a function of temperature from 25 to 80°C. Points (◊, □, ○): experimental data, Lines: Laliberte and Cooper's Density Model, Turquoise: Water; Blue: 0.52M NaOH+0.46M KOH, Green: 1.03M NaOH and 0.46M KOH, Red: 1M NaOH+0.5M Na_2CO_3, Purple: 1M LiOH+2M NaOH.

The experimental density data for water and blends of hydroxides and carbonates are given in Figure 3. It can be observed that the Laliberté and Cooper density model (Laliberte and Cooper, 2004) predicts the experimental data with less than 0.3% AARD. The largest deviations are observed at 80 °C where the model deviates from the experimental data by up to ±0.5%.

Table 2: Statistics of density data comparison with Laliberté and Cooper's Density Model

Solution	Temperature range [°C]	Concentration range [wt.%]	No. of data points	%AARD	Reference
Water	25 - 80	-	60	0. 054	This work
LiOH	25 - 80	0.024 - 4.58	39	0.138	This work
NaOH	25 - 80	0.02 – 7.42	40	0.176	This work
KOH	25 - 80	0.25 – 9.12	33	0.264	This work
***Na_2CO_3**	25 - 80	5 - 30	26	0.136	(Knuutila et al., 2010b)
***K_2CO_3**	25 - 80	5 - 50	42	0.269	(Knuutila et al., 2010b)
Blends	25 - 80	1 - 10	42	0.226	This work

*** Since the blends contained carbonates, data also for pure carbonates were used to validate the empirical coefficients**

A plot of deviations between experimental and predicted densities (model of Laliberté and Cooper) is given in Figure 4, and demonstrates that the experimental density data and model agree well (maximum ±6 kg/m^3 difference) for all data sets. As shown in Table 2, the density model predicts the experimental data with less than 0.269% AARD. The lowest value of AARD is for the water density data (0.054%) while the AARD when comparing our water density

data with Wagner's water density model (Wagner and Pruß, 2002) is 0.053% as presented by Table A2. Figure 4 does, however, indicate that the Laliberté and Cooper density model slightly under-predicts KOH solution densities. It also gives larger scatter in the data for blends.

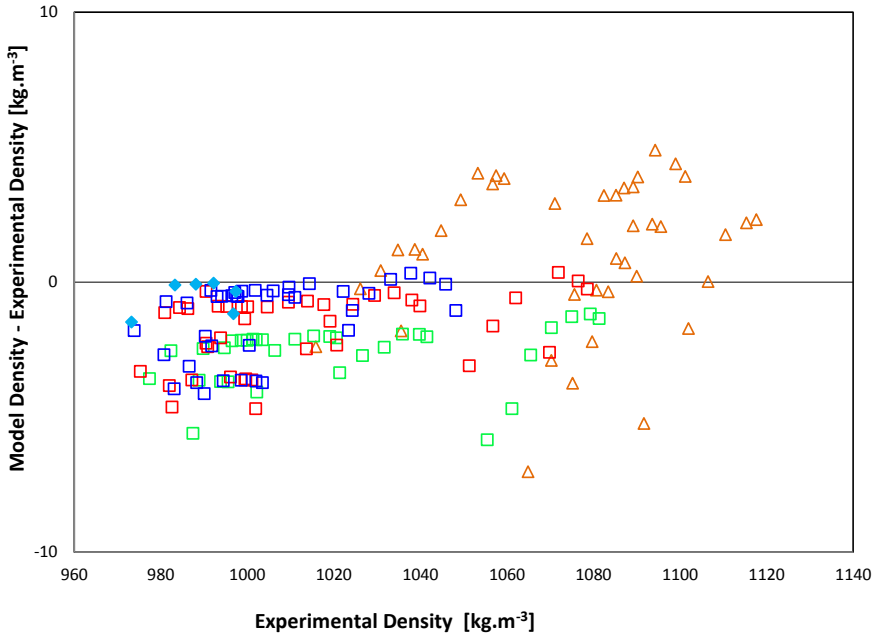

Figure 4. Plot of deviation between experimental data and prediction by Laliberté and Cooper's density model. Turquoise; Water, Blue: LiOH, Red: NaOH, Green: KOH. Diamonds (♦): water, Triangles (Δ): blends, Squares (□): hydroxides

3.2. Solubility method validation and reproducibility

To validate the methods used and to produce more data for the high temperature region, three repeated data sets in this study (set-1, set-2 and set- 3) were obtained for N_2O solubility in water. These data were also needed for calculations based on the model of Weisenberger and Schumpe (Weisenberger and Schumpe, 1996). The three data sets were spaced out in time; the first two sets were measured in the manually operated set-up and the third was measured after automation of the experimental set-up and for checking reproducibility. The results are shown in Table A4 and Figure 5.

Figure 5 presents the N_2O solubility in water in terms of an apparent Henry's law constant and comprises both data obtained in this work and found in the literature [(Knuutila et al., 2010b); (Hartono et al., 2008); (Mandal et al., 2005); (Jamal, 2002) (Li and Lee, 1996); (Li and Lai, 1995); (Al-Ghawas et al., 1989); (Versteeg and Van Swaaij, 1988); (Haimour and Sandall, 1984)]. In addition, the model developed by Jou (Jou et al., 1992) is included.

For consistency and coherence with literature, the correlation presented by Jou (Jou et al., 1992) was used. The water density correlation from (Wagner and Pruß, 2002) was incorporated to convert the units of Henry's law constant from pressure (based on mole

fraction of gas in absorbent) to often used kPa.m^3.kmol^{-1} (based on molar concentration of gas in absorbent). The correlation was used in the N_2O solubility model from Weisenberger and Schumpel (Weisenberger and Schumpe, 1996). The correlation by Jou (Jou et al., 1992) for the Henry's law constant [MPa], after conversion of units is given as:

$$H_{N_2O}^{water}[kPa.m^3.kmol^{-1}] = \frac{18020exp\left[492.0352 + 0.084942T - \frac{18560.2}{T} - 78.9292\ lnT\right]}{-0.0033461T^2 + 1.7296T + 778.53} \quad (12)$$

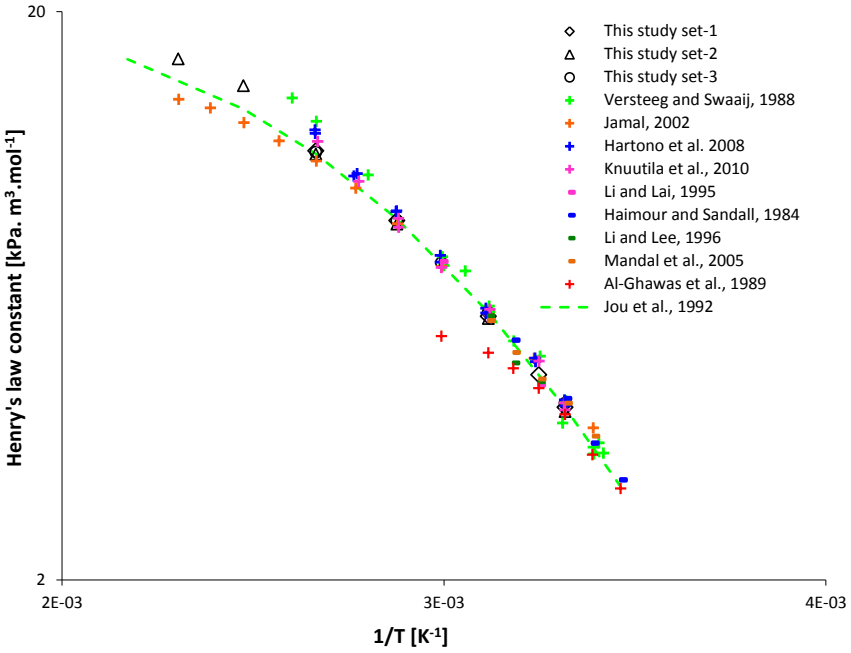

Figure 5. Henry's law constant for absorption of N_2O into water. Stippled line: Jou's correlation (Jou et al., 1992), Points: experimental data, Open points (-, +): literature data, Closed points (◊, Δ, ○): this study.

The reproducibility between the three data sets for water was good with standard deviations from 0.5-1.4% as seen in Table A4. The maximum deviation between our water solubility data and Jou's correlation, Equation (12), is 8.9% with an AARD of 2.2% for all data. We see that the largest deviations are found for the higher temperatures (8.9% at 100 °C and 7.4% at 120 °C) where also the scatter in data is high. When using only set-3 of the water experiments, which only goes up to 80°C, the AARD is only 0.76% compared to Jou's correlation (Jou et al., 1992)

For the hydroxides, most experimental repeats were performed for lithium hydroxide because of its very low solubility in water. The solubility of LiOH, as reported in (Shimonishi et al., 2011) is 5M or about 12 wt.% at room temperature. It was difficult to get clear solutions and experiments were repeated twice for improved accuracy. Here it is important to state that all solutions were prepared on molar basis but exact weight percentages of solutions were also noted. To account for the human error involved in solution making of lithium

hydroxide, a 2.5M LiOH solution was prepared and continuously stirred for 72 hours to get a clear solution. The same solution was used to perform two parallel sets of experiments and nearly identical results were obtained for set 1 and set 2. The results for water and 2.5M LiOH with identical solution are shown in Table A4. The second last column of Table A4 shows the standard deviation [$kPa.m^3.kmol^{-1}$] and last column presents %SD with respect to the average for 2 or 3 repeated sets. The statistics presented in Table A4 demonstrate very good reproducibility in the experimental method. However, as seen in Table A4, the reproducibility for 2.5M LiOH is better (0.4% average standard deviation) than for water (0.9% average standard deviation). The reason is that both sets of experiments for lithium hydroxide were performed after automation of the apparatus, whereas set-1 and set-2 of the water experiments were performed before, and only set-3 after, automation. One of the experiments for the blends of carbonates was also repeated to test the reproducibility. The overall average standard deviation for all repeated data for LiOH and the blends was found as 0.96% with a maximum of 2.7% for 1M LiOH at 80°C. Once again it is worth mentioning that one of the repeated experiments for 1M LiOH was performed manually and the other after automation. The results for repeated sets of LiOH, except for 2.5M LiOH and one of blends, as shown in Table A5 and Table A6, are not presented in Table A4 because of the fact that the solutions for repeated runs were not of exactly the same concentration.

3.3. N_2O solubility into hydroxides and blends of hydroxides with carbonates

Experimental results for N_2O solubility into hydroxides and blends are presented in Table A5 and Table A6 respectively. The results for hydroxides are graphically illustrated by Figure 6 and Figure 7. Figure 6 presents the apparent Henry's law constant [$kPa.m^3.mol^{-1}$] for absorption of N_2O into aqueous solutions of lithium hydroxide as a function of temperature for the concentration range (0.1M-2.5M) and temperature range (25-80°C).

As shown by Figure 6, the difference in results for repeated sets of experiments is negligible at lower temperatures, but at 80°C the differences for 0.5M, 1M and 2M LiOH are slightly higher. Even though the results for 1M and 2M LiOH show higher differences in repeated sets, these differences are still within the overall experimental uncertainties estimated by error propagation from the various readings, as indicated by ±6% error bars on these data sets. It is also worth mentioning that uncertainties in the evaluation of experimental results are higher at higher temperatures due to the low solubility of N_2O in liquid phase. Slightly different wt. fractions of LiOH and water obtained during solution preparation (since solutions were prepared on molar basis) for the repeated sets, as shown in Table A5 can be another reason for differences seen. As previously mentioned, the results for two repeated experiments on identical solutions of 2.5M LiOH by the automated experimental set-up demonstrate very good repeatability.

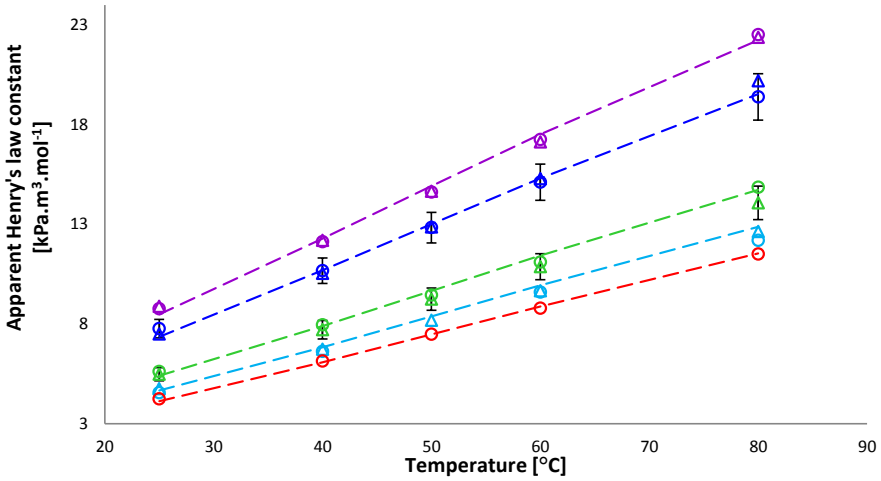

Figure 6. Henrys' law constant for absorption of N_2O into aqueous solutions of lithium hydroxide as function of temperature for concentration range (0.1M-2.5M). Points: experimental data with ±6% error bars, Circles (○): First sets of experiments, Triangles (Δ): Repeated sets of experiments, Purple: 2.5M LiOH, Blue: 2M LiOH, Green: 1M LiOH, Turquoise: 0.5M LiOH, Red: 0.1M LiOH, Lines: Weisenberger and Schumpe's model with refitted h_{Li^+} , $h_{CO_3^{2-}}$ and h_T parameters.

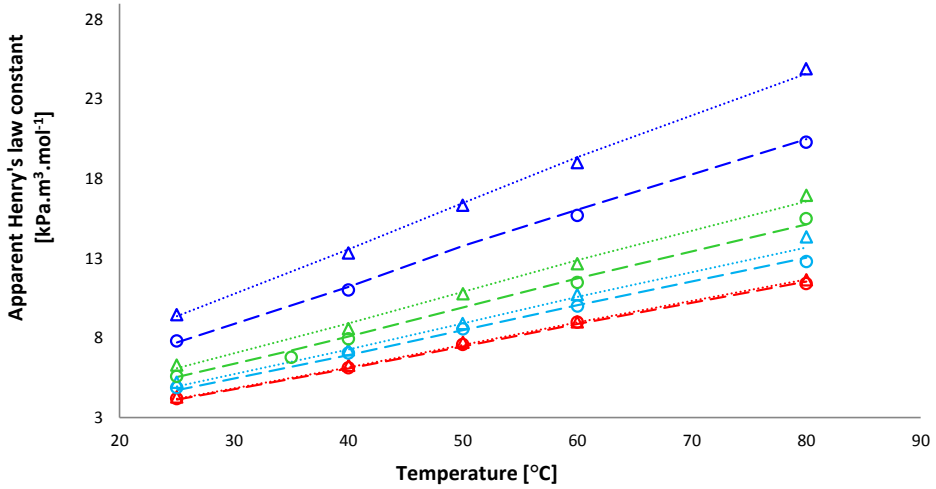

Figure 7. Apparent Henry's law constants for N_2O into aqueous solutions of sodium hydroxide and potassium hydroxide as function of temperature for the concentration range (0.08M-2M). Points: experimental data, Triangles (Δ): NaOH, Circles (○): KOH, Blue: 2M NaOH and 1.76M KOH, Green: 1M NaOH and 0.88M KOH, Turquoise: 0.5M NaOH and 0.44M KOH, Red: 0.1 M NaOH and 0.09M KOH, Lines: Weisenberger and Schumpe's model with refitted h_{Li^+} , $h_{CO_3^{2-}}$ and h_T parameters, Dotted Lines: NaOH solutions, Dashed Lines: KOH solutions.

Figure 7 presents the apparent Henry's law constants for N_2O into aqueous solutions of sodium and potassium hydroxide as function of temperature for the concentration range (0.08M-2M) and temperature range (25-80°C). As mentioned earlier, initially all solutions

were prepared on molar basis but with noted weights also. All KOH results are presented after correcting KOH for measured purity. As shown by Figure 7, the values of apparent Henry's law constant are higher for NaOH solutions (shown by Δ) than those for KOH solutions (shown by ○) for comparable molar concentrations. Comparing the results for the same concentrations of all hydroxides, LiOH, NaOH and KOH, one finds that the values of the apparent Henry's law constant vary as follows:

$$\textbf{\textit{On molar basis}}: \qquad Na^+ > K^+ > Li^+$$

$$\textbf{\textit{On weight basis}}: \qquad Li^+ > Na^+ > K^+$$

The difference increases with increasing temperature and concentration. The same trend has been reported in the literature (Knuutila et al., 2010b) for Na^+ and K^+ as cations. The difference in N_2O solubility in 0.1M NaOH, 0.08M KOH and 0.1M LiOH solutions is almost negligible at 25°C but significant at 80°C and also significant for all temperatures for concentrations greater than 1M. This trend can be clearly observed in Figure 10 where, for all hydroxides, the apparent Henry's law constant is presented as function of molar concentration [mol.L^{-1}] at different temperatures.

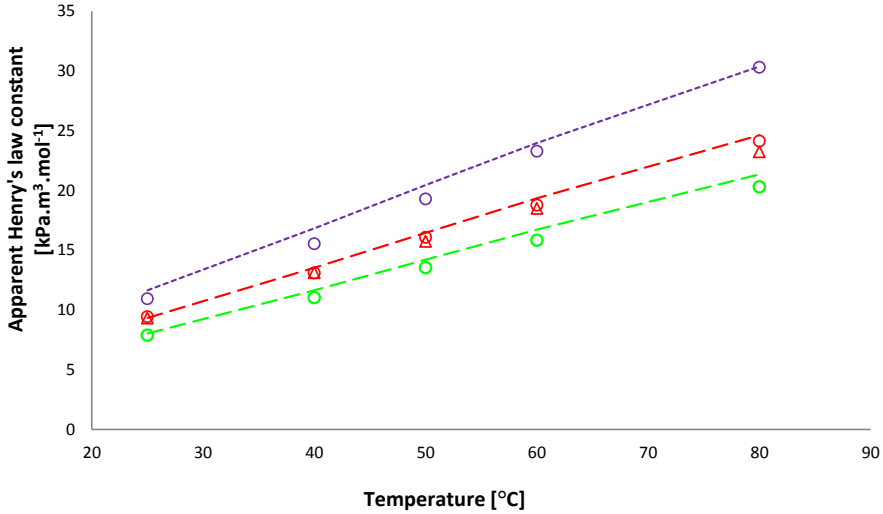

Figure 8. Apparent Henry's law constant for absorption of N_2O into blends of aqueous hydroxides and carbonates with the same cation but different anions. Lines: Weisenberger and Schumpe's model with refitted h_{Li^+} , $h_{CO_3^{2-}}$ and h_T parameters, Points: experimental data, Purple Circles (○): 0.51MNaOH+1M Na_2CO_3, Red Circles (○): 1MNaOH+0.5MNa_2CO_3, Red Triangles (Δ): Repeated 1MNaOH+0.5MNa_2CO_3, Green Circles (○): 0.89MKOH+0.5MK_2CO_3.

The results for the apparent Henry's law constant for N_2O in blends of hydroxides and carbonates are graphically illustrated in Figure 8 and Figure 9. Figure 8 presents blends of hydroxides and carbonates with the same cation (Na^+ or K^+), while Figure 9 shows blends with different cations in hydroxide and carbonate. It has been observed that carbonates, compared to hydroxides, exhibit higher values of apparent Henry's law constant for the same total cation concentration It has also been found that Na^+ , compared to K^+ and Li^+, shows the

highest value for the apparent Henry's law constant at the same molar concentration. Further discussions on blends is given after the modeling results

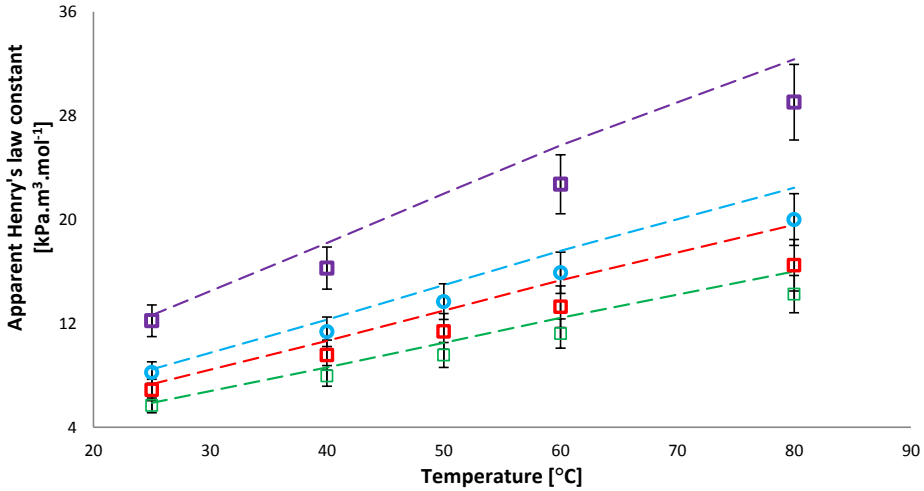

Figure 9. Apparent Henry's law constant for absorption of N_2O into blends of aqueous hydroxides and carbonates with different cations. Lines: Weisenberger and Schumpe's model with refitted h_{Li^+} , $h_{CO_3^{2-}}$ and h_T parameters, Points: experimental data with ±10% error bars, Squares (□): blends of hydroxides, Circles (○): blends of hydroxides and carbonates, Purple: 1MLiOH+2MNaOH, Turquoise: 0.89MKOH+0.5MNa_2CO_3, Red: 1MNaOH+0.46MKOH, Green: 0.52MNaOH+0.45MKOH.

3.4. Henry's law constant for infinite dilution of hydroxides

At a particular temperature, when plotting the experimental data for the apparent Henry's law constant as a function of concentration of the absorbents (hydroxides in this work), the curves should end at the N_2O solubility in water when extrapolated back to zero concentration. Figure 10 presents apparent Henry's law constants for N_2O absorption into the aqueous hydroxides of Li^+, Na^+ and K^+ cations as function of molarity for the temperatures; 25°C, 40°C, 50°C, 60°C and 80°C. Apparent Henry's law constant isotherms (constant temperature lines) for the above mentioned temperatures can be obtained as 2nd order polynomials fitted to the experimental data for H vs. molarity as:

$$H[kPa.m^3.mol^{-1}] = aM^2 + bM + c \quad (13)$$

Here $M[mol.L^{-1}]$ is the molar concentration of the hydroxides and $c[kPa.m^3.mol^{-1}]$ is the y-intercept which represents the value of the apparent Henry's law constant for infinite dilution of hydroxides, *i.e.* for zero hydroxide concentration.

As the solubility of N_2O in all the studied solutions is very low, see section 2.3, the Henry's law constants obtained can be considered as for infinite dilution in N_2O. Details and statistics of the apparent Henrys' law constant for infinite dilution of hydroxides, $H^{\infty}_{N_2O}[kPa.m^3.mol^{-1}]$ deduced from the experimental data are provided in Table 3. Both

experimental data and Weisenberger and Schumpe's model (Weisenberger and Schumpe, 1996) with refitted h_{Li^+} , $h_{CO_3^{2-}}$ and h_T parameters reduce to the apparent Henry's law constant for infinite dilution of hydroxides, $H^{\infty}_{N_2O}\,[kPa.m^3.mol^{-1}]$, when extrapolated to zero concentration of hydroxides.

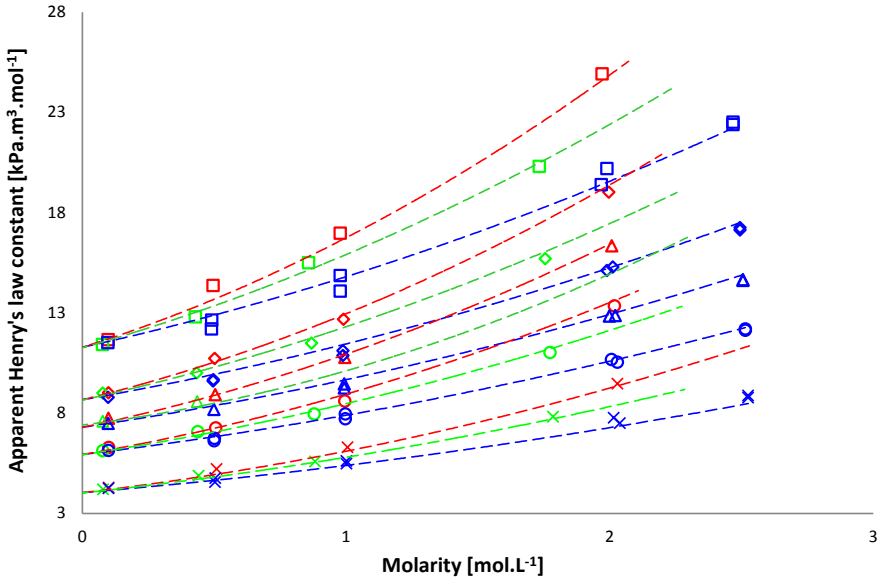

Figure 10. Apparent Henry's law constant for absorption of N_2O into aqueous solutions of hydroxides. Lines: 2nd order polynomials fitted to experimental data and Weisenberger and Schumpe's model with refitted h_{Li^+} , $h_{CO_3^{2-}}$ and h_T parameters and extended back to zero value of concentration to get infinite dilution Henry's law constant $H^{\infty}_{N_2O}$, Points: experimental data, Blue: Li^+ cation, Red: Na^+ cation, Green: K^+ cation, Cross (×): 25°C, Circles(○): 40°C, Triangles (Δ): 50°C, Diamonds (◊): 60°C; Squares (□): 80°C.

Table 3: Apparent Henry's law constant for infinite dilution of hydroxides Li^+, Na^+ and K^+ cations from 25-80°C

T (°C)	$H^{\infty}_{N_2O}\,[kPa.m^3.mol^{-1}]$ as obtained from Figure 10					$H^{water}_{N_2O}[kPa.m^3.mol^{-1}]$		Comparison of average $H^{\infty}_{N_2O}$ with $H^{water}_{N_2O}$ from Experiments and Jou's correlation	
	LiOH	NaOH	KOH	Avg. of hydro-xides	SD for hydro-xides	Exp.	Jou's corre-lation	Avg. of hydroxides, water and Jou's correlation	SD for hydroxides, water and Jou's correlation
25	4.0353	4.0332	4.0209	4.0298	0.008	4.093	4.0135	4.0455	0.04
40	5.9366	5.9363	5.9251	5.9327	0.007	5.911	5.9069	5.9168	0.01
50	7.2963	7.2937	7.406	7.332	0.064	7.227	7.2617	7.2736	0.05
60	8.6693	8.6647	8.6476	8.6605	0.011	8.569	8.6305	8.6202	0.05
80	11.282	11.279	11.255	11.272	0.015	11.31	11.2376	11.2723	0.03
Average					**0.021**				**0.04**

As presented in Table 3, the apparent Henry's law constant for infinite dilution of hydroxides, obtained from LiOH, NaOH and KOH data shows an average standard deviation of 0.021 [kPa.m^3.mol^{-1}] from the average value. This is within the average standard deviation of $H_{N_2O}^{\infty}[kPa.m^3.mol^{-1}]$ from experimental values of $H_{N_2O}^{water}[kPa.m^3.mol^{-1}]$ and values of $H_{N_2O}^{water}[kPa.m^3.mol^{-1}]$ obtained from Jou's correlation (Jou et al., 1992), found as 0.04 [kPa.m^3.mol^{-1}]. The good agreement with solubilities in water when extrapolating to zero concentration of hydroxides, and the fact that the three cations give the same values, well within experimental uncertainty, is gratifying and also shows that the data obtained constitute a consistent data set.

3.5. Modeling and Parameter Fitting

The experimental data obtained in this study, together with the literature data referred in Table 5, were used for parameter fitting in the Weisenberger and Schumpe model (Weisenberger and Schumpe, 1996). First of all the data were compared with the original Weisenberger and Schumpe model.

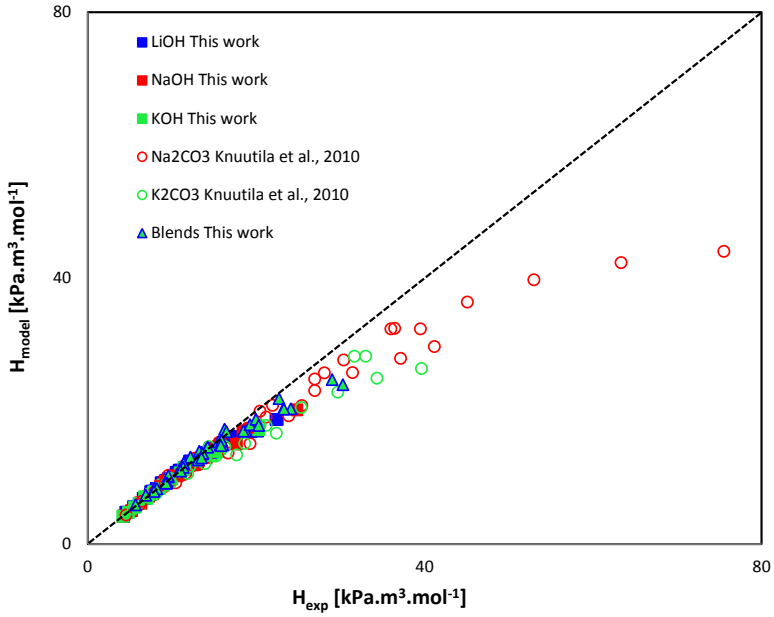

Figure 11. Parity plot showing a comparison between predictions by the original Weisenberger and Schumpe model and experimental data. Blue: Li^+ cation, Red: Na^+ cation, Green: K^+ cation, Squares (□): hydroxides, Circles (○): carbonates, Triangles(Δ): blends.

The parity plot presented as Figure 11 shows the model with the original parameters and it is observed to give very good representation of data at lower temperatures, up to 40°C, but it under-predicts the apparent Henry's law constants at temperatures higher than 40°C. It has also been observed and reported by (Knuutila et al., 2010b)that the gas-specific parameter for temperature effect, h_T , given by (Weisenberger and Schumpe, 1996) is far too low and is the cause of the under-estimation of the Henry's law constants at the higher temperatures.

The reason for the under-prediction at higher temperatures is that the parameter h_T in the original model, which describes the temperature effect on gas solubility, is valid only up to 40°C whereas the experimental data go up to 80°C. Another weak point of the original model parameters, as also described by the authors, is the concentration limitation of 2 kmol.m^{-3}. The presented experimental data for hydroxides, carbonates and blends used for parameter fitting in this work go up to 3 kmol.m^{-3}.

In a first adjustment of the model, the parameter h_T was re-fitted to all the experimental data mentioned in Table 5 using a nonlinear model fitting program, MODFIT, previously used by several authors e.g., (Øyaas et al., 1995). The objective function used for refitting of parameters was minimization of the Average Absolute Relative Deviation given as:

$$AARD[-] = \frac{1}{n}\sum_{i=1}^{n}\frac{\left|\rho_i^{Exp} - \rho_i^{Model}\right|}{\left|\rho_i^{Exp}\right|} \quad (14)$$

The parity plot, comparing the model with the new h_T and the experimental data, is presented in Figure 12. It can be observed that the model presented by Figure 12 represents the experimental data at higher temperatures much better than the original model. The original value of h_T suggested by (Weisenberger and Schumpe, 1996) was -4.79×10^{-4} [m^3.kmol^{-1}.K^{-1}] while the value given by (Knuutila et al., 2010b) is -0.1809×10^{-4} [m^3.kmol^{-1}.K^{-1}]. The h_T values suggested by both authors appear with negative sign and the higher negative value suggested by (Weisenberger and Schumpe, 1996) is the reason for the under-predictions of the apparent Henry's law constant by the model at temperatures above 40°C. The refitted value of h_T in the model presented by Figure 12 is +0.318×10^{-4} [m^3.kmol^{-1}.K^{-1}]. Although the model with refitted h_T parameter improves the predictions at temperatures higher than 40°C, especially for Na_2CO_3, it results in over-predictions for hydroxides (especially LiOH) and blends. Moreover K_2CO_3 is still under-predicted at higher temperatures.

As a final approach, the results for K_2CO_3 and LiOH were improved by refitting h_{Li^+} and $h_{CO_3^{-2}}$, together with h_T, in the model. The gas specific parameter h_{G_O} for the N_2O solubility and other ion specific parameters were not changed because nothing was gained by refitting them. Figure 13 gives the parity plot for the model with refitted h_{Li^+}, $h_{CO_3^{2-}}$ and h_T parameters. As displayed by the red circles in Figure 13, the data points for 20 wt.% (2.23M) Na_2CO_3 at 70°C and 80°C are still not predicted well by the model. An attempt to fit these two data points, either by refitting h_T or h_{Na^+} and $h_{CO_3^{2-}}$ resulted in larger deviations for the rest of the data sets including Na_2CO_3 itself. Blends are slightly over-predicted (maximum up to 18%), but improving the fit for blends results in higher deviations for carbonates and hydroxides. One explanation to this could be related to the amount of data for single cation systems (KOH, NaOH, LiOH, K_2CO_3, Na_2CO_3) compared to blends. As seen from Table 5, total of 151 data points for single cation systems were fitted where as the number for the blends was 39. All the data points were given the same weight during the fitting, thus resulting in more overall weight for the single cation systems. It is not possible to conclude, based on this work, if the over-predictions for the blends are due to the simplicity of the Weisenberger and Schumpe model or the fitting procedure.

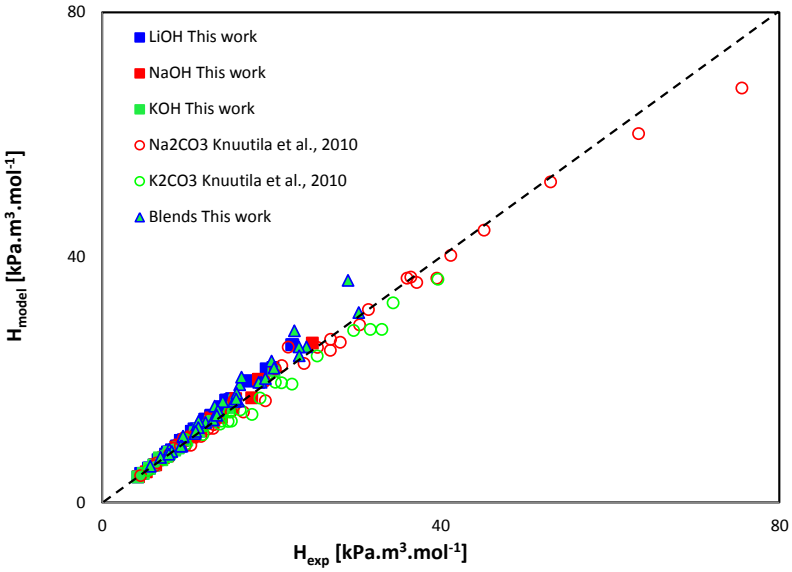

Figure 12. Parity plot for the Weisenberger and Schumpe's model with refitted h_T parameter and experimental data. Blue: Li^+ cation, Red: Na^+ cation, Green: K^+ cation, Squares (□): hydroxides, Circles (○): carbonates, Triangles(Δ):blends.

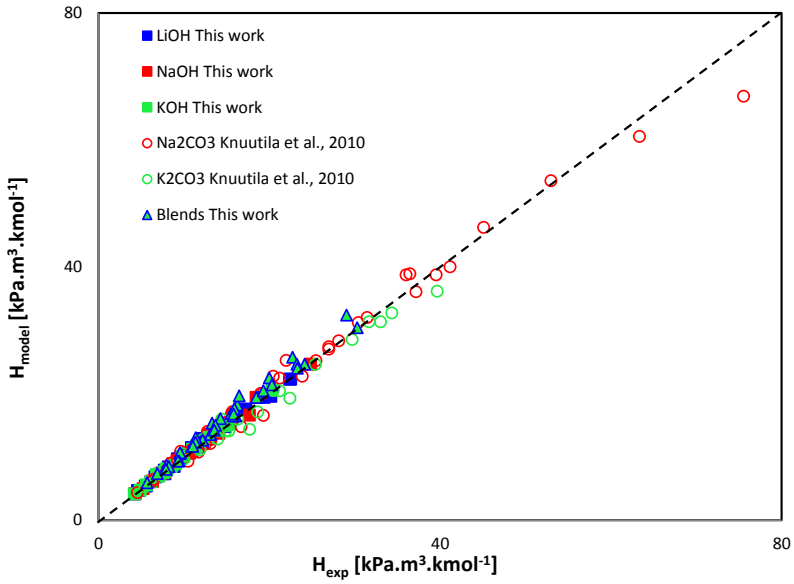

Figure 13. Parity plot for the Weisenberger and Schumpe's model with refitted h_{Li^+} , $h_{CO_3^{2-}}$ and h_T parameters and experimental data. Blue: Li^+ cation, Red: Na^+ cation, Green: K^+ cation, Squares (□): hydroxides, Circles (○): carbonates, Triangles(Δ):blends.

The parameters used in the above mentioned three approaches are presented in Table 4. The second column of Table 4 gives the original Weisenberger and Schumpe's model parameters (Weisenberger and Schumpe, 1996). The third column of Table 4 highlights the

refitted h_T parameter only and the last column presents the suggested model with refitted h_{Li^+}, $h_{CO_3^{2-}}$ and h_T. The last column shows also the change in values of refitted parameters with respect to those originally proposed by Weisenberger and Schumpe (Weisenberger and Schumpe, 1996). The new determined gas specific parameter for temperature effect h_T, indicates the stronger dependence of solubility on temperature.

Table 4: The sets of parameters for Weisenberger and Schumpe's model to estimate Henry's Law constant for N_2O solubility in aqueous solutions containing Li^+, Na^+, K^+ cations and OH^-, CO_3^{2-} anions (equations 3-4)

Parameters	Original	With refitted h_T	With refitted h_{Li^+}, $h_{CO_3^{2-}}$ and h_T
$h_{Li^+}\,[m^3.kmol^{-1}]$	0.0754	0.0754	**0.0618 (18 % decrease)**
$h_{Na^+}\,[m^3.kmol^{-1}]$	0.1143	0.1143	0.1143
$h_{K^+}\,[m^3.kmol^{-1}]$	0.0922	0.0922	0.0922
$h_{OH^-}\,[m^3.kmol^{-1}]$	0.0839	0.0839	0.0839
$h_{CO_3^{2-}}\,[m^3.kmol^{-1}]$	0.1423	0.1423	**0.1582 (11 % increase)**
$h_{N_2O}\,[m^3.kmol^{-1}]$	- 0.0085	- 0.0085	-0.0085
$h_T\,[m^3.kmol^{-1}.K^{-1}]\times 10^4$	**- 4.79****	**+0.318**	**-0.7860 (84 % increase)**

****Experimental temperature range for the validation of original h_T parameter is 0-40°C**

Table 5: Statistics of parameter fitting in Weisenberger and Schumpe's Model for N_2O solubility in hydroxides, carbonates and blends of Li^+, Na^+ and K^+

			% AARD (Average Absolute Relative Deviation)			
Data Set	**Temperature range (°C)**	**Conc. range (wt.%)**	**No. of data points**	**With original parameters**	**With refitted h_T**	**With refitted h_{Li^+}, $h_{CO_3^{2-}}$ and h_T**
Hydroxides (This work)			**83**	**3.8**	**5.0**	**2.1**
LiOH	25 - 80	0.24 – 5.67	44	3.6	7.1	2.1
NaOH	25 - 80	0.4 – 7.48	19	4.6	2.9	2.4
KOH	25 - 80	0.5 – 8.18	20	3.6	2.4	1.8
Carbonates (Knuutila et al., 2010b)			**68**	**11.9**	**5.9**	**5.3**
Na_2CO_3	25 - 80	1- 20	43	11.1	5.0	5.3
K_2CO_3	25 - 80	5 - 30	25	13.2	7.5	5.5
Blends (This work)	25 - 80	1.99- 11.38	**39**	**5.9**	**8.5**	**6.9**
Total			**190**	**7.1**	**6.1**	**4.3**

The suggested set of parameters given by the last column of Table 4 is, in our view, close to an optimal solution with adequate representation of the experimental data (4.3% AARD), reasonable coherence with the original model, as only 3 out of 7 parameters were refitted, and good agreement between all the three data sets (hydroxides, carbonates and blends). The model with only refitted h_T as shown by the third column of Table 4, is still reasonable and by using this, one avoids losing the generality of the original (Weisenberger and Schumpe, 1996) model. The suggested model with refitted h_{Li^+}, $h_{CO_3^{2-}}$ and h_T, however, is better for hydroxide and carbonate systems with Li^+, Na^+ and K^+ cations and represents the experimental results with very good accuracy. The statistical details with comparisons of average absolute relative deviation (AARD) for the three datasets, hydroxides, carbonates and blends, are provided in Table 5. As shown by Table 5, a total of 190 experimental points were used for the parameter fitting. The original Weisenberger and Schumpe's model shows

7.1% AARD, the model with refitted h_T improves the AARD to 6.1% and finally, the suggested model with refitted h_{Li^+}, $h_{CO_3^{2-}}$ and h_T represents the experimental data with 4.3% AARD. Hydroxides are the best represented data where the suggested refitted model has only 2.1% AARD.

As previously mentioned, Figure 8 presents the blends of hydroxides and carbonates with the same cation while Figure 9 shows the blends of hydroxides and carbonates with different cations. It has been observed that blends with same cation and different anions, as shown by Figure 8, are well predicted (less than 6% AARD) by the proposed model while the blends with different cations and same anion as shown by Figure 9, display higher deviations. The deviations for blends are within experimental uncertainties as shown by the ±10% error bars on the experimental data. Although all experimental work was performed with intense care, it is evident from repeated experiments on identical solutions of 2.5M LiOH (0.4% average SD), 0.5M, 1M and 2M LiOH (1.3% average SD), and 1M NaOH+0.5M Na_2CO_3 (0.9% average SD), that experimental uncertainties, apart from other factors related to experimental set-up and procedure, strongly depend on human error involved in preparation of solutions, especially when solutions of solid solutes are prepared on molar basis. These uncertainties are expected to increase with the addition of more components, as in the case of blends. Hence, the experimental data for LiOH are presented with ±6% error bars and the data for blends with ±10% error bars.

Conclusions

The apparent Henry's law constant for the solubility of N_2O into water, aqueous solutions of hydroxides containing lithium, sodium and potassium counter ions and blends of hydroxides with carbonates were experimentally determined in the temperature range (25-80°C) and the concentration (0.08-3M). The values for the apparent Henry's law constant at infinite dilution of hydroxides deduced from experimental data, experimental data for water measured in this work and Jou's correlation (Jou et al., 1992) for the solubility of N_2O into water, agree well with a standard deviation of 0.04 [kpa.m^3.mol^{-1}]. Additionally, the densities of water, aqueous solutions of hydroxides and/or carbonates were measured with an Anton Paar Stabinger Density meter for the temperature range (25-80°C). The density data measured in this work display less than 0.3% AARD when compared with the Laliberté and Cooper density model (Laliberte and Cooper, 2004) based on literature data. By using the experimental data from this work and from(Knuutila et al., 2010b), the ion specific parameters in the model of Weisenberger and Schumpe (Weisenberger and Schumpe, 1996) for Li^+, CO_3^{2-} and the gas specific parameter for the temperature effect on N_2O, h_T , were refitted. The range of the model with refitted parameters is extended to concentrations up to 3M and temperatures up to 80°C providing reasonably good representation (4.3% AARD) of experimental data for hydroxides, carbonates and blends of Li^+, Na^+, and K^+ counter ions.

Acknowledgement

The financial and technical support for this work by Faculty of Natural Sciences and Technology and Chemical Engineering Department of NTNU, Norway is greatly appreciated.

References

Akerlof, G., and Kegeles, G. (1939). The density of aqueous solutions of sodium hydroxide. *Journal of the American Chemical Society* **61**(5)**,** 1027-1032.

Al-Ghawas, H. A., Hagewiesche, D. P., Ruiz-Ibanez, G., and Sandall, O. C. (1989). Physicochemical properties important for carbon dioxide absorption in aqueous methyldiethanolamine. *Journal of Chemical and Engineering Data* **34**(4)**,** 385-391.

Anderson, C., Harkin, T., Ho, M., Mumford, K., Qader, A., Stevens, G., and Hooper, B. (2013). Developments in the CO_2CRC UNO MK 3 Process: A Multi-component Solvent Process for Large Scale CO_2 Capture. *Energy Procedia* **37,** 225-232.

Aronu, U. E., Hartono, A., and Svendsen, H. F. (2012). Density, viscosity, and N_2O solubility of aqueous amino acid salt and amine amino acid salt solutions. *The Journal of Chemical Thermodynamics* **45**(1)**,** 90-99.

Clarke, J. (1964). Kinetics of Absorption of Cardon Dioxide in Monoethanolamine Solutions at Short Contact Times. *Industrial & Engineering Chemistry Fundamentals* **3**(3)**,** 239-245.

Corti, A. (2004). Thermoeconomic evaluation of CO_2 alkali absorption system applied to semi-closed gas turbine combined cycle. *Energy* **29**(3)**,** 415-426.

Cullinane, J. T., and Rochelle, G. T. (2004). Carbon dioxide absorption with aqueous potassium carbonate promoted by piperazine. *Chemical Engineering Science* **59**(17)**,** 3619-3630.

Dindore, V., Brilman, D., and Versteeg, G. (2005). Modelling of cross-flow membrane contactors: mass transfer with chemical reactions. *Journal of membrane science* **255**(1)**,** 275-289.

Green, D., and Perry, R. (2007). "Perry's Chemical Engineers' Handbook, Eighth Edition." McGraw-Hill Education.

Haimour, N., and Sandall, O. C. (1984). Absorption of carbon dioxide into aqueous methyldiethanolamine. *Chemical Engineering Science* **39**(12)**,** 1791-1796.

Hartono, A., Juliussen, O., and Svendsen, H. F. (2008). Solubility of N_2O in aqueous solution of diethylenetriamine. *Journal of Chemical & Engineering Data* **53**(11)**,** 2696-2700.

Hershey, J., Damesceno, R., and Millero, F. (1984). Densities and compressibilities of aqueous HCl and NaOH from 0 to 45 °C. The effect of pressure on the ionization of water. *Journal of solution chemistry* **13**(12)**,** 825-848.

Hikita, H., Asai, S., Ishikawa, H., and Esaka, N. (1974). Solubility of nitrous oxide in sodium carbonate-sodium bicarbonate solutions at 25. deg. and 1 atm. *Journal of Chemical and Engineering Data* **19**(1)**,** 89-92.

Hitchcock, L. B. (1937). Mechanism of Gas-Liquid Reaction Batch Absorption of Carbon Dioxide by Stirred Alkaline Solutions. *Industrial & Engineering Chemistry* **29**(3)**,** 302-308.

Hitchcock, L. B., and McIlhenny, J. (1935). Viscosity and density of pure alkaline solutions and their mixtures. *Industrial & Engineering Chemistry* **27**(4)**,** 461-466.

Jamal, A. (2002). Absorption and desorption of CO_2 and CO in alkanolamine systems. *Ph.D. Thesis. University of British Columbia, Vancouver, B.C.*

Joosten, G. E., and Danckwerts, P. V. (1972). Solubility and diffusivity of nitrous oxide in equimolar potassium carbonate-potassium bicarbonate solutions at 25 degree and 1 atm. *Journal of Chemical and Engineering Data* **17**(4)**,** 452-454.

Jou, F.-Y., Carroll, J. J., Mather, A. E., and Otto, F. D. (1992). The solubility of nitrous oxide in water at high temperatures and pressures. *Zeitschrift fur physikalische chemie-frankfurt am main then wiesbaden then munchen-* **177,** 225-239.

Knuutila, H., Juliussen, O., and Svendsen, H. F. (2010). Density and N_2O solubility of sodium and potassium carbonate solutions in the temperature range 25 to 80 degrees C. *Chemical Engineering Science* **65**(6)**,** 2177-2182.

Knuutila, H., Svendsen, H. F., and Anttila, M. (2009). CO_2 capture from coal-fired power plants based on sodium carbonate slurry; a systems feasibility and sensitivity study. *International Journal of Greenhouse Gas Control* **3**(2)**,** 143-151.

Kohl, A. L., and Nielsen, R. (1997). "Gas purification." Gulf Professional Publishing.

Kumar, P. S., Hogendoorn, J., Feron, P., and Versteeg, G. (2001). Density, viscosity, solubility, and diffusivity of N_2O in aqueous amino acid salt solutions. *Journal of Chemical & Engineering Data* **46**(6)**,** 1357-1361.

Laddha, S., Diaz, J., and Danckwerts, P. (1981). The N_2O analogy: The solubilities of CO_2 and N_2O in aqueous solutions of organic compounds. *Chemical Engineering Science* **36**(1)**,** 228-229.

Laliberte, M., and Cooper, W. E. (2004). Model for calculating the density of aqueous electrolyte solutions. *Journal of Chemical & Engineering Data* **49**(5)**,** 1141-1151.

Lanman, E. H., and Mair, B. J. (1934). The compressibility of aqueous solutions. *Journal of the American Chemical Society* **56**(2)**,** 390-393.

Li, M.-H., and Lai, M.-D. (1995). Solubility and Diffusivity of N_2O and CO_2 in (Monoethanolamine+ N-Methyldiethanolamine+ Water) and in (Monoethanolamine+ 2-Amino-2-methyl-1-propanol+ Water). *Journal of Chemical and Engineering Data* **40**(2)**,** 486-492.

Li, M.-H., and Lee, W.-C. (1996). Solubility and Diffusivity of N_2O and CO_2 in (Diethanolamine+ N-Methyldiethanolamine+ Water) and in (Diethanolamine+ 2-Amino-2-methyl-1-propanol+ Water). *Journal of Chemical & Engineering Data* **41**(3)**,** 551-556.

Mandal, B. P., Kundu, M., and Bandyopadhyay, S. S. (2005). Physical solubility and diffusivity of N_2O and CO_2 into aqueous solutions of (2-amino-2-methyl-1-propanol+ monoethanolamine) and (N-methyldiethanolamine+ monoethanolamine). *Journal of Chemical & Engineering Data* **50**(2)**,** 352-358.

Mumford, K. A., Smith, K. H., Anderson, C. J., Shen, S., Tao, W., Suryaputradinata, Y. A., Qader, A., Hooper, B., Innocenzi, R. A., and Kentish, S. E. (2011). Post-combustion capture of CO_2: results from the solvent absorption capture plant at Hazelwood power station using potassium carbonate solvent. *Energy & fuels* **26**(1)**,** 138-146.

Øyaas, J., Storrø, I., Svendsen, H., and Levine, D. W. (1995). The effective diffusion coefficient and the distribution constant for small molecules in calcium-alginate gel beads. *Biotechnology and bioengineering* **47**(4)**,** 492-500.

Rachinskiy, K., Kunze, M., Graf, C., Schultze, H., Boy, M., and Büchs, J. (2014). Extension and application of the “enzyme test bench” for oxygen consuming enzyme reactions. *Biotechnology and bioengineering* **111**(2)**,** 244-253.

Randall, M., and Scalione, C. C. (1927). The conductance of dilute aqueous solutions of the alkali hydroxides at 25°C. *Journal of the American Chemical Society* **49**(6)**,** 1486-1492.

Rischbieter, E., Stein, H., and Schumpe, A. (2000). Ozone solubilities in water and aqueous salt solutions. *Journal of Chemical & Engineering Data* **45**(2)**,** 338-340.

Rochelle, G. T. (2012). Thermal degradation of amines for CO_2 capture. *Current Opinion in Chemical Engineering* **1**(2)**,** 183-190.

Roux, A., Perron, G., and Desnoyers, J. (1984). Heat Capacities, Volumes, Expansibilities, and Compressibilities of Concentrated Aqueous Solutions of LiOH, NaOH, and KOH. *Can. J. Chem* **62,** 878-885.

Schumpe, A. (1993). The estimation of gas solubilities in salt solutions. *Chemical Engineering Science* **48**(1)**,** 153-158.

Sechenov, M. (1889). Über die Konstitution der Salzlösungen auf Grund ihres Verhaltens zu Kohlensäure. *Z. Phys. Chem* **4,** 117.

Shimonishi, Y., Zhang, T., Imanishi, N., Im, D., Lee, D. J., Hirano, A., Takeda, Y., Yamamoto, O., and Sammes, N. (2011). A study on lithium/air secondary batteries—Stability of the

NASICON-type lithium ion conducting solid electrolyte in alkaline aqueous solutions. *Journal of Power Sources* **196**(11)**,** 5128-5132.

Sipos, P. M., Hefter, G., and May, P. M. (2000). Viscosities and densities of highly concentrated aqueous MOH solutions (M^+= Na^+, K^+, Li^+, Cs^+,$(CH_3)_4N^+$) at 25°C. *Journal of Chemical & Engineering Data* **45**(4)**,** 613-617.

Smith, K., Xiao, G., Mumford, K., Gouw, J., Indrawan, I., Thanumurthy, N., Quyn, D., Cuthbertson, R., Rayer, A., and Nicholas, N. (2013). Demonstration of a concentrated potassium carbonate process for CO_2 capture. *Energy & fuels* **28**(1)**,** 299-306.

Tham, M. J., Gubbins, K. E., and Walker Jr, R. D. (1967). Densities of potassium hydroxide solutions. *Journal of Chemical and Engineering Data* **12**(4)**,** 525-526.

Vas Bhat, R., Kuipers, J., and Versteeg, G. (2000). Mass transfer with complex chemical reactions in gas–liquid systems: two-step reversible reactions with unit stoichiometric and kinetic orders. *Chemical Engineering Journal* **76**(2)**,** 127-152.

Versteeg, G. F., and Van Swaaij, W. (1988). Solubility and diffusivity of acid gases (carbon dioxide, nitrous oxide) in aqueous alkanolamine solutions. *Journal of Chemical and Engineering Data* **33**(1)**,** 29-34.

Wagner, W., and Pruß, A. (2002). The IAPWS formulation 1995 for the thermodynamic properties of ordinary water substance for general and scientific use. *Journal of Physical and Chemical Reference Data* **31**(2)**,** 387-535.

Weisenberger, S., and Schumpe, A. (1996). Estimation of gas solubilities in salt solutions at temperatures from 273 K to 363 K. *AIChE Journal* **42**(1)**,** 298-300.

Welge, H. J. (1940). Absorption of carbon dioxide in aqueous alkalies. *Industrial & Engineering Chemistry* **32**(7)**,** 970-972.

Xu, Z. C., Wang, S. J., and Chen, C. H. (2013). Kinetics Study on CO_2 Absorption with Aqueous Solutions of 1,4-Butanediamine,2-(Diethylamino)-ethanol, and Their Mixtures. *Industrial & Engineering Chemistry Research* **52**(29)**,** 9790-9802.

Appendices

Table A1: Density Data for water form 25-80°C

Density [g.cm^{-3}]	Temperature [°C]						Average
Experimental	25	30	40	50	60	80	
	0.99809	0.99572	0.99222	0.98813	0.98327	0.97410	
	0.99818	0.99571	0.99223	0.98812	0.98328	0.97529	
	0.99812	0.99549	0.99221	0.98811	0.98329	0.97291	
	0.99710	0.99948	0.99224	0.98813	0.98330	0.97305	
	0.99709	0.99948	0.99223	0.98812	0.98329	0.97187	
	0.99704	0.99948	0.99226	0.98812	0.98328	0.97423	
	0.99710	0.99570	0.99222	0.98810	0.98339	0.97227	
	0.99709	0.99569	0.99223	0.98810	0.98338	0.97095	
	0.99704	0.99572	0.99236	0.98811	0.98329	0.97409	
	0.99707	0.99571	0.99233	0.98812	0.98328	0.97405	
Average [g.cm^{-3}]	**0.99739**	**0.99682**	**0.99225**	**0.98812**	**0.98331**	**0.97328**	
***Standard Deviation**	4.8E-04	1.7E-03	4.8E-05	1.0E-05	4.1E-05	1.2E-03	**6.0E-04**
Density model of Wanger et al., 2002 [g.cm^{-3}]	**0.99676**	**0.99535**	**0.99203**	**0.98803**	**0.98337**	**0.97204**	
% AARD	0.033	0.131	0.087	0.002	0.003	0.064	**0.053**

Table A2: Density data for Hydroxides of Li^+, Na^+ and K^+ from 25-80°C

	LiOH		NaOH		KOH	
Temperature [°C]	Conc. [wt.%]	Density [kg.m^{-3}]	Conc. [wt.%]	Density [kg.m^{-3}]	Conc. [wt.%]	Density [kg.m^{-3}]
25	0.024	997.86	0.02	1001.95	0.246	1001.34
25	0.12	998.76	0.04	1001.11	0.491	1003.54
25	0.239	1003.5	0.2	1000.13	2.414	1020.64
25	1.187	1011.02	1.959	1020.71	4.731	1041.56
25	2.343	1024.27	3.846	1039.91	9.115	1081.33
25	4.579	1048.22	7.417	1078.61	-	-
30	0.024	996.44	0.02	999.5	0.246	999.97
30	0.12	997.55	0.04	999.67	0.491	1002.12
30	0.239	1002.05	0.2	998.72	2.414	1019.06
30	1.187	1009.54	1.959	1017.71	4.731	1039.81
30	2.343	1022.19	3.846	1038.08	9.115	1079.28
30	4.579	1045.86	7.417	1076.51	-	-
40	0.024	993.03	0.02	993.32	0.246	996.53
40	0.12	994.12	0.04	996.16	0.491	998.65
40	0.239	998.6	0.2	995.26	2.414	1015.35
40	1.187	1006.02	1.959	1013.92	4.731	1035.87
40	4.579	1042.2	3.846	1033.95	9.115	1075
40	-	-	7.417	1071.93	-	-
50	0.024	990.32	0.02	990.51	0.246	993.84
50	0.12	991.79	0.04	990.85	0.491	994.7
50	0.239	994.45	0.2	990.5	2.414	1011.03

50	1.187	1001.85	1.959	1009.55	4.731	1031.67
50	2.343	1014.38	3.846	1029.41	9.115	1070.28
50	4.579	1037.82	7.417	1069.83	-	-
60	0.024	986.6	0.02	984.35	0.246	988.92
60	0.12	988.32	0.04	987.24	0.491	989.84
60	0.239	990.1	0.2	986.28	2.414	1006.35
60	1.187	997.11	1.959	1004.64	4.731	1026.65
60	2.343	1009.69	3.846	1024.42	9.115	1065.54
60	4.579	1033.15	7.417	1062.07	-	-
70	0.024	980.75	0.02	982.61	0.246	982.37
70	0.12	983.12	0.04	982.02	0.491	987.49
70	0.239	981.26	0.2	980.97	2.414	1002.21
70	1.187	991.62	1.959	999.4	4.731	1021.36
70	2.343	1004.58	3.846	1019.13	9.115	1061.19
70	4.579	1028.15	7.417	1056.75	-	-
80	0.024	973.88	0.02	975.31	0.246	977.42
80	1.187	986.13	1.959	993.87	2.414	995.61
80	2.343	1000.46	3.846	1013.68	9.115	1055.48
80	4.579	1023.45	7.417	1051.31	-	-

Table A3: Density data for blends of hydroxides and carbonates of Li^+, Na^+ and K^+ from 25-80°C

Solution	T [°C]	Density [kg.m^{-3}]	Solution	T [°C]	Density [kg.m^{-3}]
***1M (2.18 wt.%) LiOH + 2 M(7.27 wt.%) NaOH**	**25**	1101.2	***1M (3.71 wt.%) NaOH + 0.5M (4.91wt.%) Na_2CO_3**	**25**	1089.2
	30	1099		**30**	1087.1
	40	1094.3		**40**	1082.5
	50	1090.3		**50**	1078.5
	60	1085.2		**60**	1071.1
	80	1075.6		**80**	1056.7
***0.52M(1.96wt.%)NaOH + 0.46 M(2.45 wt.%)KOH**	**25**	1040.6	***1.17M(4.28 wt.%) KOH + 0.5M(4.89 wt.%) Na_2CO_3**	**25**	1090
	30	1038.7		**30**	1087.3
	40	1034.8		**40**	1083.4
	50	1030.9		**50**	1079.7
	60	1026.2		**60**	1075.2
	80	1015.9		**80**	1064.9
***1.03M(3.9 wt.%)NaOH + 0.46M(2.44 wt.%) KOH**	**25**	1059.4	***1.24M(4.54 wt.%) KOH + 0.5M(6.34 wt.%) K_2CO_3**	**25**	1095.6
	30	1057.5		**30**	1093.6
	40	1053.3		**40**	1089.2
	50	1049.3		**50**	1085.3
	60	1044.8		**60**	1080.7
	80	1035.6		**80**	1070.3
***0.5M(1.79 wt.%) NaOH + 1M (9.49 wt.%) Na_2CO_3**	**25**	1117.6			
	30	1115.4			
	40	1110.5			
	50	1106.5			
	60	1102			
	80	1091.7			

*** All molar concentrations are stated at 25°C.**

Table A4: Reproducibility of results for apparent Henry's law constant from 25-80°C

Solution Identity	T [°C]	H [kPa.m^3.kmol^{-1}]					
		Set-1	Set-2	Set-3	Average	SD	%SD
Water	25	4025.1	3957.6	4093.2	4025.3	55.4	1.4
	30	4589.4		-	4589.4	-	-
	40	5819.9	5767.9	5910.8	5832.8	59.1	1
	50	-	-	7227.1	7227.1	-	-
	60	8570.8	8457.3	8569.7	8532.6	53.3	0.6
	80	11376.7	11225.6	11307.2	11303.1	61.7	0.5
	100	-	14806	-	14806	-	-
	120	-	16504	-	16504	-	-
Average		-	-	-	-	**57.4**	**0.9**
2.5M LiOH	25	8763.3	8880.8	-	8822.1	58.7	0.7
	40	12129.4	12194.2	-	12161.8	32.4	0.3
	50	14611	14650.6	-	14630.8	19.8	0.1
	60	17247.6	17126.9	-	17187.2	60.4	0.4
	80	22510.9	22379.9	-	22445.4	65.5	0.3
Average		-	-	-	-	**47.4**	**0.4**

Table A5: N_2O solubility data for hydroxides of Li^+, Na^+ and K^+ from 25-80°C

T [°C]	[wt. %]	Molarity [mol.L^{-1}] LiOH	H [kPa.m^3.kmol^{-1}]	T [°C]	[wt. %]	Molarity [mol.L^{-1}] NaOH	H [kPa.m^3.kmol^{-1}]
25	0.239	0.10	4246	**25**	0.402	0.1	4291
25	1.193	0.50	4550	**25**	2.000	0.51	5211
25	1.195*	0.50	4754	**25**	3.867	1.01	6293
25	2.344	1.00	5612	**25**	7.483	2.03	9462
25	2.344*	1.00	5478	**40**	0.402	0.1	6285
25	4.588	2.02	7770	**40**	2.000	0.51	7261
25	4.658*	2.04	7503	**40**	3.867	1	8593
40	0.239	0.10	6136	**40**	7.483	2.02	13340
40	1.193	0.50	6620	**50**	0.402	0.1	7735
40	1.195*	0.50	6733	**50**	2.000	0.5	8910
40	2.344	1.00	7958	**50**	3.867	1	10773
40	2.344*	1.00	7708	**50**	7.483	2.01	16334
40	4.588	2.01	10668	**60**	0.402	0.1	9007
40	4.658*	2.03	10532	**60**	2.000	0.5	10724
50	0.239	0.10	7485	**60**	3.867	0.99	12671
50	1.195	0.50	8183	**60**	7.483	2	19013
50	2.344	0.99	9452	**80**	0.402	0.1	11662
50	2.344*	0.99	9244	**80**	2.000	0.5	14356
50	4.588	2.00	12834	**80**	3.867	0.98	16962
50	4.658*	2.02	12859	**80**	7.483	1.97	24917

60	0.239	0.10	8784			**KOH**	
60	1.193	0.50	9590	**25**	0.504	0.08	4199
60	1.195*	0.50	9659	**25**	2.459	0.44	4878
60	2.344	0.99	11103	**25**	4.800	0.88	5589
60	2.344*	0.99	10870	**25**	8.118	1.79	7817
60	4.588	1.99	15106	**40**	0.504	0.08	6123
60	4.658*	2.01	15282	**40**	2.459	0.44	7063
80	0.239	0.10	11510	**40**	4.800	0.88	7949
80	1.193	0.49	12192	**40**	8.118	1.77	11020
80	1.195*	0.49	12638	**50**	0.504	0.08	7593
80	2.344	0.98	14852	**50**	2.459	0.44	8572
80	2.344*	0.98	14077	**60**	0.504	0.08	8988
80	4.588	1.97	19391	**60**	2.459	0.43	9995
80	4.658*	1.99	20190	**60**	4.800	0.87	11482
				60	8.118	1.76	15692
				80	0.504	0.08	11423
				80	2.459	0.43	12800
				80	4.800	0.86	15501
				80	8.118	1.73	20298

*** Repeated sets of experiments with almost same molar concentrations but solutions were not identical.**

****The results for 2.5M (5.647 wt.%) LiOH are given in Table A4. The molarity of this solution changed from 2.53M to 2.47M in temperature range 25-80°C.**

Table A6: N_2O solubility data for blends of hydroxides and carbonates from 25-80°C

Solution	T [°C]	H [kPa.m^3.kmol^{-1}]	Solution	T [°C]	H [kPa.m^3.kmol^{-1}]
1.01M (2.2 wt.%) LiOH + 2.02M (7.3 wt.%) NaOH	**25**	12207	**0.89M (5.19 wt.%) KOH + 0.5M (4.9 wt.%) Na_2CO_3**	**25**	8228
	40	16261		**40**	11365
	50	-		**50**	13678
	60	22725		**60**	15902
	80	29035		**80**	20003
0.52M(1.99 wt.%) NaOH + 0.45M (2.78 wt.%) KOH	**25**	5699	**0.88M (4.54 wt.%) KOH + 0.5M (6.34 wt.%) K_2CO_3**	**25**	7882
	40	7955		**40**	11038
	50	9575		**50**	13540
	60	11221		**60**	15824
	80	14260		**80**	20305
1.04M (3.9 wt.%) NaOH + 0.46M (2.8 wt.%) KOH	**25**	6888	**0.58M (2.02 wt.%) NaOH + 1.23M(11.38wt.%)Na_2CO_3**	**25**	10948
	40	9564		**40**	15535
	50	11394		**50**	19296
	60	13287		**60**	23296
	80	16481		**80**	30308
1.01M (3.7 wt.%) NaOH + 0.51M (4.9 wt.%)Na_2CO_3	**25**	9444	***1M (3.68 wt.%) NaOH + 0.5M (4.85 wt.%) Na_2CO_3**	**25**	9321
	40	13100		**40**	13125
	50	16074		**50**	15744
	60	18781		**60**	18496
	80	24141		**80**	23241

*** Repeated set of experiments show standard deviation of 0.89%.**

6. Paper II

VLE and Apparent Henry's Law Constant Modeling of Aqueous Solutions of Unloaded and Loaded Hydroxides of Lithium, Sodium and Potassium

*Shahla Gondal, Muhammad Usman, Juliana G.M.S. Monteiro, Hallvard F. Svendsen, Hanna Knuutila**

Department of Chemical Engineering, Norwegian University of Science and Technology, N-7491 Trondheim, Norway

Is not included due to copyright

*** Corresponding Author: Hanna.Knuutila@ntnu.no**

7. Paper III

Kinetics of the absorption of carbon dioxide into aqueous hydroxides of lithium, sodium and potassium and blends of hydroxides and carbonates

*Shahla Gondal, Naveed Asif, Hallvard F. Svendsen, Hanna Knuutila**

Department of Chemical Engineering, Norwegian University of Science and Technology, N-7491 Trondheim, Norway

ABSTRACT

In the present work the rates of absorption of carbon dioxide into aqueous hydroxides (0.01–2.0 kmol m^{-3}) and blends of hydroxides and carbonates with mixed counter ions (1–3 kmol m^{-3}) containing Li^+, Na^+ and K^+ as cations were studied in a String of Discs Contactor (SDC). The temperature range was 25–63°C and the conditions were such that the reaction of CO_2 could be assumed pseudo-first-order. The dependence of the reaction rate constant on temperature and concentration/ionic strength and the effect of counter ions were verified for the reaction of CO_2 with hydroxyl ions (OH^-) in these aqueous electrolyte solutions. The infinite dilution second order rate constant $k^{\infty}_{OH^-}$ was derived as an Arrhenius temperature function and the ionic strength dependency of the second order rate constant, k_{OH^-}, was validated by the widely used Pohorecki and Moniuk model (Pohorecki and Moniuk, 1988) with refitted parameters. The contribution of ions to the ionic strength and the model itself, was extended to the given concentration and temperature ranges. The model with refitted parameters represents the experimental data with less than 12% AARD.

*** Corresponding Author: Hanna.Knuutila@ntnu.no**

1. Introduction

The reactions occurring during absorption of CO_2 into aqueous solutions of hydroxides can be expressed by the following equations:

$$CO_{2_{(g)}} \leftrightarrow CO_{2_{(l)}} \quad (1)$$

$$CO_{2_{(l)}} + OH^- \leftrightarrow HCO_3^- \quad (2)$$

$$HCO_3^- \leftrightarrow CO_3^{-2} + H^+ \quad (3)$$

The rate of physical dissolution of gaseous CO_2 into the liquid solution, Eq. (1), is high and the equilibrium at the interface can be described by Henry's law (Pohorecki and Moniuk, 1988). Since reaction Eq. (3) is a proton transfer reaction, it has a very much higher rate constant than reaction Eq. (2) (Hikita et al., 1976). Hence, reaction Eq. (2) governs the overall rate of the process. Hydration of CO_2, Eq. (2), is second order, i.e. first order with respect to both CO_2 and OH^- ions and the rate of reaction on concentration basis can be expressed by the equation:

$$r[kmol.m^{-3}.s^{-1}] = k_{OH^-}[OH^-][CO_2] \quad (4)$$

Here $k_{OH^-}[m^3.kmol^{-1}.s^{-1}]$ is the second order rate constant, $[OH^-]$ and $[CO_2]$ are molar concentrations $[kmol.m^{-3}]$ of hydroxide and carbon dioxide respectively.

It has been known that in the concentration based kinetic expression, the second order rate constant $k_{OH^-}[m^3.kmol^{-1}.s^{-1}]$ depends both on the counter ion and the composition of the solution [(Pohorecki and Moniuk, 1988); (Haubrock et al., 2007); (Knuutila et al., 2010c)]. Since both OH^- and CO_2 concentrations have a direct effect on the reaction rate kinetics, correct modeling or measurement of them is important (Knuutila et al., 2010c). The concentration of CO_2 at the interface is typically found via solubility models proposed by [(Schumpe, 1993); (Weisenberger and Schumpe, 1996); (Gondal et al., 2014a)] or earlier methods, like the models given by (Danckwerts, 1970b) or (Van Krevelen and Hoftijzer, 1948). However, due to the chemical reaction between CO_2 and hydroxyl ions, it is suggested that the N_2O analogy can be employed to estimate the concentration of CO_2 at the interface (Versteeg and Van Swaalj, 1988).

The reaction rate constant for reaction Eq. (2) has previously been published by several authors [(Knuutila et al., 2010c), (Kucka et al., 2002), (Pohorecki and Moniuk, 1988), (Pohorecki, 1976), (Barrett, 1966), (Nijsing et al., 1959), (Himmelblau and Babb, 1958), (Pinsent et al., 1956), (Pinsent and Roughton, 1951)]. The rate constants measured by above mentioned authors were limited either by temperature and concentration ranges or were based on only one counter ion (Na^+ or K^+). The motivation behind the present work is to see the effect of different counter ions (Li^+, Na^+ and K^+) on the reaction rate constant for wider range of temperatures and concentrations.

Classically, the kinetic constant for electrolyte solutions is expressed as function of ionic strength (Astarita et al., 1983)

$$logk_{OH^-} = logk^{\infty}_{OH^-} + bI \quad (5)$$

In Eq. (5), $k_{OH^-}^{\infty}$ is the infinite dilution reaction rate constant, I is the ionic strength of solution and b is a solution dependent constant.

Ideally, the infinite dilution kinetic constant should be independent of cation and is an Arrhenius type temperature function expressed as,

$$k_{OH^-}^{\infty}[m^3.kmol^{-1}.s^{-1}] = Aexp\left(\frac{E_A}{RT}\right) \quad (6)$$

where A [m^3.$kmol^{-1}$.s^{-1}] is the pre-exponential factor, E_A [kJ.$kmol^{-1}$] is the reaction activation energy, R [8.3144 kJ.$kmol^{-1}$.K^{-1}] is the ideal gas law constant and T [K] is absolute temperature.

In the model proposed by (Pohorecki and Moniuk, 1988), they theoretically justified that it seems more logical to use a correlation containing contributions characterizing the different ions, rather than different compounds present in the solution. They proposed the model given by Eq. (7).

$$log\frac{k_{OH^-}}{k_{OH^-}^{\infty,e}} = \sum b_{ion}I_{ion} \quad (7)$$

where I_{ion} [kmol.m^{-3}] is the ionic strength of an ion, b_{ion} [m^3.$kmol^{-1}$] is an ion specific parameter and $k_{OH^-}^{\infty,e}$ is the apparent rate constant for the reaction in Eq.(2) in the infinite dilute solution. Its value at any temperature (18-41°C) can be calculated by Eq.(8) (Pohorecki and Moniuk, 1988).

$$logk_{OH^-}^{\infty,e} = 11.916 - \frac{2382}{T[K]} \quad ; where \;\; k_{OH^-}^{\infty,e}[m^3.kmol^{-1}.s^{-1}] \quad (8)$$

2. Experimental section

2.1. Materials

The purity and suppliers of all chemicals used for the experimental work are given in Table 1. The purity of KOH as provided by the chemical batch analysis report from MERCK was relatively low. Thus it was determined analytically by titration against 0.1N HCl and was found to be 88 wt.%; the rest being water. All other chemicals were used as provided by the manufacturer without further purification or correction.

Table 1: Purity and suppliers of chemicals used for experimental work

Name of Chemical	Purity	Supplier
LiOH	Powder, reagent grade, > 98%	SIGMA-ALDRICH
NaOH	> 99 wt.%, Na_2CO_3 < 0.9% as impurity	VWR
KOH	*88 wt.%	MERCK
Na_2CO_3	> 99.9 wt.%	VWR
K_2CO_3	> 99 wt.%	SIGMA-ALDRICH
CO_2 gas	≥ 99.999 mol%	YARA-PRAXAIR
N_2 gas	≥ 99.6 mol%	YARA-PRAXAIR

*** The purity is based on the titration results against 0.1M HCl. Since the purity was relatively low, all experimental data of KOH are presented after correction for purity.**

All the solutions used for absorption experiments were prepared at room temperature on molar basis by dissolving known weights of chemicals in deionized water and the total weight of deionized water required to make a particular solution was also noted. Therefore the weight fractions of all chemicals and water for all molar solutions were always known.

2.2. Kinetic experiments

The absorption rate of CO_2 into solutions of hydroxides and blends of hydroxides and carbonates were measured for concentrations 0.01–3 kmol.m^{-3} and for temperatures 25–60°C using the string of discs contactor (SDC) apparatus shown in Fig. 1. The SDC apparatus was previously used for kinetics measurements by [(Luo et al., 2012); (Aronu et al., 2011); (Knuutila et al., 2010c); (Hartono et al., 2009); (Ma'mun et al., 2007)].

The apparatus consists of a fan driven gas circulation loop where the gas passes along the string of discs at a velocity independent of the CO_2 absorption flux. This ensures low gas film resistance. The absorption flux is determined by a mass balance between inert gas and CO_2 entering the gas circuit through calibrated mass flow meters, and the gas leaving the circuit through the CO_2 analyzer. Two Bronkhorst Hi-tech mass flow controllers were applied to control the feed gas mixture of CO_2 and N_2. The gas flow in the circulation loop fan was controlled by a Siemens Micro Master Frequency Transmitter. A Fisher–Rosemount BINOS 100 NDIR CO_2 analyzer measured the circuit gas phase CO_2 concentration while a peristaltic liquid pump (EH Promass 83) was used to adjust the liquid rate. The apparatus is equipped with K-type thermocouples at the inlet and outlet of both the gas and liquid phases. Calibration mixtures of CO_2 and N_2 were used for calibration of the analyzers before the start of each experiment. The SDC column operated in counter current flow with liquid from top and gas from bottom.

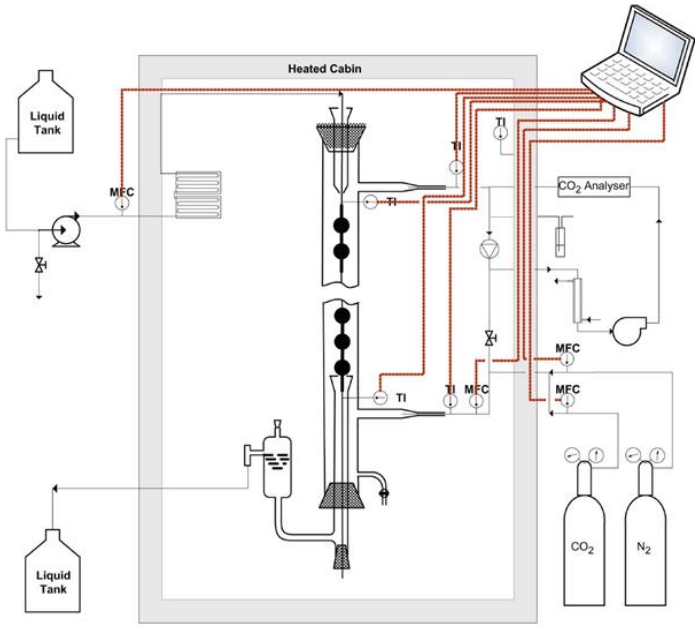

Figure 1: String of Discs Contactor (SDC) kinetic apparatus (Hartono et al., 2009)

The unloaded solutions of hydroxide or blends with carbonate were passed through the column with a flow rate of ~51 mL/min. For every concentration and temperature, the set liquid rate was above the minimum value required to ensure that the flux of CO_2 into solution was independent of liquid flow rate; a condition required for the pseudo-first order assumption to be valid. The same procedure was used by (Luo et al., 2012); (Aronu et al., 2011); (Knuutila et al., 2010c) and (Hartono et al., 2009). When the column attained the required temperature, a known mixture of CO_2 and N_2 was circulated through the column with makeup gas added to maintain the CO_2 level in the gas. Steady state was considered to be achieved when the CO_2-analyzer and temperature transducers indicated constant values. All the data were recorded, using Field Point and LabVIEW data acquisition systems. Average values of state variables were calculated over a 10–25 minutes of steady state operation and were used for the evaluation of kinetics. A more detailed description of the apparatus and experimental procedure is found in (Ma'mun et al., 2007).

3. Overall mass transfer coefficient

The absorption of CO_2 into an aqueous solution can be imagined as a process of CO_2 transfer from the bulk gas phase to the gas/liquid interface and then through a reaction zone to the bulk of liquid. Using a film model, the driving force for mass transfer can be taken as the bulk-interface concentration difference in the liquid phase and the partial pressure difference in the gas phase. Due to continuity, the CO_2 flux from the bulk gas to the interface equals that from the interface to the bulk liquid. According to the two film theory (Lewis and Whitman, 1924), the steady state absorption of CO_2 can then be described by

$$N_{CO_2}[mol.m^{-2}.s^{-1}] = k_g\left(P_{CO_{2,bulk}} - P_{CO_{2,i}}\right) = E_A k_L^o\left(C_{CO_{2,i}} - C_{CO_{2,bulk}}\right) \quad (9)$$

Where $P_{CO_{2,bulk}}[kPa]$ and $P_{CO_{2,i}}[kPa]$ are the partial pressures of CO_2 in bulk gas and at the interface respectively while $C_{CO_{2,i}}[mol.m^{-3}]$ and $C_{CO_{2,bulk}}[mol.m^{-3}]$ are CO_2 concentrations at the interface and in bulk liquid. Here $k_L^0[m.s^{-1}]$ and $k_g[mol.m^{-2}.kpa^{-1}.s^{-1}]$ are liquid side and gas side mass transfer coefficients respectively while $E_A[-]$ is the enhancement factor. The gas film mass transfer coefficient $k_g[mol.m^{-2}kPa^{-1}.s^{-1}]$ can be calculated as:

$$k_g[mol.m^{-2}.kpa^{-1}.s^{-1}] = \frac{k_G[m.s^{-1}]}{RT[kPa.m^3.mol^{-1}]} \quad (10)$$

where $R[kJ.mol^{-1}.K^-]$ is ideal gas law constant, $T[K]$ is absolute temperature. The value of $k_G[m.s^{-1}]$ is calculated according to the method described by (Ma'mun et al., 2007).

The enhancement factor describes the effect of chemical reaction on the liquid side mass transfer coefficient, and can be defined as the ratio of k_L, in the presence of chemical reaction, to the k_L^0, in the absence of chemical reaction, for identical mass transfer driving force.

The CO_2 flux $N_{CO_2}[mol.m^2.s^{-1}]$ can be expressed as the product of an overall mass transfer coefficient and the logarithmic mean pressure difference between inlet and outlet of the SDC contactor.

$$N_{CO_2}[mol.m^{-2}.s^{-1}] = N_{CO_2}^{in} - N_{CO_2}^{out} = K_{ov,G}\Delta p_{CO_{2,LM}} \quad (11)$$

where $K_{ov,G}[mol.m^{-2}.kPa^{-1}.s^{-1}]$, is gas phase based overall mass transfer coefficient, $N_{CO_2}^{in}$ $[mol.m^{-2}.s^{-1}]$ is CO_2 fed to the system from the mass flow controllers and $N_{CO_2}^{out}[mol.m^{-2}.s^{-1}]$ is CO_2 going out from system through the bleed. $\Delta p_{CO_{2,LM}}[kPa]$ is the log mean pressure difference defined as:

$$\Delta p_{CO_{2,LM}}[kPa] = \frac{\left(P_{CO_2}^{in} - P_{CO_{2,b}}^{in}\right) - \left(P_{CO_2}^{out} - P_{CO_{2,b}}^{out}\right)}{ln\frac{\left(P_{CO_2}^{in} - P_{CO_{2,b}}^{in}\right)}{\left(P_{CO_2}^{out} - P_{CO_{2,b}}^{out}\right)}} \tag{12}$$

where $P_{CO_{2,b}}^{in}[kPa]$ and $P_{CO_{2,b}}^{out}[kPa]$ are the equilibrium pressures of CO_2 over the liquid at the SDC contactor inlet and outlet. These can be considered to be zero because the solution is unloaded when it enters the column and the degree of absorption of CO_2 in the column is very small. It should be noted that since the gas flow rate in the SDC is large compared to the flow of CO_2 through the system, the difference between $P_{CO_2}^{in}$ and $P_{CO_2}^{out}$ is very small and the driving force can be equally well calculated by the arithmetic mean $(P_{CO_2}^{in} + P_{CO_2}^{out})/2$.

Hence the overall mass transfer coefficient $K_{ov,G}[mol.m^{-2}.kPa^{-1}.s^{-1}]$ can be calculated directly, merely based on the absorbed CO_2 flux and measured partial pressure of CO_2 in the column as shown in Eq. (11).

4. Evaluation of kinetic constants

The liquid phase equilibrium concentration of CO_2 at the interface is governed by Henry's law and can be calculated by use of an apparent Henry's law constant

$$H_{CO_2}^{app}[kpa.m^3.mol^{-1}] = \frac{P_{CO_2}^*}{C_{CO_2}^*} \tag{13}$$

By introduction of the apparent Henry's law constant $H_{CO_2}^{app}[kPa.m^3.mol^{-1}]$ for equilibrium concentration at interface in Eq. (9), the experimentally determined gas phase mass transfer coefficient can be expressed as:

$$K_{ov,G}[mol.m^{-2}.kPa^{-1}.s^{-1}] = \frac{1}{\frac{1}{k_g} + \frac{H_{CO_2}^{app}}{k_L^o E_A}} \tag{14}$$

The enhancement factor, E_A $[-]$, can be typically estimated by use of Hatta number. The Hatta number $Ha[-]$ is defined as

$$Ha[-] = \frac{\sqrt{k_1 D_{CO_2}}}{k_L^o} \tag{15}$$

where $D_{CO_2}[m^2.s^{-1}]$ is the diffusivity of CO_2 in the liquid solution, $k_L^0[m.s^{-1}]$ is the liquid side mass transfer coefficient and $k_1[s^{-1}]$ is the pseudo first order rate constant.

If the reaction kinetics is to be derived from determination of enhancement factors, the experiment should be carried out in the pseudo first order regime. For pseudo first order irreversible reactions, without the presence of CO_2 in the liquid bulk, the expressions for the enhancement factor E_A $[-]$ from different mass transfer models can be found in (Van Swaaij and Versteeg, 1992). In this work, the two film theory (Lewis and Whitman, 1924) is used and the enhancement factor can be calculated by

$$E_A[-] = \frac{Ha}{\tanh(Ha)} \tag{16}$$

For a first order reaction, in the fast reaction regime (Ha>3), the enhancement factor is

$$E_A[-] = Ha \tag{17}$$

The requirements for the use of the pseudo first order approximation (Danckwerts, 1970b), must be fulfilled. The CO_2 absorption rate must be independent of liquid flow rate, and the Hatta number must be

$$3 < Ha \ll E_{A,\infty} \tag{18}$$

Here, the infinite enhancement factor $E_{A,\infty}[-]$ is defined as the enhancement factor with instantaneous conversion of reactants and the rate of absorption thus completely being limited by the diffusion of governing components. For the film model, it can be calculated by

$$E_{A,\infty,film}[-] = 1 + \frac{D_{reactant} C_{reactant}}{\nu D_{CO_2} C_{CO_2,i}} \tag{19}$$

Here $D_{reactant}[m^2.s^{-1}]$ and $D_{CO_2}[m^2.s^{-1}]$ are diffusivities of the reactant and CO_2 respectively, $\nu[-]$ is the stoichiometric coefficient of reactant in a balanced chemical equation while $C_{reactant}[mol.m^{-3}]$ and $C_{CO_2,i}[mol.m^{-3}]$ are the liquid phase concentrations of the reactant and CO_2 at interface respectively. The infinite enhancement factor for the different mass transfer models can be found in (Van Swaaij and Versteeg, 1992).

Although Eqs. (18) and (19) are valid only for irreversible reactions, in this work, initial rate measurements were performed, where the back reaction is negligible.

Incorporating the definition of Hatta number $Ha[-]$, by Eq. (15) to replace the enhancement factor $E_A[-]$ in Eq. (14) gives:

$$k_1[s^{-1}] = \frac{\left(H_{CO_2}^{app}\right)^2}{\left(\frac{1}{K_{ov,G}} - \frac{1}{k_g}\right)^2 D_{CO_2}} \tag{20}$$

Hence the pseudo first order rate constant $k_1[s^{-1}]$ can be calculated from the experimentally determined value of $K_{ov,G}[mol.m^{-2}.kPa^{-1}.s^{-1}]$, diffusivity of CO_2 , $D_{CO_2}[m^2.s^{-1}]$ and the value of apparent Henry's law constant, $H_{CO_2}^{app}[kPa.m^3.mol^{-1}]$ by use of Eq. (20). The definition of the pseudo first order concentration based kinetic constant for reaction Eq. (2) is

$$r[kmol.m^{-3}.s^{-1}] = k_1[CO_2] \tag{21}$$

From this, the second order rate constant $k_2[m^3.kmol^{-1}.s^{-1}]$ or $k_{OH^-}[m^3.kmol^{-1}.s^{-1}]$ can be calculated by

$$k_{OH^-}[m^3.kmol^{-1}.s^{-1}] = \frac{k_1}{[OH^-]} \quad (22)$$

Various enhancement factor $E_A\ [-]$ models have been suggested based on a number of mass transfer models, ranging from the two film model (Lewis and Whitman, 1924) to the penetration model (Higbie, 1935b) and the surface renewal model (Danckwerts, 1970b). For pseudo first order reactions, these models yield almost same values at high Hatta numbers $Ha[-]$ and the difference at Hatta numbers above 4 is less than 1% (Knuutila et al., 2010c).

5. Physicochemical properties

The calculation of film coefficients and interpretation of the CO_2 absorption rates in aqueous solutions requires the physicochemical properties including density, viscosity, diffusivity and solubility.

The densities of aqueous solutions were taken from (Gondal et al., 2014a)while Laliberte and Cooper's density model (Laliberte and Cooper, 2004) was used for interpolation of density data at required temperatures. The viscosities of aqueous solutions were calculated by Laliberte's viscosity model (Laliberté, 2007) and diffusivities were calculated from viscosities by use of the Stokes–Einstein viscosity-diffusivity correlations [(Barrett, 1966); (Pohorecki and Moniuk, 1988); (Haubrock et al., 2007); (Knuutila et al., 2010c)]. The diffusivity of CO_2 in water was taken from (Danckwerts, 1970b).

The N_2O solubility in aqueous solutions predicted by the refitted Schumpe's model (Weisenberger and Schumpe, 1996) was taken from (Gondal et al., 2014a) and the N_2O analogy was used for calculation of CO_2 solubility. The N_2O and CO_2 solubilities in water, to be used in the N_2O analogy, were taken from (Jou et al., 1992) and (Carroll et al., 1991) respectively. The diffusivity ratio ($\frac{D_{OH^-}}{D_{CO_2}}$) for the calculation of the infinite enhancement factor, $E_{A,\infty,film}[-]$ was set equal to 1.7 as suggested by (Hikita et al., 1976).

6. Results and discussion

6.1. Mass transfer coefficients

The gas film coefficient, $k_g[mol.m^{-2}.kPa^{-1}.s^{-1}]$ and the physical liquid film mass transfer coefficient, $k_L^o[m.s^{-1}]$ for the SDC apparatus were calculated in the same way as in prior publications by [(Luo, Hartono, and Svendsen, 2012); (Aronu, Hartono, and Svendsen, 2011); (Knuutila, Juliussen, and Svendsen, 2010); (Hartono, da Silva, and Svendsen, 2009); (Ma'mun, Dindore, and Svendsen, 2007)]. The overall mass transfer coefficient $K_{ov,G}[mol.m^{-2}.kPa^{-1}.s^{-1}]$ based on the absorbed CO_2 flux and logarithmic mean pressure difference in the column was calculated from Eq. (11). The results for aqueous solutions of LiOH, NaOH, KOH and their blends are given in Tables A1-A4 respectively.

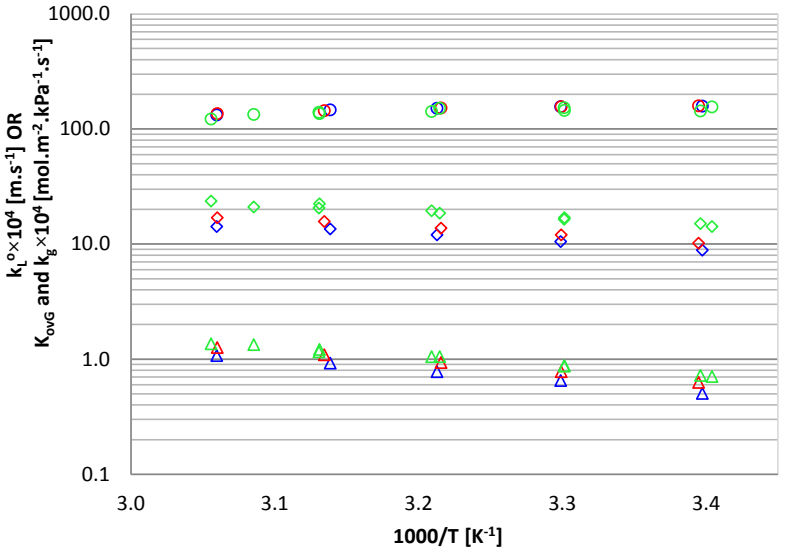

Figure 2: Mass transfer coefficients as function of temperature for 2M LiOH (blue), 2M NaOH (red) and 1.76M KOH (green): Liquid film mass transfer coefficient $k_L^o \times 10^4$ (Δ); Gas film mass transfer coefficient $k_g \times 10^4$ (○); Overall mass transfer coefficient $K_{ov_G} \times 10^4$ (◊).

The mass transfer coefficients for 2M LiOH, 2M NaOH and 1.76M KOH are illustrated in Figure 2 for comparison. The highest concentrations of hydroxides are selected for comparison because the biggest differences based on counter ion (Li^+, Na^+, K^+) are observed for the highest concentrations. As shown by Figure 2, it can be observed that values of the gas side mass transfer coefficient $k_g[mol.m^{-2}.kPa^{-1}.s^{-1}]$ are higher than the values of the physical liquid side mass transfer coefficient $k_L^o[m.s^{-1}]$ for all hydroxides. The values of liquid side mass transfer coefficient $k_L^o[m.s^{-1}]$ and overall mass transfer coefficient $K_{ov,G}[mol.m^{-2}.kPa^{-1}.s^{-1}]$ increase while the values of gas side mass transfer coefficient $k_g[mol.m^{-2}.kPa^{-1}.s^{-1}]$ slightly decrease with increasing temperature.

The effect of counter ion on overall and liquid side mass transfer coefficients can be observed by viewing the difference in values for different cations; the order of values being Li^+<Na^+< K^+. The comparison of the values of gas phase overall mass transfer coefficient, $K_{ov,G}[mol.m^{-2}.kPa^{-1}.s^{-1}$, and gas film mass transfer coefficient, $k_g[mol.m^{-2}.kPa^{-1}.s^{-1}]$, show that gas side film resistance is very small as compared to overall mass transfer resistance. The contribution of gas side resistance to overall mass transfer resistance is less than 1% for the lowest concentrations (0.01M LiOH, 0.01M NaOH and 0.0089M KOH) and increases as concentration increases. The highest contribution of gas side resistance to overall resistance is observed for 1.76M KOH at 56.3°C where the contribution is 15.7%. It is worth mentioning that the increase in contribution of gas side resistance for the higher concentrations is actually increased by the decrease in overall resistance due to enhancement by chemical reaction because the gas side resistance does not change significantly either by concentration or counter ion as illustrated by Figure 2.

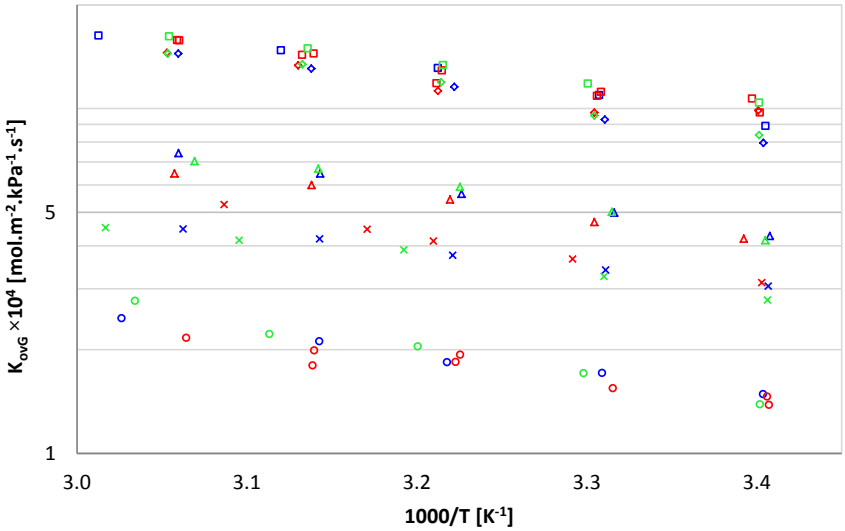

Figure 3: Overall mass transfer coefficient $K_{ov_G} \times 10^4$ as function of temperature for various concentrations of LiOH (blue), NaOH (red) and KOH (green). Circles (○): 0.01M (LiOH and NaOH) and 0.0089M (KOH); Cross (×): 0.05M (LiOH and NaOH) and 0.045M (KOH); Triangles (Δ): 0.1M (LiOH and NaOH) and 0.088M (KOH); Diamonds (◊): 0.5M (LiOH and NaOH) and 0.0447M (KOH); Squares (□): 1M (LiOH and NaOH) and 0.88M (KOH).

Figure 3 presents the gas phase based overall mass transfer coefficient $K_{ov_G}[mol.m^{-2}.kPa^{-1}.s^{-1}]$ of hydroxides as function of temperature for various ion concentrations other than 2M. It can be observed that the values of $K_{ov_G}[mol.m^{-2}.kPa^{-1}.s^{-1}]$ increase with increasing concentration at all temperatures for all the three hydroxides.

6.2. Kinetic constants at infinite dilution

The calculated values of the pseudo first order rate constant $k_1[s^{-1}]$ and second order rate constant $k_{OH^-}[m^3.kmol^{-1}.s^{-1}]$ are given in the last two columns of Tables A1-A4. Both rate constants are strong functions of temperature and concentration and depend on the counter ion with the same trend as seen for liquid side and overall mass transfer coefficients. The effect of counter ion is very significant at higher concentrations but becomes negligibly small for dilute solutions.

To obtain an Arrhenius expression for $k_{OH^-}[m^3.kmol^{-1}.s^{-1}]$ at infinite dilution, the second order rate constant data for all hydroxides were regressed as function of temperature by linear regression. The obtained data points were plotted as function of concentration for all hydroxides at 25°C, 35°C, 40°C, 50°C and 60°C. The same procedure was used by various authors [(Knuutila et al., 2010c); (Kucka et al., 2002); (Pohorecki and Moniuk, 1988); (Nijsing et al., 1959)].

The 25°C isotherms for all hydroxides are presented in Figure 4. The same trend for the three counter ions has been reported in literature at 20°C [(Nijsing et al., 1959); (Pohorecki and Moniuk, 1988)].

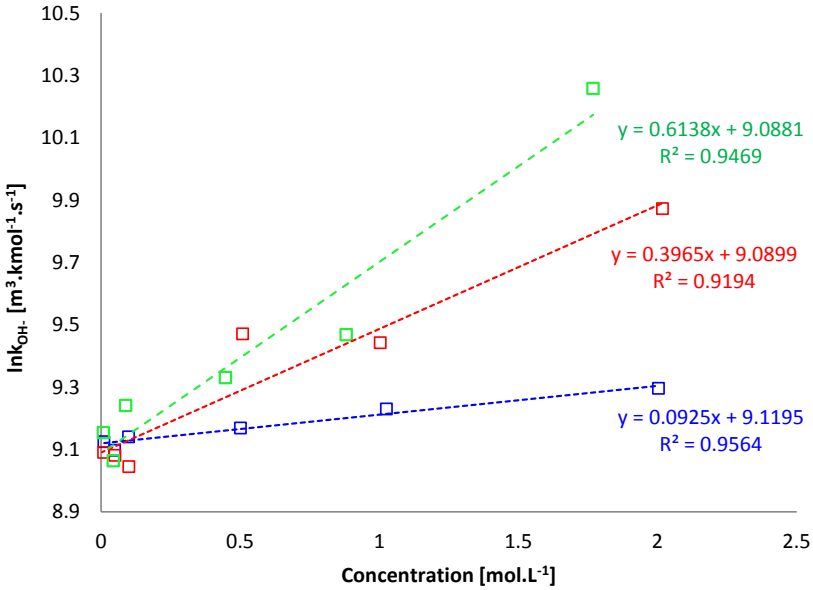

Figure 4: Second order rate constant, k_2 or k_{OH^-} as function of concentration at 25°C for LiOH (blue), NaOH (red) and KOH (green). Points (□): Experimental data; Dashed lines: Linear regression trend lines to obtain infinite dilution value, $k^{\infty}_{OH^-}$.

The y-intercept values obtained from the linear regression line of $lnk_{OH^-}[m^3.kmol^{-1}.s^{-1}]$ *vs.* Concentration $[mol.L^{-1}]$ plot as shown by Figure 4 at a particular temperature yield the infinite dilution value of $lnk_{OH^-}[m^3.kmol^{-1}.s^{-1}]$. The y-intercept values obtained from the isotherms for all the three hydroxides are given in Table 2. The table also provides the infinite dilution values for the second order rate constant $lnk^{\infty}_{OH^-}[m^3.kmol^{-1}.s^{-1}]$ based on an average value for all hydroxides along with the standard deviation from the average. As shown by the standard deviation values, the differences obtained between the three hydroxides is negligible.

Table 2: Pseudo second order rate constant (k_{OH^-}) for hydroxides of Li^+, Na^+ and K^+ at infinite dilution

	$lnk^{\infty}_{OH^-}$, where $k^{\infty}_{OH^-}$ [m^3.$kmol^{-1}$.s^{-1}]					$lnk^{0.01M}_{OH^-}$, where $k^{0.01M}_{OH^-}$[m^3.$kmol^{-1}$.s^{-1}]	
T (°C)	**LiOH**	**NaOH**	**KOH**	**Average**	**SD**	$= 26.064 - \frac{5056.9}{T\,[K]}$	**% Difference**
25	9.1195	9.0899	9.0811	9.0968	0.016	9.1031	0.07
35	9.6707	9.6234	9.6634	9.6525	0.021	9.6535	0.01
40	9.9331	9.8775	9.9375	9.9160	0.027	9.9155	0.01
50	10.434	10.362	10.460	10.4187	0.041	10.4152	0.03
60	10.904	10.817	10.952	10.8910	0.056	10.885	0.06

$$\text{SD} = \text{Standard Deviation}\,[lnk^{\infty}_{OH^-}\,[\text{m}^3.\text{kmol}^{-1}.\text{s}^{-1}]] = \sqrt[2]{\frac{\sum_{j=1}^{n}(lnk^{\infty}_{OH^-{}_i} - \frac{1}{n}\sum_{j=1}^{n} lnk^{\infty}_{OH^-{}_i})^2}{n}}$$

As mentioned previously the effect of the counter ion on the first and second order rate constants become small at lower concentrations. For consistency and as a second approach, the combined results of both rate constants for 0.01M LiOH, 0.01M NaOH and 0.0089M KOH are presented in Figure 5.

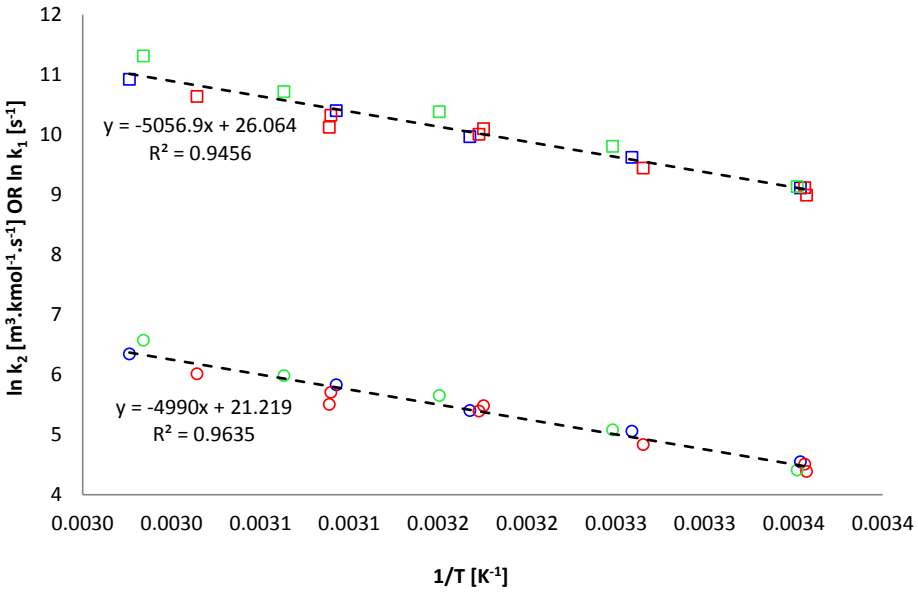

Figure 5: Pseudo first order rate constant, k_1 (○) and second order rate constant, k_2 or k_{OH^-} (□) as function of temperature taken as an average based on the lowest concentrations used (0.01M LiOH, 0.01M NaOH and 0.0089M KOH). Blue: LiOH; Red: NaOH; Green: KOH; Points: Experimental data; Dashed lines: Linear regression trend lines.

As shown by the linear regression lines in Figure 5, regardless of cation, all data come together. The data for both rate constants can be expressed as Arrhenius expressions fitted to all the three hydroxides for dilute solutions as follows:

$$lnk_1 = 21.219 - \frac{4990}{T[K]} \quad ; \quad where \ k_1[s^{-1}] \tag{23}$$

$$lnk_2 \ or \ lnk_{OH^-} = 26.064 - \frac{5056.9}{T[K]} \quad ; \quad where \ k_2 \ or \ k_{OH^-} \ [m^3.kmol^{-1}.s^{-1}] \tag{24}$$

The last two columns of Table 2 show the values $lnk_{OH^-}^{0.01M}$ obtained from Eq. (24) and the % difference from the values obtained as an average of all hydroxides obtained from infinite dilution values $lnk_{OH^-}^{\infty}$ given by the different isotherms; as 25°C isotherms are shown in Figure 4. It can be noted that the difference between the two values, i.e. $lnk_{OH^-}^{\infty}$ and $lnk_{OH^-}^{0.01M}$, is very small. This reflects the consistency of the results.

The infinite dilution second order rate constant, $lnk_{OH^-}^{\infty}$ obtained for LiOH, NaOH, KOH and the average for all hydroxides given in Table 2 were plotted as function of reciprocal of absolute temperature to obtain an Arrhenius plot, as shown in Figure 6. The figure illustrates that KOH seems to exhibit slightly higher values and a steeper slope compared to LiOH and NaOH. The linear regression lines with corresponding equations are also displayed in the

figure. The differences in the values at infinite dilution also seem influenced by the counter ion. The effect increases with increasing temperature due to the different slopes for the cations.

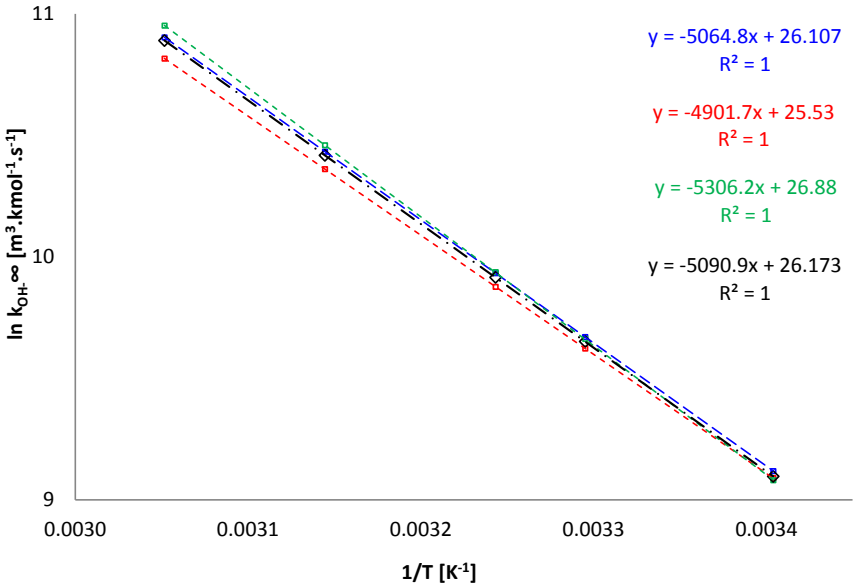

Figure 6: Arrhenius plot for infinite dilution second order rate constant, $k_{OH^-}^{\infty}$ as function of temperature. Points (□,◊): $lnk_{OH^-}^{\infty}$ as obtained from infinite dilution values (y-intercepts of k_{OH^-} isotherms as function of concentration at 25°C, 35°C , 40°C, 50°C and 60°C); Blue: LiOH; Red: NaOH; Green: KOH; Black: Averages of LiOH, NaOH and KOH; Dashed lines: Linear regression trend lines.

The Arrhenius expression shown by Eq. (6) for $k_{OH^-}^{\infty}[m^3.kmol^{-1}.s^{-1}]$ was obtained by linear regression trend line for the average of all three hydroxides obtained from Figure 6 as follows:

$$lnk_{OH^-}^{\infty} = 26.173 - \frac{5090.9}{T[K]} \quad ; \quad where\ k_{OH^-}^{\infty}[m^3.kmol^{-1}.s^{-1}] \tag{25a}$$

$$k_{OH^-}^{\infty}[m^3.kmol^{-1}.s^{-1}] = 2.327 \times 10^{11} exp\left(\frac{-42328[kJ.kmol^{-1}]}{RT[K]}\right) \tag{25b}$$

When compared to Eq. (6), 2.327×10^{11} is the value of pre-exponential factor, 42328 is the value obtained for activation energy $E_A[k].kmol^{-1}]$, *R* [8.3144 kJ.kmol^{-1}.K^{-1}] is the ideal gas law constant and T [K] is absolute temperature.

The same expression can be modified to get an expression in the shape of Eq. (8) which is an expression from (Pohorecki and Moniuk, 1988).

$$log_{10}k_{OH^-}^{\infty,e} = 11.365 - \frac{2211}{T[K]} \quad ; where\ \ k_{OH^-}^{\infty,e}[m^3.kmol^{-1}.s^{-1}] \tag{25c}$$

The infinite dilution models given by Eqs. (25a, 25b, 25c) are valid for a range of temperature (25-60°C). A comparison of $lnk^{\infty}_{OH^-}[m^3.kmol^{-1}.s^{-1}]$ values obtained in the present work, Eq. (25a) and those from literature is given in Table 3 and illustrated by Figure 7.

Table 3: Comparison of second order rate constant at infinite dilution ($\mathbf{k^{\infty}_{OH^-}}$) with literature

	$lnk^{\infty}_{OH^-}$ [m^3.$kmol^{-1}$.s^{-1}]									
T (°C)	**0**	**10**	**18**	**20**	**25**	**30**	**41**	**52**	**60**	**70**
This work (Model)	-	-	-	*8.81	9.1	9.38	9.97	10.52	10.89	-
Knuutila et al., 2010 (Model)	-	-	-	-	-	-	10.31	10.95	11.39	11.9
Kucka et al., 2002 (Model)	-	-	-		8.95	9.31	10.08	10.79	-	-
Pohorecki and Moniuk, 1976 (Model)	-	-	8.55	8.68	8.99	9.29	9.930	-	-	-
Pohorecki and Moniuk, 1988 (Model)	-	-	-	8.73	9.04	9.35	9.98	-	-	-
Barrett, 1966	-	-	-	8.94	-	-	-	-	-	-
Nijsing et al., 1959	-	-	-	8.46	-	-	-	-	-	-
Himmelblau and Babb, 1958	-	-	-	12.5	-	-	-	-	-	-
Pinsent et al., 1956	-	-	-	8.61	9.05	9.36	-	-	-	-
Pinsent et al., 1951	6.95	7.74	-	-	-	-	-	-	-	-
This work+ Pinsent et al., 1951 and 1956 (Model)	**7.06**	**7.84**	**8.42**	**8.56**	**8.91**	**9.25**	**9.93**	**10.58**	**11.02**	**-**

*** Extrapolated value**

As shown by Table 3 and Figure 7, the values of $lnk^{\infty}_{OH^-}[m^3.kmol^{-1}.s^{-1}]$ obtained by the present work (based on averages for LiOH, NaOH and KOH) agree well (less than 1% difference) with the apparent value from the infinite dilution model by (Pohorecki and Moniuk, 1988) at all temperatures even when extrapolated to higher temperatures beyond the given ranges of both models. The values obtained by this work agree well (less than 0.5% difference) with those from (Pinsent et al., 1956) at 25°C and 30°C. The values from (Pinsent et al., 1956) are slightly lower and the reason may be that they used NaOH which shows slightly lower values and a less steep slope. The extrapolation of this work to 20°C agrees (less than ±2% difference) with other literature data available except those from (Himmelblau and Babb, 1958) which are 42% higher than this work. The model from (Kucka et al., 2002) shows lower values (up to 1%) than this work at 25°C and 30°C but higher values (up to 3%) at 41°C and 52°C because the slope given by their model is steeper than that obtained by this work. The model given by (Knuutila et al., 2010c) shows higher values (3.5 - 5%) than this work and the difference increases with increasing temperature because the slope from their model is slightly steeper than that from this work. As earlier discussed, the values obtained by this work are lower than those from (Knuutila et al., 2010c) and slopes are less steep than those of models from (Knuutila et al., 2010c) and (Kucka et al., 2002). One of the reasons of this trend could be that in both aforementioned publications, infinite dilution values were based on the K^+ cation only, K_2CO_3 and KOH respectively. It has been shown in Figure 6 that the values obtained from KOH data are slightly higher than those from LiOH and NaOH, moreover the slope of KOH data is steeper than those of the other hydroxides especially NaOH.

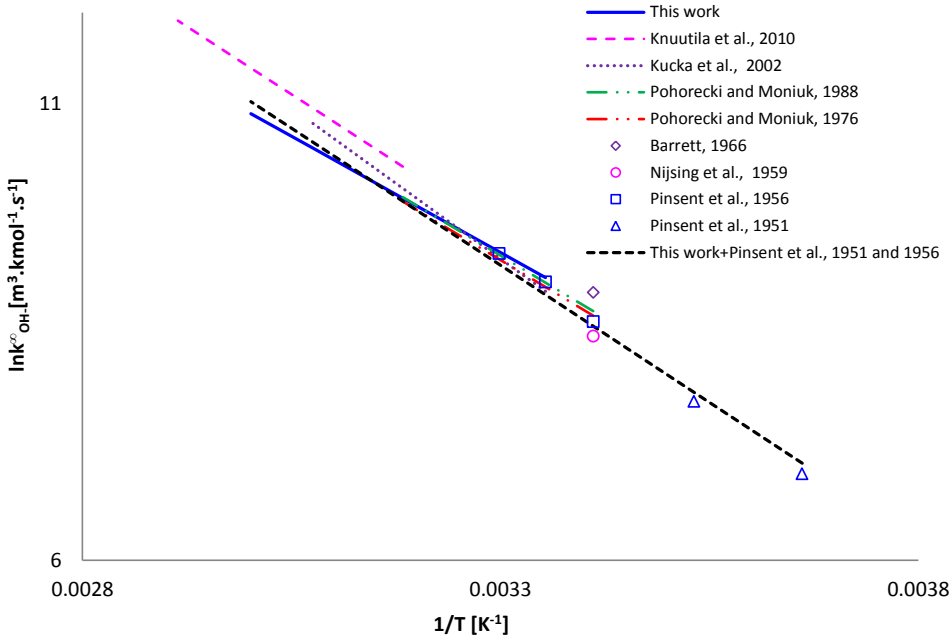

Figure 7: Arrhenius plot for infinite dilution second order rate constant, $k^{\infty}_{OH^-}$ as function of temperature. Points (◊, ○, □, Δ): Experimental data from different literature sources; Dashed lines: Models from literature and this work.

The Figure 7 also presents a model obtained by linear regression of data from (Pinsent and Roughton, 1951), (Pinsent et al., 1956) plus the averaged values obtained by this work to extend the range of the combined model to 0°C. This model is given by Eq. (26) and the validity range is 0-63 °C.

$$lnk^{\infty}_{OH^-} = 29.051 - \frac{6005.9}{T[K]}\ ;\ where\ \ k^{\infty}_{OH^-}[m^3.kmol^{-1}.s^{-1}] \quad (valid\ for\ 0-63°C)\ (26)$$

The values obtained by this model are shown in the last row of Table 3.

6.3 Second order rate constant predicted by Pohorecki and Moniuk's Model

As mentioned earlier, a model for higher concentrations, based on an ionic strength contribution of individual ions, as presented by Eq. (7) and Eq. (8), was proposed by (Pohorecki and Moniuk, 1988). The model is valid for 18–41°C and is widely used and typically referred in literature for the second order rate constant, k_{OH^-} [(Kreulen et al., 1993) ;(Versteeg et al., 1996); (Kucka et al., 2002); (Haubrock et al., 2005); (Li and Chen, 2005); (Haubrock et al., 2007); (Stolaroff et al., 2008); (Knuutila et al., 2010c)].The values for the second order kinetic constant, $k_{OH^-}[m^3.kmol^{-1}.s^{-1}]$ obtained in this work for hydroxides and blends of hydroxides with carbonates were compared with this model and the parity plot comparing experimental data with the model is given in Figure 8.

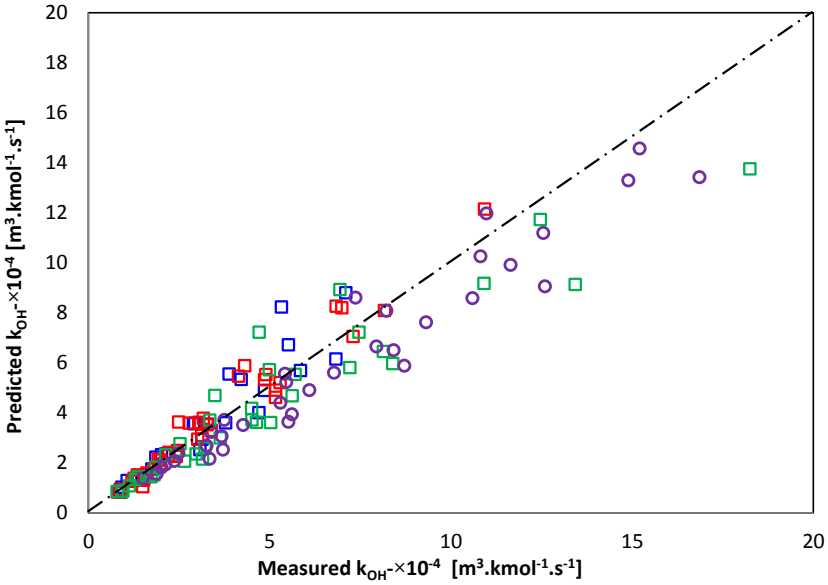

Figure 8: Parity plot for the original Pohorecki and Moniuk's model and experimental data. Blue (□): LiOH; Red (□): NaOH; Green (□): KOH; Purple (○): Blends of hydroxides and carbonates.

Table 4: Statistics comparing new data with Pohorecki and Moniuk Model (Pohorecki and Moniuk, 1988)

Solutions	No. of Data points	%AARD with Original parameters	%AARD with refitted parameters
LiOH	30	13.5	9.3
NaOH	38	11.2	11.4
KOH	35	16.7	14.4
Blends	35	12.9	12.0
Total	**138**	**14.2**	**11.6**

$$AARD\,[\%] = \frac{1}{n}\sum_{i=1}^{n} 100\frac{\left|k_{OH^-_i}^{Exp} - k_{OH^-_i}^{Model}\right|}{\left|k_{OH^-_i}^{Exp}\right|}$$

The original model by (Pohorecki and Moniuk, 1988) represents the experimental data with 14.2% AARD (Average Absolute Relative Deviation). From Figure 8 it is seen that data for KOH and blends are under-predicted at higher temperatures and concentrations while data for LiOH are over-predicted at higher concentrations. Detailed statistics for the comparison are given in Table 4. As shown by the last column in Table 4, the parameters in the model were refitted and the AARD reduced to 11.57%. The values of all parameters used in the original and refitted models are given in Table 5 and the parity plot for the refitted model is shown in Figure 9. The refitted values for parameters A and B shown in Table 5 are those obtained for the infinite dilution model in this work as given by Eq. (25c).

Table 5: Pohorecki and Moniuk Model (Pohorecki and Moniuk, 1988) with original and re-fitted parameters

$log_{10}\frac{k_{OH^-}}{k^{\infty}_{OH^-}} = \sum b_{ion} I_{ion}$; $I_{ion}[kmol.m^{-3}] = \frac{1}{2} c_i z_i^2$

and $log_{10} k^{\infty}_{OH^-} = A - \frac{B}{T[K]}$; $k^{\infty}_{OH^-}\ [m^3.kmol^{-1}.s^{-1}]$

Parameters	Original	Refitted	Change w.r.t. original value
A	11.916	11.365	4.6% decrease
B [K]	2382	2211	7.2% decrease
b_{Li^+} [$m^3.kmol^{-1}$]	-0.050	-0.193	286% increase
b_{Na^+} [$m^3.kmol^{-1}$]	0.12	0.0971	19.1% decrease
b_{K^+} [$m^3.kmol^{-1}$]	0.22	0.301	36.8% increase
b_{OH^-} [$m^3.kmol^{-1}$]	0.22	0.28	27.3% increase
$b_{CO_3^=}$ [$m^3.kmol^{-1}$]	0.085	0.134	57.7% increase

I_{ion} is ionic strength of the ion in solution, z_i is charge number of the ion and c_i is concentration of the ion in solution.

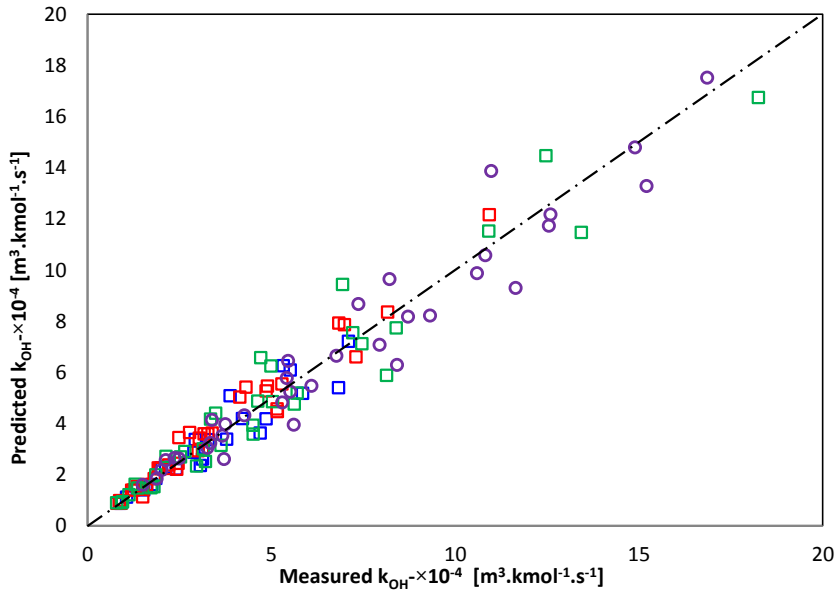

Figure 9: Parity plot for the Pohorecki and Moniuk's model with refitted parameters and experimental data. Blue (□): LiOH; Red (□): NaOH; Green (□): KOH; Purple (○): Blends of hydroxides and carbonates.

As shown by Figure 9, the under-predictions for KOH and the blends and the over-predictions for LiOH were improved by re-fitting the parameters. The AARD for KOH is reduced from 16.7% to 14.4% and for LiOH from 13.5% to 9.3%. Any other attempt to refit the parameters did not result in further improvement of AARD. Here it is important to see that the contribution of Li^+ to the value of $k_{OH^-}[m^3.kmol^{-1}.s^{-1}]$ appears with negative sign in both models although the effect is more significant in the re-fitted model. The effect on AARD for NaOH is very small (11.2% to 11.4%) and the improvement for the blends is from 12.9% to 12.0%.

In the re-fitted model, due to slightly lower values of A, B and $k_{OH^-}^{\infty}$ obtained in this work as given by Eq. (25c) when compared to (Pohorecki and Moniuk, 1988); the contribution of all ions is increased (for Li^+ negative effect) except that of Na^+ which is decreased by 19.1%. This decrease is justified by the fact that $k_{OH^-}^{\infty}$ values obtained from NaOH data are slightly lower than the used average value of $k_{OH^-}^{\infty}$ in this work and the effect is compensated by a lower value for the Na^+ contribution.

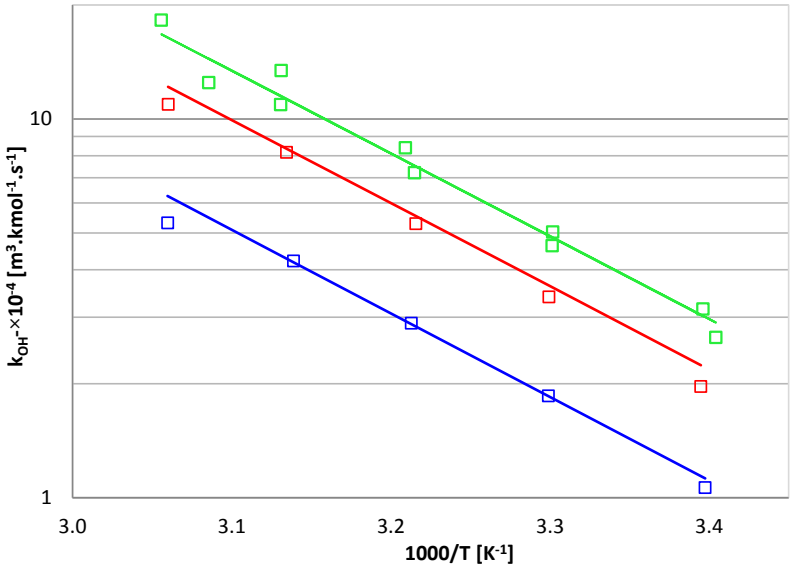

Figure 10: Second order rate constant, k_2 or k_{OH^-} as function of temperature for 2M LiOH (blue), 2M NaOH (red) and 1.76M KOH (green). Points (□): Experimental data; Lines: Pohorecki and Moniuk's model with refitted parameters.

Figure 10 illustrates the second order rate constant, k_2 or k_{OH^-} as function of temperature for 2M LiOH, 2M NaOH and 1.76M KOH. As previously discussed, the reason for the graphical illustration of the results at the highest concentration level is to demonstrate the effect of counter ion on the value of the kinetic constants. This effect increases with increasing concentration. The data for KOH were obtained by two different sets of experiments and the values obtained show good reproducibility and agree well. It can be seen that experimental and re-fitted model predictions agree well (less than 12% AARD) and show the relatively strong effect of the counter ion. The effect of the counter ion on the kinetic constant values varies in the same order as earlier discussed for the mass transfer coefficients i.e. $Li^+ < Na^+ < K^+$.

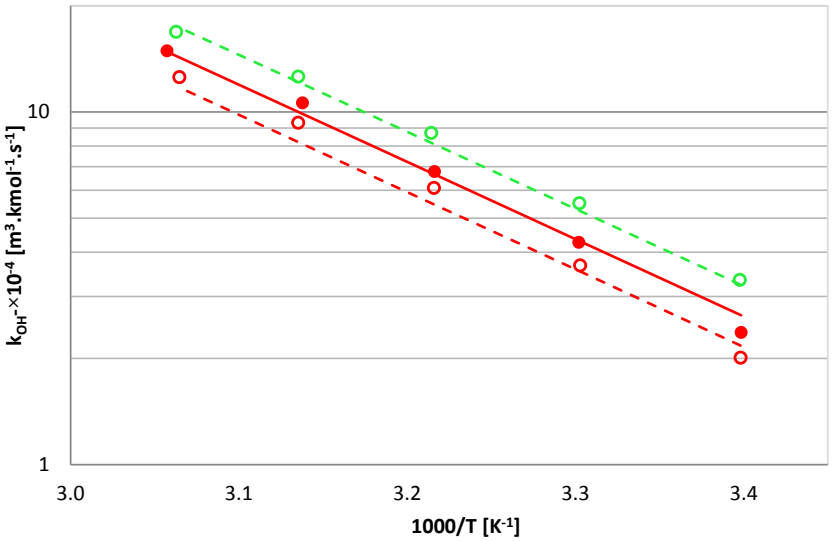

Figure 11: Second order rate constant, k_2 or k_{OH^-} as function of temperature for blends of hydroxides and carbonates with same cations, Points: Experimental data; Filled red circles (•): 0.5MNaOH+1M Na_2CO_3; Open red circles (○): 1MNaOH+0.5MNa_2CO_3; Open green circles (○): 0.89MKOH+0.5MK_2CO_3; Lines: Pohorecki and Moniuk's model with refitted parameters.

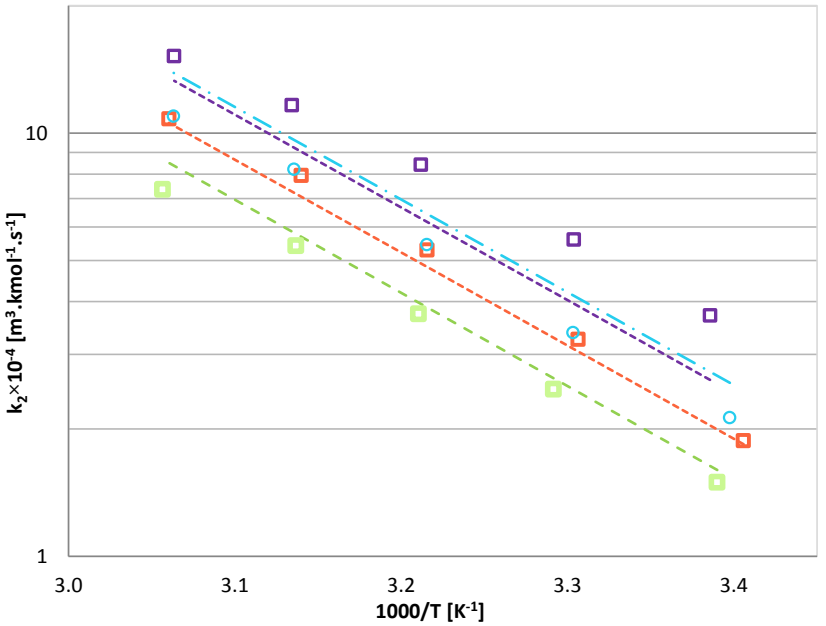

Figure 12: Second order rate constant, k_2 or k_{OH^-} as function of temperature for blends of hydroxides and carbonates with mixed cations. Points (□, ○): Experimental data; Purple: 1MLiOH+2MNaOH; Turquoise: 0.89MKOH+0.5MNa_2CO_3; Orange: 1MNaOH+0.44MKOH; Lemon green: 0.5MNaOH+0.44MKOH; Lines: Pohorecki and Moniuk's model with refitted parameters.

Figure 11 and Figure 12 present the k_{OH^-} results for blends of hydroxides and carbonates. The results demonstrate that blends with same cations, as shown in Figure 11, are better predicted by the model than those with mixed cations, as illustrated in Figure 12. The latter values show large deviations from the model predictions. The largest deviations were observed for 1MLiOH+2MNaOH where under predictions were from 12 to 30%. A similar behavior of blends with mixed cations was reported in (Gondal et al., 2014a) for apparent Henry's law constant predictions by a refitted Weisenberger and Schumpe's model (Weisenberger and Schumpe, 1996). For under prediction of 1MLiOH+2MNaOH, it may be assumed that calculated experimental values of k_{OH^-} for this blend might be higher due to the higher values of apparent Henry's law constant obtained from re-fitted Weisenberger and Schumpe's model by (Gondal et al., 2014a). The over predictions of k_{OH^-} for 0.89MKOH+0.5MNa_2CO_3 cannot be justified in the same manner because the model values for the apparent Henry's law constant for this blend were also reported to be over-predicted.

7. Conclusions

The experimental data measured in a String of Discs Contactor (SDC) under pseudo-first-order conditions are presented for absorption of carbon dioxide into aqueous hydroxides (0.01–2.0 kmol.m^{-3}) and blends of hydroxides and carbonates with mixed counter ions (1–3 kmol.m^{-3}) containing Li^+, Na^+ and K^+ for a range of temperatures (25–63°C).

The dependence of the reaction rate constant on temperature and concentration/ionic strength and effect of counter ion is verified for the reaction of CO_2 with hydroxyl ions (OH^-) in these aqueous electrolyte solutions.

The infinite dilution second order rate constant, $k^{\infty}_{OH^-}[m^3.kmol^{-1}.s^{-1}]$ for LiOH, NaOH and KOH are derived as Arrhenius temperature function from measured experimental data. It is observed that though slightly but the infinite dilution values of k_{OH^-} are also affected by counter ion. An Arrhenius model for infinite dilution second order rate constant, $k^{\infty}_{OH^-}$ based on average value of LiOH, NaOH and KOH obtained in this work along with data from (Pinsent et al., 1956) and (Pinsent and Roughton, 1951) has been proposed also which is valid from 0 to 63°C.

The dependence of second order rate constant, k_{OH^-} on ionic strength is validated by the original Pohorecki and Moniuk model (Pohorecki and Moniuk, 1988) with less than 15% AARD. The model with re-fitted parameters is valid for range of temperatures (25–63°C) and concentrations (0.01–3 kmol.m^{-3}) and predicts the experimental data with less than 12% AARD. The blends with same counter ions are better predicted by model with re-fitted parameters but blends with mixed counter ions show as large as 30% deviations.

Acknowledgement

The financial and technical support for this work by Faculty of Natural Sciences and Technology and Chemical Engineering Department of NTNU, Norway is greatly appreciated.

References

Aronu, U. E., Hartono, A., and Svendsen, H. F. (2011). Kinetics of carbon dioxide absorption into aqueous amine amino acid salt: 3-(methylamino) propylamine/sarcosine solution. *Chemical Engineering Science* **66**(23)**,** 6109-6119.

Astarita, G., Savage, D. W., and Bisio, A. (1983). "Gas treating with chemical solvents." John Wiley.

Barrett, P. V. L. (1966). Gas Absorption on a Sieve Plate. Ph.D. Thesis, University of Cambridge.

Carroll, J. J., Slupsky, J. D., and Mather, A. E. (1991). The solubility of carbon dioxide in water at low pressure. *Journal of Physical and Chemical Reference Data* **20**(6)**,** 1201-1209.

Danckwerts, P. V. (1970). "Gas–liquid reactions." McGraw-Hill, New York.

Gondal, S., Asif, N., Svendsen, H. F., and Knuutila, H. (2014). Density and N_2O solubility of aqueous Hydroxide and Carbonate Solutions in the temperature range from 25 to 80 °C. *Accepted for publication in Chemical Engineering Science*.

Hartono, A., da Silva, E. F., and Svendsen, H. F. (2009). Kinetics of carbon dioxide absorption in aqueous solution of diethylenetriamine (DETA). *Chemical Engineering Science* **64**(14)**,** 3205-3213.

Haubrock, J., Hogendoorn, J., and Versteeg, G. (2007). The applicability of activities in kinetic expressions: A more fundamental approach to represent the kinetics of the system CO_2–OH-–salt in terms of activities. *Chemical Engineering Science* **62**(21)**,** 5753-5769.

Haubrock, J., Hogendoorn, J., and Versteeg, G. F. (2005). The Applicability Of Activities In Kinetic Expressions: a More Fundamental Approach To Represent the Kinetics Of the System CO(-OH-) In Terms Of Activities. *International Journal of Chemical and Reactor Engineering* **3**(3)**,** 1290.

Higbie, R. (1935). "The rate of absorption of a pure gas into still liquid during short periods of exposure."

Hikita, H., Asai, S., and Takatsuka, T. (1976). Absorption of carbon dioxide into aqueous sodium hydroxide and sodium carbonate-bicarbonate solutions. *The Chemical Engineering Journal* **11**(2)**,** 131-141.

Himmelblau, D. M., and Babb, A. (1958). Kinetic studies of carbonation reactions using radioactive tracers. *AIChE Journal* **4**(2)**,** 143-152.

Jou, F.-Y., Carroll, J. J., Mather, A. E., and Otto, F. D. (1992). The solubility of nitrous oxide in water at high temperatures and pressures. Zeitschrift fur physikalische chemie-frankfurt am main then wiesbaden then munchen- **177,** 225-225.

Knuutila, H., Juliussen, O., and Svendsen, H. F. (2010). Kinetics of the reaction of carbon dioxide with aqueous sodium and potassium carbonate solutions. *Chemical Engineering Science* **65**(23)**,** 6077-6088.

Kreulen, H., Smolders, C., Versteeg, G., and Van Swaaij, W. (1993). Microporous hollow fibre membrane modules as gas-liquid contactors Part 2. Mass transfer with chemical reaction. *Journal of Membrane Science* **78**(3)**,** 217-238.

Kucka, L., Kenig, E. Y., and Gorak, A. (2002). Kinetics of the gas-liquid reaction between carbon dioxide and hydroxide ions. *Industrial & engineering chemistry research* **41**(24)**,** 5952-5957.

Laliberté, M. (2007). Model for calculating the viscosity of aqueous solutions. *Journal of Chemical & Engineering Data* **52**(2)**,** 321-335.

Laliberte, M., and Cooper, W. E. (2004). Model for calculating the density of aqueous electrolyte solutions. *Journal of Chemical & Engineering Data* **49**(5)**,** 1141-1151.

Lewis, W., and Whitman, W. (1924). Principles of gas absorption. *Industrial & Engineering Chemistry* **16**(12)**,** 1215-1220.

Li, J.-L., and Chen, B.-H. (2005). Review of CO_2 absorption using chemical solvents in hollow fiber membrane contactors. *Separation and Purification Technology* **41**(2)**,** 109-122.

Luo, X., Hartono, A., and Svendsen, H. F. (2012). Comparative kinetics of carbon dioxide absorption in unloaded aqueous monoethanolamine solutions using wetted wall and string of discs columns. *Chemical Engineering Science* **82,** 31-43.

Ma'mun, S., Dindore, V. Y., and Svendsen, H. F. (2007). Kinetics of the reaction of carbon dioxide with aqueous solutions of 2-((2-aminoethyl) amino) ethanol. *Industrial & engineering chemistry research* **46**(2)**,** 385-394.

Nijsing, R., Hendriksz, R., and Kramers, H. (1959). Absorption of CO_2 in jets and falling films of electrolyte solutions, with and without chemical reaction. *Chemical Engineering Science* **10**(1)**,** 88-104.

Pinsent, B., Pearson, L., and Roughton, F. (1956). The kinetics of combination of carbon dioxide with hydroxide ions. *Transactions of the Faraday Society* **52,** 1512-1520.

Pinsent, B., and Roughton, F. (1951). The kinetics of combination of carbon dioxide with water and hydroxide ions. *Transactions of the Faraday Society* **47,** 263-269.

Pohorecki, R. (1976). Mass transfer with chemical reaction during gas absorption on a sieve plate. *Chemical Engineering Science* **31**(8)**,** 637-644.

Pohorecki, R., and Moniuk, W. d. w. (1988). Kinetics of reaction between carbon dioxide and hydroxyl ions in aqueous electrolyte solutions. *Chemical Engineering Science* **43**(7)**,** 1677-1684.

Schumpe, A. (1993). The estimation of gas solubilities in salt solutions. *Chemical Engineering Science* **48**(1)**,** 153-158.

Stolaroff, J. K., Keith, D. W., and Lowry, G. V. (2008). Carbon dioxide capture from atmospheric air using sodium hydroxide spray. *Environmental science & technology* **42**(8)**,** 2728-2735.

Van Krevelen, D., and Hoftijzer, P. (1948). *Chimie et Industrie: Numero Speciale du XXIe Congress International de Chimie Industrielle, Bruxelles*.

Van Swaaij, W., and Versteeg, G. (1992). Mass transfer accompanied with complex reversible chemical reactions in gas—liquid systems: an overview. *Chemical Engineering Science* **47**(13)**,** 3181-3195.

Versteeg, G., Van Dijck, L., and Van Swaaij, W. (1996). On the kinetics between CO_2 and alkanolamines both in aqueous and non-aqueous solutions. An overview. *Chemical Engineering Communications* **144**(1)**,** 113-158.

Versteeg, G. F., and Van Swaalj, W. (1988). Solubility and diffusivity of acid gases (carbon dioxide, nitrous oxide) in aqueous alkanolamine solutions. *Journal of Chemical and Engineering Data* **33**(1)**,** 29-34.

Weisenberger, S., and Schumpe, A. (1996). Estimation of gas solubilities in salt solutions at temperatures from 273 K to 363 K. *AIChE Journal* **42**(1)**,** 298-300.

Appendices

Table A1: Kinetic data of CO_2 absorption into aqueous lithium hydroxide (LiOH) solutions

Experiment	T [°C]	[R]$LMPD_{CO_2}$ [kPa]	[§]$N_{CO_2}\times10^4$ [mol.m^{-2}.s^{-1}]	[a]k_L^o $\times10^4$ [m.s^{-1}]	[b]$k_g\times10^2$ [mol. m^{-2}. kPa^{-1}.s^{-1}]	[c]$K_{ov_G}\times10^4$ [mol. m^{-2}. kPa^{-1}.s^{-1}]	[d]$E_{A,\infty,film}$ [-]	[e]Ha [-]	[*]k_1 [s^{-1}]	[**]k_2 $\times10^{-4}$ [m^3. kmol^{-1}.s^{-1}]
0.01M	25.02	0.2284	0.339	0.8282	1.58	1.48	195	5	94	0.9
LiOH	33.69	0.2578	0.4402	1.0241	1.57	1.71	177	6	157	1.51
	42.52	0.2502	0.4595	1.2263	1.54	1.84	185	7	221	2.13
	50.19	0.2353	0.4966	1.4472	1.5	2.11	197	8	340	3.28
	62.84	0.2119	0.5214	1.7445	1.37	2.46	207	9	567	5.51
0.05M	24.75	0.2653	0.8098	0.8119	1.53	3.05	797	11	431	0.87
LiOH	33.49	0.2685	0.9121	0.9979	1.5	3.4	810	13	669	1.35
	42.2	0.2665	1.0006	1.1917	1.47	3.76	838	14	993	2.01
	50.17	0.2778	1.1619	1.3762	1.43	4.18	818	16	1441	2.93
	58.81	0.266	1.189	1.6233	1.38	4.47	861	17	1898	3.88
0.1M LiOH	24.67	0.23	0.9823	0.8094	1.59	4.27	1854	16	897	0.9
	33.01	0.2109	1.0525	0.9835	1.57	4.99	2082	19	1524	1.53
	41.68	0.1995	1.129	1.1871	1.51	5.66	2264	22	2397	2.41
	50.14	0.1918	1.2437	1.3609	1.46	6.49	2406	26	3741	3.78
	59.1	0.1896	1.4084	1.599	1.37	7.43	2466	30	5764	5.85
0.5M LiOH	25	0.2097	1.6663	0.7199	1.57	7.95	10345	40	4693	0.94
	33.54	0.203	1.886	0.903	1.55	9.29	11033	46	8017	1.6
	42.09	0.1894	2.1886	1.0826	1.52	11.56	12229	59	15326	3.07
	50.68	0.2031	2.6532	1.3016	1.49	13.06	11715	66	23360	4.7
	59.12	0.2035	2.9379	1.4572	1.34	14.44	11977	77	33803	6.83
1M LiOH	24.89	0.2123	1.8896	0.6318	1.52	8.9	20969	59	9399	0.92
	33.85	0.2106	2.3011	0.7855	1.5	10.93	21880	74	17887	1.75
	43.06	0.2038	2.6719	0.9668	1.46	13.11	23397	90	31916	3.13
	52.58	0.1989	2.9326	1.1245	1.32	14.74	24748	106	49361	4.86
	64.37	0.1914	3.1162	1.437	1.32	16.28	26109	112	71695	7.1
2M LiOH	25.59	0.2988	2.6341	0.5027	1.58	8.82	29107	100	21312	1.06
	34.65	0.285	2.9901	0.6527	1.56	10.49	31578	115	37122	1.86
	43.02	0.287	3.4467	0.7758	1.51	12.01	32381	134	57626	2.89
	50.61	0.2927	3.9564	0.9235	1.46	13.51	32675	148	83753	4.22
	59.11	0.3093	4.3825	1.0707	1.32	14.17	31727	156	105281	5.32

[R] **Log mean pressure differene of CO_2.** [§] **CO_2 flux.** [a] **Liquid film mass transfer coefficient.** [b] **Gas film mass transfer coefficient.** [c] **Overall mass transfer coefficient.** [d] **Infinite Enhancement factor based on film theory.** [e] **Hatta Number.** [*] **Pseudo first order rate constant.** [**] **Second order rate constant**

Table A2: Kinetic data of CO_2 absorption into aqueous sodium hydroxide (NaOH) solutions

Experiment	T [°C]	$LMPD_{CO_2}$ [kPa]	$N_{CO_2}\times10^4$ [mol.m^{-2}.s^{-1}]	k_L^o $\times10^4$ [m.s^{-1}]	$k_g\times10^2$ [mol. m^{-2}. kPa^{-1}.s^{-1}]	$K_{ov_G}\times10^4$ [mol. m^{-2}. kPa^{-1}.s^{-1}]	$E_{A,\infty,film}$ [-]	Ha [-]	k_1 [s^{-1}]	$k_2\times10^{-4}$ [m^3. kmol^{-1}. s^{-1}]
0.01M NaOH	24.72	0.2515	0.3471	0.8262	1.52	1.38	104	5	80	0.8
	33.09	0.2186	0.3373	0.9619	1.49	1.54	124	6	125	1.26
	42.02	0.2183	0.4014	1.1899	1.47	1.84	127	7	219	2.21
	50.61	0.2324	0.4179	1.4161	1.41	1.8	120	7	246	2.49
0.01M NaOH Repeated	24.81	0.221	0.3227	0.8263	1.53	1.46	118	5	90	0.91
	41.76	0.1866	0.36	1.204	1.5	1.93	149	7	240	2.42
	50.51	0.1959	0.3888	1.4201	1.46	1.98	142	7	300	3.04
	58.6	0.19	0.4104	1.6201	1.39	2.16	143	8	408	4.14
0.05M NaOH	25.09	0.2429	0.7592	0.8252	1.53	3.13	541	12	451	0.9
	35.33	0.248	0.9071	1.0668	1.51	3.66	557	14	803	1.61
	43.32	0.264	1.0893	1.2465	1.48	4.13	535	16	1221	2.46
	47.27	0.2501	1.1162	1.3809	1.48	4.46	570	17	1549	3.13
	56.16	0.224	1.1788	1.5858	1.37	5.26	639	20	2546	5.16
0.1M NaOH	26.04	0.2709	1.136	0.8771	1.57	4.19	989	15	881	0.87
	34.12	0.3284	1.5384	1.0375	1.55	4.68	850	18	1353	1.35
	42.35	0.2728	1.4866	1.2494	1.52	5.45	1054	21	2214	2.21
	50.68	0.2772	1.6617	1.4383	1.48	6	1056	23	3164	3.17
	59.36	0.2807	1.818	1.6559	1.4	6.48	1043	26	4285	4.31
0.5M NaOH	25.27	0.2301	2.2704	0.7917	1.43	9.87	5778	49	7633	1.5
	34.12	0.2834	2.7602	0.9573	1.44	9.74	4890	50	9211	1.81
	43.05	0.249	2.8019	1.1465	1.41	11.25	5761	59	15241	3.01
	51.5	0.2181	2.9104	1.3632	1.34	13.35	6729	70	26027	5.16
	59.84	0.2029	2.9454	1.5267	1.2	14.51	7287	80	36655	7.3
1M NaOH	25.6	0.2377	2.5395	0.7536	1.35	10.68	10155	70	15246	1.52
	33.97	0.3031	3.297	0.9136	1.36	10.88	8330	72	19278	1.92
	43.14	0.3013	3.5644	1.086	1.39	11.83	8676	80	27729	2.78
	51.26	0.2895	4.1403	1.298	1.36	14.3	9271	97	48681	4.9
	59.04	0.2839	4.4759	1.5102	1.26	15.77	9545	107	69220	6.99
1M NaOH Repeated	25.18	0.2591	2.5225	0.7625	1.57	9.74	9202	61	12078	1.2
	33.75	0.2629	2.9366	0.9373	1.56	11.17	9550	71	19855	1.98
	42.82	0.2663	3.4338	1.1399	1.54	12.89	9824	83	32656	3.27
	50.54	0.2693	3.8897	1.3157	1.48	14.45	9973	95	48300	4.86
	59.19	0.2676	4.2238	1.5211	1.39	15.78	10189	105	67694	6.84
2M NaOH	25.82	0.2841	2.8864	0.6283	1.58	10.16	13338	120	39712	1.97
	34.61	0.2515	3.0163	0.7789	1.56	12	16118	143	68184	3.39
	42.74	0.2357	3.2333	0.9317	1.52	13.72	18076	164	106025	5.29
	51.05	0.2544	3.9854	1.0915	1.44	15.66	17397	190	163048	8.16
	59.08	0.2584	4.3674	1.2611	1.36	16.9	17548	205	217297	10.93

Table A3: Kinetic data of CO_2 absorption into aqueous potassium hydroxide (KOH) solutions

Experiment	T [°C]	$LMPD_{CO_2}$ [kPa]	$N_{CO_2}\times10^4$ [mol.m^{-2}.s^{-1}]	k_L^o $\times10^4$ [m.s^{-1}]	$k_g\times10^2$ [mol. m^{-2}. kPa^{-1}.s^{-1}]	$K_{ov_G}\times10^4$ [mol. m^{-2}. kPa^{-1}.s^{-1}]	$E_{A,\infty,film}$ [-]	Ha [-]	k_1 [s^{-1}]	$k_2\times10^{-4}$ [m^3. kmol^{-1}. s^{-1}]
0.0089M KOH	25.19	0.2786	0.3863	0.8246	1.53	1.39	83	5	82	0.92
	34.71	0.2334	0.3979	0.9849	1.5	1.71	104	6	161	1.81
	44.25	0.2128	0.434	1.2595	1.45	2.04	115	7	284	3.21
	53.3	0.2212	0.4903	1.4975	1.41	2.22	109	8	396	4.5
	61.95	0.1885	0.5216	1.7163	1.3	2.77	116	10	714	8.13
0.045M KOH	24.79	0.2495	0.6946	0.8149	1.52	2.78	464	10	355	0.79
	33.57	0.2534	0.8246	1.0003	1.5	3.25	478	12	610	1.37
	45.08	0.2218	0.8617	1.2497	1.43	3.89	566	15	1124	2.53
	55.2	0.2275	0.9446	1.4967	1.31	4.15	557	16	1544	3.49
	63.9	0.2263	1.0205	1.7252	1.31	4.51	549	18	2075	4.71
0.088M KOH	24.9	0.2284	0.9481	0.8249	1.57	4.15	1002	16	841	0.95
	33.16	0.1947	0.9759	1.0089	1.54	5.01	1230	19	1528	1.73
	41.77	0.1902	1.1278	1.2208	1.51	5.93	1303	23	2616	2.97
	50.26	0.1901	1.2725	1.4294	1.47	6.69	1332	26	3961	4.51
	58.05	0.193	1.3571	1.6086	1.42	7.03	1316	28	4991	5.7
0.447M KOH	25.23	0.3098	2.5955	0.7972	1.41	8.38	3633	39	5048	1.13
	34.12	0.2589	2.469	0.9771	1.41	9.54	4556	45	8276	1.85
	42.87	0.2071	2.469	1.1721	1.41	11.92	5911	58	16149	3.63
	51.24	0.2242	3.01	1.3329	1.28	13.43	5591	69	24898	5.62
	59.79	0.2181	3.1475	1.5622	1.34	14.43	5734	73	32929	7.47
0.88M KOH	25.22	0.2707	2.8152	0.7723	1.58	10.4	7803	59	11405	1.29
	34.48	0.2681	3.1652	0.9473	1.56	11.81	8272	69	18767	2.13
	42.76	0.2696	3.6035	1.1355	1.51	13.37	8521	79	29354	3.35
	50.9	0.2684	4.0072	1.3123	1.48	14.93	8742	90	43557	4.99
	59.7	0.2681	4.3406	1.5011	1.4	16.19	8842	100	60308	6.94
1.76M KOH	25.7	0.2211	3.328	0.7213	1.43	15.05	17722	133	55524	3.15
	34.39	0.2152	3.6443	0.8772	1.44	16.93	19021	153	88403	5.03
	43.39	0.2038	3.9745	1.0505	1.42	19.5	20829	182	147008	8.4
	51.41	0.1961	4.3749	1.2115	1.36	22.31	22186	216	234239	13.43
	59.55	0.1976	4.6713	1.3559	1.22	23.64	22334	242	316860	18.25
1.76M KOH Repeated	24.99	0.2535	3.5864	0.7067	1.55	14.15	15312	123	46859	2.65
	34.41	0.2336	3.8365	0.8684	1.53	16.42	17491	149	81651	4.63
	42.83	0.2355	4.3548	1.0483	1.51	18.49	17950	168	126653	7.21
	51.45	0.2268	4.6504	1.1589	1.4	20.5	19156	204	190848	10.91
	56.29	0.2329	4.8705	1.3341	1.33	20.91	18805	198	217485	12.47

Table A4: Kinetic data of CO_2 absorption into aqueous solutions of blends of hydroxides and carbonates of lithium, sodium and potassium

Experiment	T [°C]	$LMPD_{CO_2}$ [kPa]	$N_{CO_2}\times10^4$ [mol.m^{-2}.s^{-1}]	$k_L^0\times10^4$ [m.s^{-1}]	$k_g\times10^2$ [mol. m^{-2}. kPa^{-1}.s^{-1}]	$K_{ov_G}\times10^4$ [mol. m^{-2}. kPa^{-1}.s^{-1}]	$E_{A,\infty,film}$ [-]	Ha [-]	k_1 [s^{-1}]	$k_2\times10^{-4}$ [m^3. kmol^{-1}. s^{-1}]
0.5M	25.49	0.3098	0.4773	0.5151	1.54	4.3	6995	73	11987	2.37
NaOH+1M	34.35	0.3011	0.4616	0.6457	1.53	5.26	7427	88	21527	4.27
Na_2CO_3	42.67	0.318	0.4802	0.7748	1.51	6.13	7247	102	34095	6.77
	50.71	0.2936	0.436	0.9179	1.48	7.18	8059	118	53212	10.59
	59.37	0.287	0.3995	1.0821	1.39	8.02	8434	129	74626	14.89
1M	25.52	0.299	0.4726	0.6013	1.58	7.4	14681	89	20431	2.01
NaOH+0.5M	34.27	0.2774	0.4319	0.765	1.56	9.02	16360	106	37193	3.67
Na_2CO_3	42.71	0.2751	0.4224	0.9286	1.54	10.62	17029	125	61523	6.09
	50.98	0.2693	0.3969	1.1016	1.47	12.14	17904	142	93757	9.31
	58.56	0.2719	0.3643	1.2516	1.34	13.22	18181	156	125962	12.55
1M LiOH+2M	26.64	0.256	0.4032	0.506	1.58	10.94	52062	224	112991	3.71
NaOH	34.18	0.2613	0.406	0.6147	1.55	12.41	52620	251	170450	5.61
	43.12	0.2621	0.3967	0.7659	1.51	13.96	54248	276	254926	8.42
	51.07	0.2633	0.39	0.8697	1.48	15.37	55456	312	351128	11.64
	58.69	0.2718	0.3784	1.025	1.39	16.57	55098	326	456825	15.21
0.5MNaOH+	26.25	0.2604	0.3996	0.8237	1.53	11.13	15932	63	14178	1.5
0.44M KOH	35.34	0.2517	0.38	1.0039	1.51	12.69	17051	74	23450	2.48
	43.26	0.2511	0.376	1.1575	1.5	14.18	17591	86	35253	3.74
	50.83	0.2493	0.3632	1.3586	1.46	15.69	18214	95	50859	5.42
	59.46	0.2522	0.351	1.565	1.39	16.85	18414	104	68803	7.37
1M	24.84	0.2589	0.3956	0.7305	1.53	11.91	24627	93	27355	1.88
NaOH+0.44	33.94	0.2405	0.3626	0.9072	1.51	13.87	27499	110	47309	3.26
M KOH	42.74	0.2287	0.3376	1.0852	1.48	15.89	29881	129	76629	5.3
	50.49	0.2273	0.3239	1.2403	1.42	17.83	30952	150	114482	7.94
	59.04	0.2336	0.3264	1.4442	1.4	19.26	30769	162	155239	10.82
0.89M KOH	25.57	0.3019	0.4702	0.6108	1.56	7.75	12817	84	19026	2.13
+0.5M	34.23	0.3011	0.4652	0.7824	1.55	8.82	13261	92	30150	3.38
Na_2CO_3	42.75	0.2916	0.4408	0.8854	1.51	10.21	14126	115	48477	5.45
	50.95	0.2841	0.4192	1.054	1.48	11.59	14887	129	72803	8.22
	58.73	0.2911	0.4016	1.2108	1.38	12.54	14874	139	96944	10.98
0.89M	25.56	0.2715	0.4296	0.6698	1.58	10.61	14378	101	29887	3.34
KOH+0.5M	34.32	0.27	0.4135	0.819	1.53	12.11	14967	118	49218	5.51
K_2CO_3	42.87	0.2648	0.4002	0.9719	1.51	13.75	15759	137	77622	8.72
	50.97	0.2642	0.3875	1.1282	1.47	15.18	16230	154	111835	12.59
	58.78	0.265	0.3592	1.2833	1.36	16.26	16585	167	149232	16.85

8. Paper IV

Activity based kinetics of CO_2-OH^- systems with Li^+, Na^+ and K^+ counter ions

*Shahla Gondal, Hallvard F. Svendsen, Hanna Knuutila**

Department of Chemical Engineering, Norwegian University of Science and Technology, N-7491 Trondheim, Norway

Is not included due to copyright

*** Corresponding Author: Hanna.Knuutila@ntnu.no**